ANALYSIS OF SUCCINIC ACID-PRODUCING BIOFILMS OF *ACTINOBACILLUS SUCCINOGENES*

BY

SEKGETHO CHARLES MOKWATLO

THESIS SUBMITTED IN PARTIAL FULFILMENT OF THE REQUIREMENTS FOR THE DEGREE

DOCTOR OF PHILOSOPHY IN CHEMICAL ENGINEERING

IN THE

DEPARTMENT OF CHEMICAL ENGINEERING

FACULTY OF ENGINEERING, THE BUILT ENVIRONMENT AND TECHNOLOGY

UNIVERSITY OF PRETORIA

SUPERVISOR: PROFESSOR WILLIE NICOL

CO-SUPERVISOR: DR HENDRIK GIDEON BRINK

JUNE 2020

ANALYSIS OF SUCCINIC ACID-PRODUCING BIOFILMS OF *ACTINOBACILLUS SUCCINOGENES*

Author: Sekgetho Charles Mokwatlo

Supervisor: Professor Willie Nicol

Co-supervisor: Dr Hendrik Gideon Brink

Department: Chemical Engineering

Degree: Doctor of Philosophy in Chemical Engineering

SYNOPSIS

Biofilms of the bovine rumen bacterium *Actinobacillus succinogenes* have demonstrated their exceptional capabilities as biocatalysts for high productivity, titre and yield production of succinic acid (SA). Succinic acid is set to become a significant building block chemical in the biobased economy. Although substantial progress has been made towards understanding the productive aspect of this microorganism with regard to its metabolic limits and performance on unrefined biorefinery stream substrates, more research is still required to address other challenges. One aspect is to understand how the biofilm biocatalyst is affected by bioreactor conditions, which would help in developing stable and highly active biofilms. For this reason the aim of this thesis was (i) to characterise how the accumulation of acid metabolites in continuous operation impacts *A. succinogenes* biofilms with respect to biofilm development, biofilm structure and cell activity within the biofilm, (ii) to show how shear conditions in the fermenter can be used to manipulate the biofilm structure and viable cell content of biofilms, leading to improved cell-based succinic acid productivities, and lastly (iii) to investigate the internal mass transfer effects on biofilm performance, further showing the role played by differences in shear and acid accumulation conditions in this respect.

The first part of the study addressed the interaction between the biofilm and the accumulation of metabolites produced. The results showed that biofilms of *A. succinogenes* develop rapidly and with high activity when cultivated under low product accumulation (LPA) conditions (< 10 g L^{-1} SA). High product accumulation (HPA) conditions considerably slowed down biofilm

development, and increased cell mortality. Under HPA conditions some cells exhibited severe elongation while maintaining a cross-sectional diameter like the rod/cocci-shaped cells predominantly found in LPA conditions. The elongated cells formed in HPA conditions were found to be more viable and thus more resistant than the clusters of rod-shaped or cocci-shaped cells. The global microscopic structure of the HPA biofilms also differed significantly from that of the LPA biofilms. Although both exhibited shedding after 4 days of growth, the LPA biofilms were more homogenous (less patchy), thicker and had high viability throughout the biofilm depth.

In the second part of the study, two custom-designed bioreactors were used to evaluate the effect of shear on the biofilms. The first bioreactor allowed for in situ removal of small biofilm samples used for microscopic imaging. The second bioreactor allowed for complete removal of all biofilm and was used to analyse biofilm composition and productivity. Results clearly indicated that high shear biofilm cultivation in LPA conditions has beneficial morphological, viability and cell-based productivity characteristics. The smooth, low-porosity biofilms obtained under high shear and LPA conditions had an average cell viability of 79% (over a 3-day cultivation period) compared with the low shear value of 57%, also developed under LPA conditions. The EPS content of the high shear biofilm was 58% compared with 7% of the low shear equivalent. The cell-based (EPS excluded) succinic acid productivity for the high shear biofilm was 2.4 g g^{-1}DCW h^{-1} compared with the 0.8 g g^{-1}DCW h^{-1} for the low shear biofilm. This threefold increase in productivity obtained from the second bioreactor corresponded to the cell viability differences obtained from the first bioreactor. Clear evidence was provided for shear-induced shaping of the biofilm which resulted in improved volumetric glucose turnover attributes within the biofilm matrix.

The last section of the study investigated internal mass transfer effects in biofilm fermentations of *Actinobacillus succinogenes* by performing batch fermentations using attached and resuspended biofilms as biocatalysts. In the latter, the biofilms were resuspended after initial development to simulate mass transfer-free fermentations. Intrinsic kinetics for succinic acid production obtained from resuspended fermentations predicted faster production rates than for the attached biofilm runs (biofilm thicknesses in the range of 120–200 μm), indicating internal mass transfer limitations. A developed biofilm reaction diffusion model gave good prediction of attached biofilm batch operation results by accounting for internal mass transfer in the biofilm. Biofilm effectiveness factors ranged from 75% to 97% for all batches at the inception

of batch conditions, but increased with the progression of batch operation due to the increased succinic acid titres which inhibited the production rates. Analysis of pseudo-steady-state continuous fermentation data from the literature, as well as from the second part of the study, using the model developed, showed that active biofilm thickness and effectiveness factors were dependent on the shear conditions and succinic acid titres in the biofilm reactors. A simplified algorithm was developed to estimate the pseudo-steady-state glucose penetration and biofilm effectiveness of *A. succinogenes* biofilms without the requirement to solve the overall mass transfer model. The results clearly showed that internal mass transfer needs to be considered in biofilm fermentations involving *A. succinogenes* as high biomass concentrations may not always equate to increased productivities if mass transfer effects dominate.

Keywords: *Actinobacillus succinogenes,* succinic acid, biofilms, shear, internal mass transfer, metabolite accumulation

ACKNOWLEDGEMENTS

To my Heavenly Father, who hearkened unto my humble prayers and lavished me with His unfailing mercies throughout my PhD journey, I send my foremost gratitude and thanksgiving. Without His mercies nothing worth doing can be done. Thank you to Yahweh for choosing this path for me and my family.

To my supervisor (soon to be friend) Prof. Willie Nicol, I want to thank you for your continued guidance and insight throughout the duration of my postgrad studies. Through your outstanding supervision you created a free environment that encouraged learning and gave me courage to explore ideas. I have honestly learned so much from you, both in the academic sphere and my personal capacity. I will not forget our countless talks over drinks through which I got introduced to a proud African with big dreams for this country and Africa. You have indeed left a big impression on me, I'm so very proud of the person you are, the budding "*Yoga Master!!!*".

To Dr Deon Brink, who is also my co-supervisor, I thank you for the continuous discussions we had concerning my research – we spent ample time either over the phone, or in both our offices, and even around campus (walking) – they have helped me considerably. It has been a pleasure working with you.

I would also like to acknowledge the late Frank Simmonds, for continuously encouraging and supporting me from my early years at school until he passed on. Frank always believed in me, and for that I am forever grateful.

I have met incredible individuals in the Bioreaction Engineering Group who have made my stay bearable. To the veterans – Dr Michael Bradfield, Dr Andre Naude, Jolandi Herselman and Uma Vijayan – thank you for the encouragement, and the patience you had in teaching me the ropes of continuous fermentations as well as for the interesting conversations we had. The new guys always bring fresh ideas which are not always linked to our research work; in this respect I thank Monique Geyer, Deon Durand, Makhine Nchabeleng and Waldo Lexow for introducing the movie and quiz nights, and the now traditional journal club meetings. To the recent batch of new recruits – Reuben Swart, Nico de Jongh, Eleanor Reynecke and Naas van Rooyen – thank you for the discussions, supporting my campaign for the "smoothie club", and for general assistance with the running of the lab.

Several members of the Department of Chemical Engineering staff have proved to be key for the efficient and successful running of our laboratory. I would like to thank Shadrack Phosane and Gerrie Claassen for keeping our facilities running and being available to help at a moment's notice. Thank you to the ever-smiling Mrs Elmarie Otto for gracefully helping us with the countless orders we sent her way. Thanks also to Paul Sonnendecker who helped with machining my bioreactor, without which this research would not have been possible. Beyond the Chemical Engineering Department, I would like to thank Dr Eudri Venter, Dr Chantelle Venter, Allan Hall and other staff members at the Laboratory for Microscopy and Microanalysis for their assistance with my microscope work.

To the members of the TAP ZCCSF family, I convey my ever-present gratitude for the spiritual and social support they have provided me with. I single out Pastor Johannes Mothiba, who has led us with humility, encouraged us at every obstacle, and whose fervent prayers have safeguarded us. I also thank my church, the ZCC, and its exemplary leadership for much more that simply cannot be put into words.

To all my friends, thank you so much for the calls, the texts, the outings, the visits, the prayers and for understanding when I could not make it to the arrangements we had. You all played an instrumental role in my life, and for this I'm grateful.

Lastly, I thank my family for their love, support and encouragement throughout my studies – from my first year to my postgrad years. My mother Mokete Mokwatlo has sacrificed much for me, so thank you. My siblings, Tommy, Masi and Hloni have always been a delight to hang out with, thanks guys.

FUNDING

The financial assistance of the Sugar Milling Research Institute via the Step-Bio programme is hereby gratefully acknowledged. The financial assistance of the National Research Foundation (NRF) towards this research is hereby acknowledged. Opinions expressed, and conclusions arrived at, are those of the author and are not necessarily to be attributed to the NRF.

NOTE ON PDF NAVIGATION

All in text references of figures, tables, sections and subsections in the PDF version of this thesis are cross-referenced to their respective locations in the document by hyperlinks. The links are visible (blue font). Furthermore, when using Adobe Acrobat Reader, it is possible to return to the point from which the link was clicked by pressing the "Alt" and "Left arrow" keys together, or by following View → Page Navigation → Previous View in the menu bar.

CONTENTS

LIST OF FIGURES

LIST OF TABLES

NOMENCLATURE

a_1	effectiveness factor equation parameter	
a_2	effectiveness factor equation parameter	
AA	acetic acid	
AceCoA	acetyl-CoenzymeA	
A_p	solid liquid interface biofilm area per volume	(m^2 m^{-3})
ATP	adenosine triphosphate	
c_1	effectiveness factor equation parameter	
CER	cation exchange resin	
C_{Glc}	glucose concentration	(g L^{-1})
C_j	concentration of component j in the biofilm	(g L^{-1})
$C_{j\text{-}aq}$	concentration of component j in the liquid phase	(g L^{-1})
C_{SA}	succinic acid concentration	(g L^{-1})
$C_{SA_{avg}}$	average succinic acid concentration in the biofilm	(g L^{-1})
C^*_{SA}	non-dimensional succinic acid concentration	
CSLM	confocal scanning laser microscope	
$C_{X,aq}$	cell concentration in the liquid phase	(gDCW L^{-1})
C_{XB}	biofilm cell concentration	(gDCW L^{-1})
DCW	dry cell weight	
D_{e_j}	effective diffusivity of component j in the biofilm	(m^2 s^{-1})

D_{aq-j}	diffusivity of component j in water	(m^2 s^{-1})
D_{cr}	diffusivity of component j in the cell	(m^2 s^{-1})
D_{eo-j}	effective diffusivity of component j in the EPS	(m^2 s^{-1})
D_{pr}	diffusivity of component j in the EPS	(m^2 s^{-1})
EPS	extracellular polymeric substances	
F6P	fructose 6-phosphate	
FA	formic acid	
FDH	formate dehydrogenase	
G3P	glyceraldehyde 3-phosphate	
G6P	glucose 6-phosphate	
Glc	glucose	
HPA	high product accumulation	
HSC	hydrodynamic shear conditions	
J_j	flux of component j	(g L^{-1} h^{-1})
k	maximum maintenance-based production rate	(g $gDCW^{-1}$ h^{-1})
Ki	product inhibition constant	(g. L^{-1})^2
Kp	product half saturation constant	(g. L^{-1})
L	biofilm thickness	(m)
L^*	active biofilm thickness	(m)
LPA	low product accumulation	
MTT	3-(4,5-dimethylthiazol-2-yl)-2,5-diphenyl tetrazolium bromide	

NADH	nicotinamide adenine dinucleotide	
OAA	oxaloacetic acid	
OPPP	oxidative pentose phosphate pathway	
PBS	phosphate buffered saline	
PDH	pyruvate dehydrogenase	
PEP	phosphoenolpyruvate	
PFL	pyruvate formate lyase	
q_{SA}	succinic acid productivity	(g L^{-1} h^{-1})
r'_{Glc}	cell-based glucose consumption rate	(g $gDCW^{-1}$ h^{-1})
$\overline{r'_{Glc}}$	average glucose consumption rate in the biofilm	(g $gDCW^{-1}$ h^{-1})
r'_{AA}	cell-based acetic acid production rate	(g $gDCW^{-1}$ h^{-1})
r'_{FA}	cell-based formic acid production rate	(g $gDCW^{-1}$ h^{-1})
r'_{SA}	cell-based succinic acid production rate	(g $gDCW^{-1}$ h^{-1})
r'_j	cell based production rate of component j	(g $gDCW^{-1}$ h^{-1})
SA	succinic acid	
SEM	scanning electron microscope	
TCA	tricarboxylic acid	
$Y_{AA/SA}$	acetic acid to succinic acid mass ratio	(g g^{-1})
$Y_{FA/SA}$	formic acid to succinic acid mass ratio	(g g^{-1})
Z	non-dimensional biofilm thickness	
m	dimensionless parameter	

z	biofilm thickness variable	(m)

Greek symbols

η	biofilm effectiveness factor	
ε_{CELLS}	volume fraction of cells in the biofilm	
ε_{EPS}	volume fraction of EPS in the biofilm	
ε_{W}	volume fraction of water in the biofilm	
α	thiele moduli equivalent parameter	
β	non-dimensional product saturation parameter	
γ	non-dimensional product inhibition parameter	
θ	maintenance associated production	(g $gDCW^{-1}$)
μ	specific growth rate	(h^{-1})
ϕ	growth associated succinic acid production	(g $gDCW^{-1}$)

1 INTRODUCTION

The rate of environmental degradation as a result of anthropogenic activities is fast approaching a tipping point. For a long time humanity has embraced a linear economic model [1] with a "take, make and dispose" production philosophy. This model prioritised profits at the cost of depleting natural resources, and generated excessive waste and pollution. Since the survival and prosperity of humanity is tied to that of the environment, it appears that human civilisation was unwittingly built on a bedrock of an economic model that is a ticking time bomb, ticking ever so fast as the world population grows and industrialisation spreads. To address this growing danger, debates about the circular economy concept and sustainability are currently gaining traction in academia, industry and policy making [1, 2]. In a circular economy, minimisation of both waste creation and the use of virgin resources will ideally be achieved through employing principles such as reusing, recycling, repairing, remanufacturing, etc. to create a closed loop of material flows in the market [2]. Moreover, themes of cleaner production, eco-designs and various other green technologies will conceptually be integrated into industry to mitigate or reverse ongoing harmful anthropogenic effects.

In particular, the sector for fuel, power and bulk chemicals supply – a strategic industry on which modern civilisation chiefly depends – requires much redress. This is because it is a sector that is highly unsustainable as the feedstocks used are almost exclusively non-renewable (coal and petroleum), and the processing thereof has had an enormous carbon footprint [2, 3]. Since it is a strategic sector, the redress cannot be a total overhaul of the current infrastructure but must be its transformation through the development of sustainable renewable resources and green processing technologies. It is within this context that the biorefinery concept was developed [4–6]. Conceptually, in a biorefinery, biomass (preferably obtained from agricultural and forestry residue) will be transformed through bioprocessing technologies into a spectrum of biochemicals and biomaterials products, as well as energy [4]. However, the low energy content of biomass resources as compared with petroleum-based feedstocks implies that biofuel production will constitute a smaller part of biorefineries, unlike in traditional refineries. In this way, a significantly larger part of biorefineries will include the production of biochemicals and biomaterials with a greater variety compared with traditional refineries [5, 7]. This will help to

compensate for the loss of the economies-of-scale benefit obtainable from fuel production. Overall, the renewable nature of biomass resources, the use of biotechnological conversion processes, as well as the integrated use of waste streams by other processes in a biorefinery to avoid waste generation, will, taken as a whole, render the biorefinery concept highly sustainable.

The use of biological conversion technologies is fundamental to the success of biorefineries. Here, microbial catalysis and enzyme catalysts will play a major role as they provide several key advantages [7]. As a result of their biodegradable nature, the biocatalysts can be easily disposed of or even used as feed additives, and the conversion process will operate at lower temperatures and pressures, thereby saving immense energy costs. Furthermore, since a single microbe can catalyse multiple reactions, a substantial reduction in the amount of processing equipment required can be realised [8, 9]. Most importantly, however, biocatalysts are amenable to various types of manipulation using concepts of metabolic engineering as well as systems biology, and thus they can potentially be optimised for particular processing needs [8, 9].

Among the US DOE's reported "top value-added chemicals from biomass" [10], succinic acid (SA) is most sought after and well established as a top bio-based platform chemical with an estimated market of USD132 million in 2018, which is expected grow to USD183 million by 2023. Succinic acid finds application in the pharmaceutical industry, in the food industry as a pH regulator and flavouring agent, as an ion chelator and surfactant, and mostly as a building block chemical. It is a precursor for a plethora of high-value chemicals, including 1,4-butanediol, tetrahydrofuran, adipic acid, γ-butyrolactone and n-methylpyrrolidone. Various microorganisms have been used for bench-scale fermentation experiments to produce succinic acid. Wild-type microbes reported in the literature include *Mannheimia succiniciproducens* [11], *Anaerobiospirillum succiniciproducens* [12], *Basfia succiniciproducens* [13] and modified strains of *Escherichia coli* [14]. However, among these, it is the bovine rumen bacterium *Actinobacillus succinogenes* 130Z that is the most apt for industrial bio-succinic acid production, owing mainly to its capacity to produce succinic acid at titres [15–19], productivities and yields [20–23] well above its those of its competitors. In addition, *A. succinogenes* sequesters CO_2 in succinic acid production (thus offering a CO_2 sink in a biorefinery concept) while consuming a wide range of carbon sources [24] with comparatively high tolerance to acids.

Key among the traits that make *A. succinogenes* a desirable biocatalyst is its ability to form biofilms unavoidably in continuous fermentations [20, 22]. This allows the microbe to reach high cell concentrations without active cell retention strategies (which add to both capital and running costs), and thus achieve high succinic volumetric productivities and titres. High productivity, titre and yield are crucial considering the economics of the process. The superior performance of *A. succinogenes* biofilms in comparison with any suspended cell systems of the same microbe have been demonstrated in various bioreactor configurations (batch, fed-batch, continuous) with regard to rates, yield and titre [21, 25]. Furthermore, apart from productivity gains, biofilms are beneficial for their enhanced tolerance to toxic reagents and their long-term activity – qualities that are desirable in continuous processing where process stability is a concern [20, 24]. Indeed, biofilms of *A. succinogenes* were shown to metabolise non-detoxified xylose hydrolysate streams efficiently while achieving competitive titres, yield and productivities over prolonged fermentation periods [24].

The production characteristics of SA with *A. succinogenes* biofilms have been studied extensively in the open literature, exploring steady-state metabolite distributions at varying glucose consumption rates [20–22, 25], and yield comparisons of biofilm and suspended cell fermentation [20, 21], fermentations of various sugar types, including hydrolysate streams [24, 26, 27], as well as using different reactor configuration schemes [21, 25]. The biofilm process story painted thus far shows industrial promise, albeit it is also an incomplete story as the productive aspect of the *A. succinogenes* biofilm process is just but one side of the coin. Another side of this coin – which is critical for industrial implementation – is understanding how best to lay down the biofilm catalyst in such a way that it promotes stable and efficient fermenter operation. This requires understanding of how biofilm development and properties, such as its structure and activity, are influenced by conditions in the fermenter, both physically and microscopically. However, no studies thus far have explored this topic.

It was the main objective of this study to investigate the development of *A. succinogenes* biofilms. More specifically, this research aimed (i) to characterise how accumulation of acid metabolites in continuous operation impacts *A. succinogenes* biofilms with respect to biofilm development, biofilm structure and cell activity within the biofilm, and (ii) to show how shear conditions in the fermenter can be used to manipulate the biofilm structure and viable cell content of biofilms, leading to improved cell-based succinic acid productivities. In addition,

internal mass transfer effects on biofilm performance were studied, further showing the role played by differences in biofilm composition in this respect.

This research is thus divided into three main themes captured in Chapters 3, 4 and 5, with the background on the *A. succinogenes* biofilm process given in Chapter 2. In Chapter 3, a brief discussion on the custom development of a bioreactor suited for biofilm cultivation and multiple sampling for microscopic visualisation precedes a main discussion on how the accumulation of metabolite acids impacts biofilm development, structure and viability. Chapter 4 focuses on how variation in shear conditions in the fermenter influence changes in the biofilm structure, composition and viable cell content, as well as biofilm succinic acid productivity. Finally, Chapter 5 investigates internal mass transfer in biofilms of *A. succinogenes* giving consideration to how it impacts glucose availability within the biofilm, as well as the effectiveness of the biofilm as a catalyst for the production of succinic acid.

2 THE *ACTINOBACILLUS SUCCINOGENES* BIOFILM PROCESS

2.1 SUCCINIC ACID

Succinic acid (SA) is a four-carbon-chain dicarboxylic acid commonly referred to as "spirit of amber" or amber acid, as it was first obtained by distilling amber in 1550 [28] (Figure 2-1). The linear structure and carboxyl functional groups of succinic acid render it amenable to various interesting chemical transformations, hence its reputation as a potential specialty chemical. Traditionally, SA was commercially produced predominantly via petrochemical processes from the catalytic hydrogenation of maleic anhydride derived from butane [29]. However, since it is an intermediate metabolite in the TCA cycle, it can also be produced naturally by various microorganisms [30].

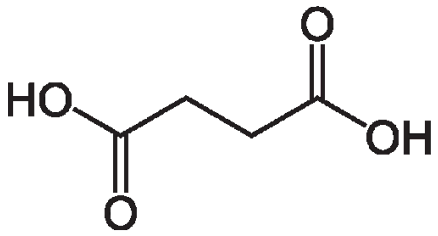

Figure 2-1: Succinic acid molecule

Alongside malic and fumaric acid, the close dicarboxylic acid counterparts, SA is included in the top 12 platform chemicals derivable from biomass resources [10] by the US Department of Energy. This is chiefly because all three acids can be produced through microbial processes and have a similar chemical structure. They can therefore be converted readily to a range of industrial chemicals with big markets, such as 1,4-butanediol [30] which had a market volume of 4.3 million tons in 2018. These acids have a higher oxygen content than the starting petrochemical chemicals used to make maleic anhydride due to the carboxyl functional groups. Costly and often harsh oxidation processes are used to add these functional groups to the carbon backbone in the petroleum industry [28]. By contrast, comparatively mild conditions are required for the microbial production of these acids. Moreover, renewable feedstocks are used, making the processes sustainable.

2.1.1 MARKET AND APPLICATIONS OF SUCCINIC ACID

There are numerous commercial applications for succinic acid (SA). In the food industry succinic acid is used primarily as a flavouring agent and as an acidulant, and it is further used in the cosmetic and personal care industries as raw material for emollients, surfactants and emulsifiers. In the pharmaceutical industry, succinic acid is used as raw material for the production of ferrous succinate, succinimide and N-bromosuccinimide [31]. The main application of SA, however, is in the chemicals and materials industry where it is used as raw material for the production of resins, coatings and pigments, and for polymers such as polybutylene succinate and polyester polyols [31]. If an economical bio-based method of producing SA were to be developed that could compete with petrochemical production routes, succinic acid could potentially serve as a building block in the synthesis of bulk chemicals such as 1,4-butanediol, γ-butyrolactone, tetrahydrofuran, adipic acid, 2-pyrrolidone, etc. [32].

Market analysis shows that the well-established SA market is expected to grow considerably in the near future, with the Asia-Pacific region responsible for most of this growth [31]. Indeed, the market size of succinic acid, valued at USD 131.7 million in 2018 [31], is projected to grow at a constant annual growth rate of 6.8% to reach a market size of USD 182.8 million in 2023. More alarming, however, is that it is the petro-based SA that is projected to be the major contributor to the anticipated market size growth of SA, instead of biobased SA. Cost effectiveness and the greater efficiency achieved in petro-based production of SA are cited as the main reasons for this disparity. This underscores the need to improve the fermentation routes by developing high-yield, -titre and -productivity processes able to compete with the petro-based counterparts.

Nevertheless, commercial bioproduction of succinic acid is currently underway with several companies such as BASF-Purac, Myrant, Riverdia and BioAmber at the forefront and though there was an expectation of considerable increases in the annual tonnage production by 2020 [33], Figure **2-2**, this was not realised by most of them. The considerable reduction in oil prices is cited as a major reason why most of these companies have either halted or stopped bio-succinic acid production. Most of these companies use genetically modified organisms and also opt for processes that use low-pH conditions, thereby gaining the advantage of keeping metabolites in acid form which significantly lowers the downstream processing and neutralisation costs.

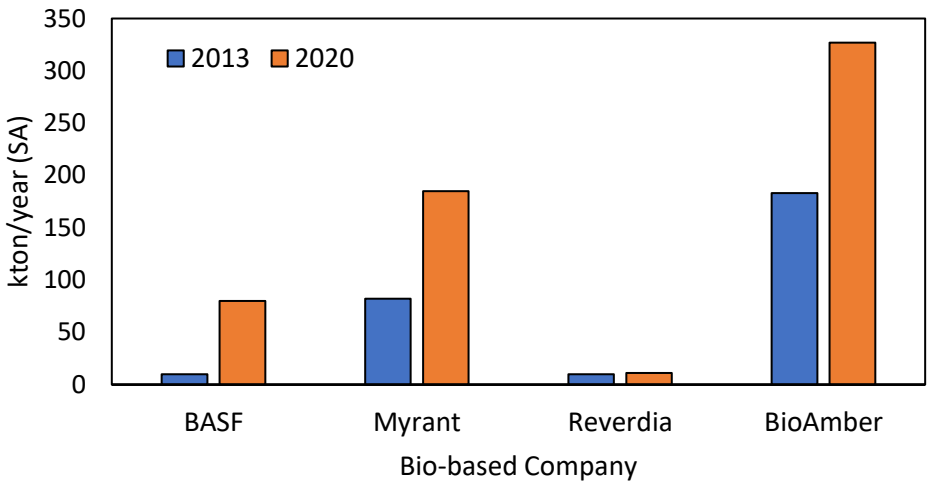

Figure 2-2: Bioproduction of succinic acid and projected growth [33]

2.1.2 MICROBIAL HOSTS FOR SUCCINIC ACID PRODUCTION

Several microorganisms have been identified for bioproduction of succinic acid from sugar substrates, and these range from natural producers to genetically modified producers (Table **2-1**). However, when screening for potential – industrially applicable – biocatalysts for succinic production, it is imperative to consider the capabilities of the microorganism to produce succinic acid at high yield, titre and productivity. Yield is a measure of the ability of the biocatalyst to channel most of the carbon substrate into the desired product metabolite and it thus affects the variable costs of the process. Product titre in the fermentation broth determines the ease of separation in downstream processes and will thus affect both the capital investment for separation equipment and the variable costs of the process. Finally, productivity reflects the efficiency of utilisation of the production capacity which affects the capital costs of the process. Extensive review work has been done on the fermentative production of succinic acid, covering aspects such as the market analysis and microbial hosts for biobased SA [34–36].

Among the natural producers of succinic acid, the microbial strains of *Mannheimia succiniciproducens, Basfia succiniciproducens and Actinobacillus succinogenes* have shown good performance with an ability to break down a wide variety of carbon substrates under anaerobic conditions for efficient succinic fermentative production [37] (Table 2-2). All these strains were isolated from the bovine rumen, where they were most probably responsible for producing succinic acid as a precursor for the propionic acid which accounts for 30% (w/w) of the volatile fatty acids in the rumen [34]. A common challenge with natural producers, however,

is their non-fastidious nature, which requires the use of expensive and complex growth media. *Escherichia coli* AFP 111/pTrc99Apyc and *Corynebacterium glutamicum* ΔldhApCRA717 are two genetically modified microorganisms which have demonstrated promising fermentative succinic acid production performance. High succinic acid titres of 146 g L^{-1} and 99.2 g L^{-1} at yields of 0.99 and 1.1 (g g^{-1}), and productivities of 3.17 g L^{-1} h^{-1} and 1.17 g L^{-1} h^{-1} for *C. glutamicum* and *E. coli* respectively have been reported [38, 39] (Table **2-2**). However, a major drawback with genetically modified microorganisms is their tendency to revert to their natural metabolism during prolonged fermentations [40]. This is a significant risk factor when considering commercialisation of the process. Strains that naturally produce succinic acid at high titres and rates may be good starting points for optimisation through metabolic engineering to enhance performance [41]. These strains would offer the advantage of requiring less genetic manipulation and stable phenotypes during prolonged fermentations.

The rumen bacterium *A. succinogenes* is most promising among competitive wild-type producers of SA. It has demonstrated a propensity to produce SA at high titre, yield and productivity in a mixed-acid bench-scale fermentation [15–23], well above its natural competitors. *A. succinogenes* is tolerant towards high acid titres [15–19], and it also has an ability to utilise a wide range of carbon sources [37], including scalable biorefinery streams [24, 26, 27]. *A. succinogenes* has consistently demonstrated an ability to self-immobilise on available surfaces, thereby attaining high cell densities which help to boost SA productivities. Cell retention is crucial in that it reduces the time and carbon investment for cell growth through prolonged use of previously produced cells. Moreover, the metabolic behaviour of *A. succinogenes* under biofilm conditions favours succinic acid production, which ultimately leads to enhanced SA yields and reduced by-product formation [22]. In this way, *A. succinogenes* shows industrial promise as a top succinic acid producer.

Table 2-1: Identified organisms for biobased production of succinic acid

Type			Organism	Cultivation	Reference
Natural species	Bacteria	Gram positive	*Enterococcus faecalis* RKY1	Facultative anaerobe	[42]
			Enterococcus flavescens	Facultative anaerobe	[43]
		Gram negative	*Bacteroides fragilis*	Obligate anaerobe	[44]
			Klebsiella pneumoniae	Facultative anaerobe	[45]
			Succinivibrio dextrinosolvens	Obligate anaerobe	[46]
			Basfia succiniciproducens	Facultative anaerobe	[13]
			Mannheimia succiniciproducens	Facultative anaerobe	[11]
			Anaerobiospirillum succiniciproducens	Obligate anaerobe	[12]
			Actinobacillus succinogenes	Facultative anaerobe	[20]
			Fibrobacter succinogenes	Obligate anaerobe	[47]
	Fungi		*Aspergillus niger*	Facultative	[48]
			Paecilomyces variotii	Facultative	[49]
			Penicillium simplicissimum	Facultative	[50]
Genetically modified	Bacteria	Gram positive	*Escherichia coli*	Facultative	[38]
			Corynebacterium gluctamicum		[39]
	Yeasts		*Saccharomyces cerevisiae*		[51]

Table 2-2: Performance of succinic acid production studies using various microbial hosts

Organism	Carbon source	Mode	Yield (g/g)	Productivity ($g\ L^{-1}\ h^{-1}$)	Succinic acid ($g\ L^{-1}$)	Reference
Basfia succiniciproducens	Glucose	Batch	0.49	0.53	20	[52]
Actinobacillus succinogenes FZ53	Glucose	Batch	0.82	1.36	105.6	[53]
Actinobacillus succinogenes 130Z	Glucose	Continuous	0.9	10.8	32.5	[20]
Mannheimia succiniciproducens LPKZ	Glucose	Batch	0.76	1.8	52.4	[54]
Anaerobiospirillum succiniciproducens	Glucose	Continuous	0.81	14.8	15.1	[55]
Escherichia coli AFP111/pTrc99A-pyc*	Glucose	Batch	1.1	1.3	99.2	[38]
Corynebacterium gluctamicum ΔldhA-pCRA717*	Glucose	Batch	0.92	3.17	146	[39]

*Genetically modified strains

2.2 ACTINOBACILLUS SUCCINOGENES 130Z

Actinobacillus succinogenes 130Z (DSM No. 22257; ATCC No. 55618) is a Gram-negative and facultative anaerobe of the *Pasteurellaceae* family isolated from bovine rumen at the Michigan State University by Guettler et al. [56] (Figure 2–3). It is a non-motile, non-spore-forming and non-pathogenic pleomorphic rod that grows well at temperatures of 36–38 °C and pH values between 6.0 and 7.4 as it is also a mesophilic neutrophile . Its mixed-acid fermentation in a nutrient-rich medium results in considerable titres of succinic acid, acetic acid, formic acid and small amounts of ethanol and pyruvic acid. As it was isolated from the rumen, an anaerobic and CO_2-rich environment, the bacterium exhibits enhanced growth rates and succinic acid production in high-CO_2 content conditions, making it capnophilic. *A. succinogenes* has shown an ability to metabolise various disaccharides as well as a wide range of C_5 and C_6 sugars and carbon sources, such as glucose, xylose, arabinose, mannose, galactose, fructose, sucrose, lactose, cellobiose, raffinose, mannitol, maltose, sorbitol, glycerol, amygdalin, ascorbate, glucarate, galactarate and idonate, among others [37].

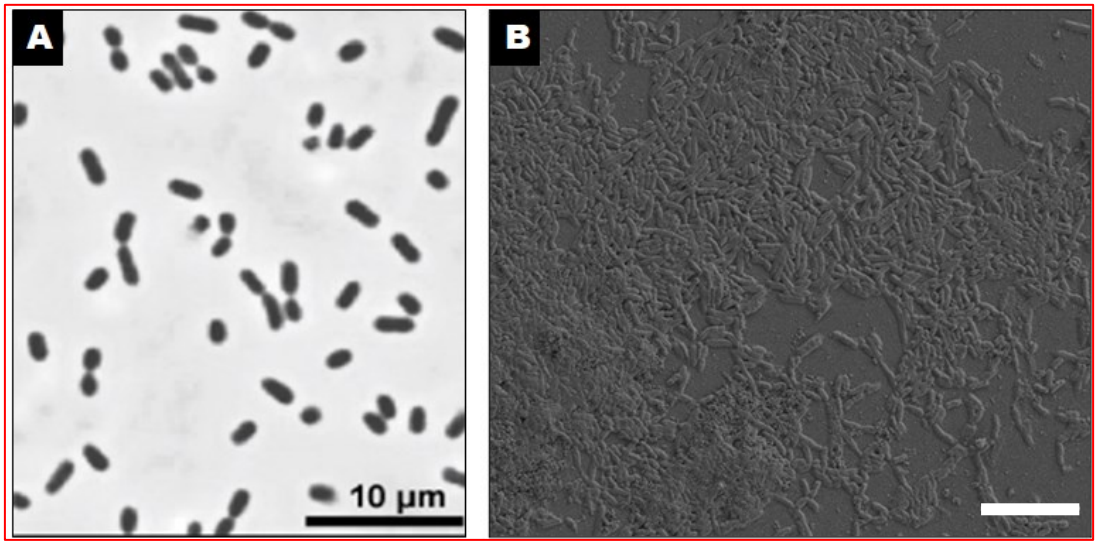

Figure 2-3: Characteristic morphology of *A. succinogenes* cells

As the bacterium is pleomorphic, it can appear in either a rod or a coccobacillus morphology (A). Early-stage biofilm formation, as captured by cryogenic SEM, rod-like cell morphology, is apparent (B). (Souce of images: (A) James Mckinlay, Michigan State University, public domain; (B) Sekgetho Mokwatlo, University of Pretoria, author)

2.2.1 METABOLISM

The metabolism of *A. succinogenes* was characterised largely by McKinlay et al. [57] through genome sequencing [58] and a ^{13}C metabolic analysis study [59, 60]. In the central metabolism of *A. succinogenes*, glucose uptake is facilitated by a phosphoenolpyruvate (PEP)-dependent phosphotransferase system, as well as through the action of a permease and subsequent phosphorylation by a hexokinase, to form glucose 6-phosphate (G6P) which is further deconstructed to PEP via glycolysis pathways [58]. Indeed, C_6 sugars are broken down via glycolysis pathways, whereas C_5 sugars are initially broken via the pentose phosphate pathways (PPP) and subsequently enter the glycolysis pathways at fructose-6-phosphate (F6P) and glyceraldehyde 3-phosphate (G3P) (Figure 2-4). The involvement of the PPP in the deconstruction of glucose was found to be minimal as determined by ^{13}C metabolic flux analysis [60]. PEP forms the first node in the central metabolism of *A. succinogenes* as the deconstructed sugars link up to the glycolysis and ultimately form PEP.

A. succinogenes lacks a complete TCA cycle since it does not contain genes that code for citrate synthase and isocitrate dehydrogenase, thus resulting in an incomplete oxidative branch of the TCA cycle [58]. In this way, once at the PEP node, carbon flux can be channelled either towards the reductive leg of the TCA cycle (C_4 pathway) where succinic is the ultimate metabolite, or towards the C_3 pathways where redox power (NADH) is generated and acetate, pyruvate, formate and ethanol are possible end metabolites. The conversion of PEP to oxaloacetate by a PEP carboxykinase enzyme (EC 4.1.1.49) is the starting point of the C_4 pathway, where a single mole of CO_2 is fixed per mole of PEP converted with subsequent formation of an ATP molecule. The formation of ATP is crucial as it means that the C4 pathway can partly satisfy the energy requirements for growth and maintenance, which favours succinic acid production in both cases. The enzymes malate dehydrogenase, fumarase and fumarate reductase subsequently catalyse the conversion of oxaloacetate to fumarate and ultimately succinate, consuming two moles of NADH and producing 2/3 of a mole of ATP in the process. In this way there is a net consumption of NADH and a net generation of ATP in the C_4 pathways leading to succinic acid production. In Figure 2-4, the central metabolism of *A. succinogenes* is presented with the essential enzymes that catalyse the reactions depicted therein.

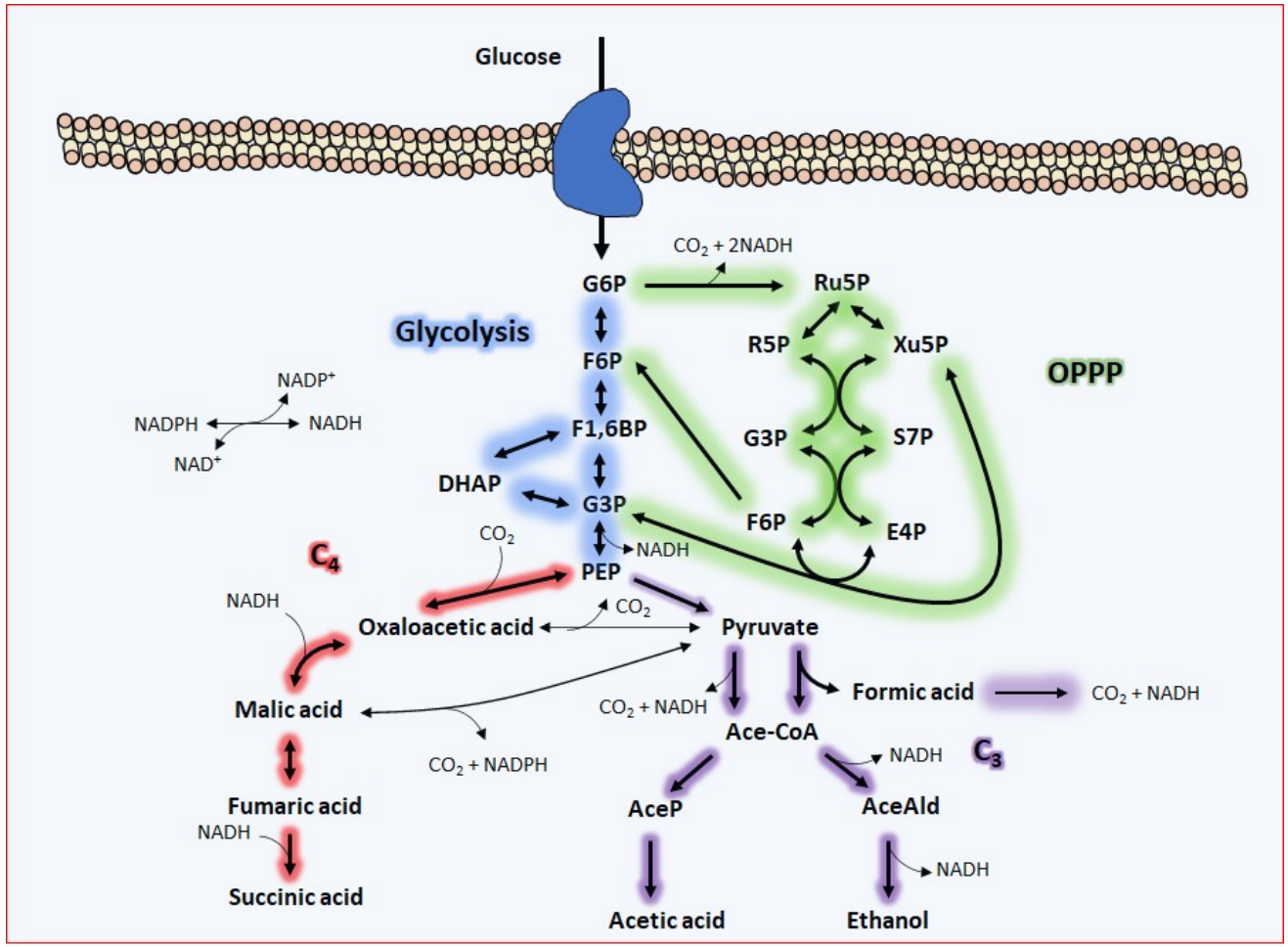

Figure 2-4: Central metabolic network of *A. succinogenes.* Every major pathway is shown in a different colour. (Abbreviations: AceP: acetyl-phosphate; Ace-CoA: acetytl-CoA; AceAld: acetaldehyde; G6P: glucose-6-phosphate; glyceraldehyde 3-phosphate; DHAP: dihydroxyacetone phosphate; E4P: erythrose 4-phosphate; F6P: fructose 6-phosphate; F1,6BP: fructose 1,6-bisphosphate; OPPP: oxidative pentose phosphate pathway; PEP: phosphoenolpyruvate; R5P: ribose 5-phosphate; Ru5P: ribulose 5-phosphate; S7P: sedoheptulose 7-phosphate; Xu5P: xylulose 5-phosphate)

The redox consumed in the reductive C_4 leg must be produced elsewhere to satisfy the redox balance of the system. Splitting some of the flux from the PEP node towards the C_3 pathways serves this purpose. PEP is converted to pyruvate by pyruvate kinase, with the generation of an ATP molecule in the process. Alternatively, Mckinlay et al. [57] determined that both oxaloacetic acid (OAA) and malic acid can serve as nodal points in the C_4 pathways, effectively redirecting carbon from the C_4 pathways to the C_3 leg by forming pyruvate via an OAA decarboxylase (for conversion of OAA) and the malic enzyme, respectively. Pyruvic acid subsequently serves as an important node in the C_3 leg, where it can be oxidized by either pyruvate dehydrogenase (PDH) or pyruvate formate lyase (PFL) to form acetyl-CoenzymeA (AceCoA). When the reaction is catalysed by PDH, a mole of NADH and a CO_2 molecule are generated. In the case of PFL, a CO_2 molecule is liberated along with formic acid, a major byproduct in *A. succinogenes* mixed-acid fermentation. It is desirable for most of the flux from the pyruvate node to be channelled via the PDH route as additional NADH is produced; this would boost the selectivity for succinic acid production. However, the formate generated in the PFL route can subsequently be broken down to CO_2 and NADH by a formate dehydrogenase (FDH), ultimately resulting in the same selectivity enhancement as the PDH route. Both the PDH and PFL routes form AceCoA which is another node in the C_3 leg, where carbon can be directed to the formation of either acetaldehyde or acetyl-phosphate, with the former consuming an NADH molecule. Acetate kinase then catalyses acetyl-phosphate producing acetic acid and an ATP molecule, whereas in the acetaldehyde route, ethanol is produced with an additional consumption of an NADH molecule. Overall, ethanol production from AceCoA consumes a net 2 NADH molecules. Ethanol production is minimal in CO_2-rich conditions. However, it is a major byproduct in CO_2-limited conditions as the C_4 pathway becomes constrained and it therefore serves to balance the redox. Another possible route from the AceCoA node is the formation of malate by the glyoxylate shunt, which would make homo-succinate production possible. However, *A. succinogenes* lacks a glyoxylate shunt [58]. The C_3 pathway results in the production of mostly acetic acid, formic acid and minor amounts of pyruvic acid and ethanol.

Theoretically, the maximum yield of succinic acid from glucose fermentation is 1.12 g g^{-1}, which can only be realised when there is no byproduct formation, including that of biomass. This would have been possible for *A. succinogenes* had it possessed a full TCA cycle or a glyoxylate shunt. According to the central metabolic pathways of *A. succinogenes*, and assuming a redox balanced fermentation, the maximum succinic acid yield is 0.67 g g^{-1} when

PFL is used at the pyruvate node (without subsequent formic dehydrogenase activity) or 0.87 g g^{-1} when the PDH is preferred. Subsequent oxidation of formate by formate dehydrogenase results in the same theoretical yield maximum of 0.87 g g^{-1} for succinic acid. The low yield in the case of the PFL-only route corresponds to a succinate selectively of 1.97g $g_{by\text{-}products}^{-1}$, whereas for the PDH (or the PFL and FDH) route, the selectivity is 3.93 g $g_{by\text{-}products}^{-1}$.

2.3 BATCH PRODUCTION STUDIES

Most of the fermentation studies by *A. succinogenes* have been performed in a batch mode. This is mainly because batch reactors are versatile, and are easy to operate and maintain, and thus many batch experiments can be operated simultaneously giving high throughputs for results and repeat runs. In this way batch experiments have mostly been used to explore various fundamental topics about succinic acid production by *A. succinogenes*, further advancing insight into the organism and the process.

2.3.1 GROWTH KINETICS

Substrate and product inhibition

Batch studies on the growth kinetics of *A. succinogenes* suggest that the specific growth of the bacterium is a stronger function of the acid metabolites produced than it is of the initial substrate concentrations [17, 19, 61–63]. Lin et. al. [17] reported a critical glucose concentration of 158 g L^{-1} at which growth is completely terminated, with a low Monod half-saturation constant of 2.03 g L^{-1}, demonstrating that substrate inhibition is limited. Optimal growth was found to be below glucose concentrations of 55 g L^{-1}, with concentrations beyond 100 g L^{-1} causing increased lag times at the beginning of fermentation [17]. Regarding product inhibition, it has been reported that at a total acid concentration of 20 g L^{-1} (accounting for succinate, formate and acetate) biomass growth terminates [61]. Of the metabolites produced, formic acid shows the most inhibition potency, followed by ethanol, acetic acid, pyruvic acid and succinic acid. In a study by Brink and Nicol [21], fermentation data from various prominent batch studies on glucose were used to calculate specific cell growth rates, estimated from biomass curves, as a function of succinic concentrations in the broth (succinic acid was used as a proxy variable). The resultant data cloud uncovered severe biomass growth inhibitions, with an eight-fold decrease in the specific biomass growth rate between succinic acid concentrations of 0 to 7 g L^{-1} (see Figure 2-5). Beyond succinic acid titres of 10 g L^{-1}, growth is negligible and subsequent

succinic acid production is maintenance driven [21]. Moreover, subsequent to growth termination, it is generally observed that byproduct formation decreases while succinic acid production continues unaffected. The changes in product selectivity are discussed in detail in Section 2.4.3.

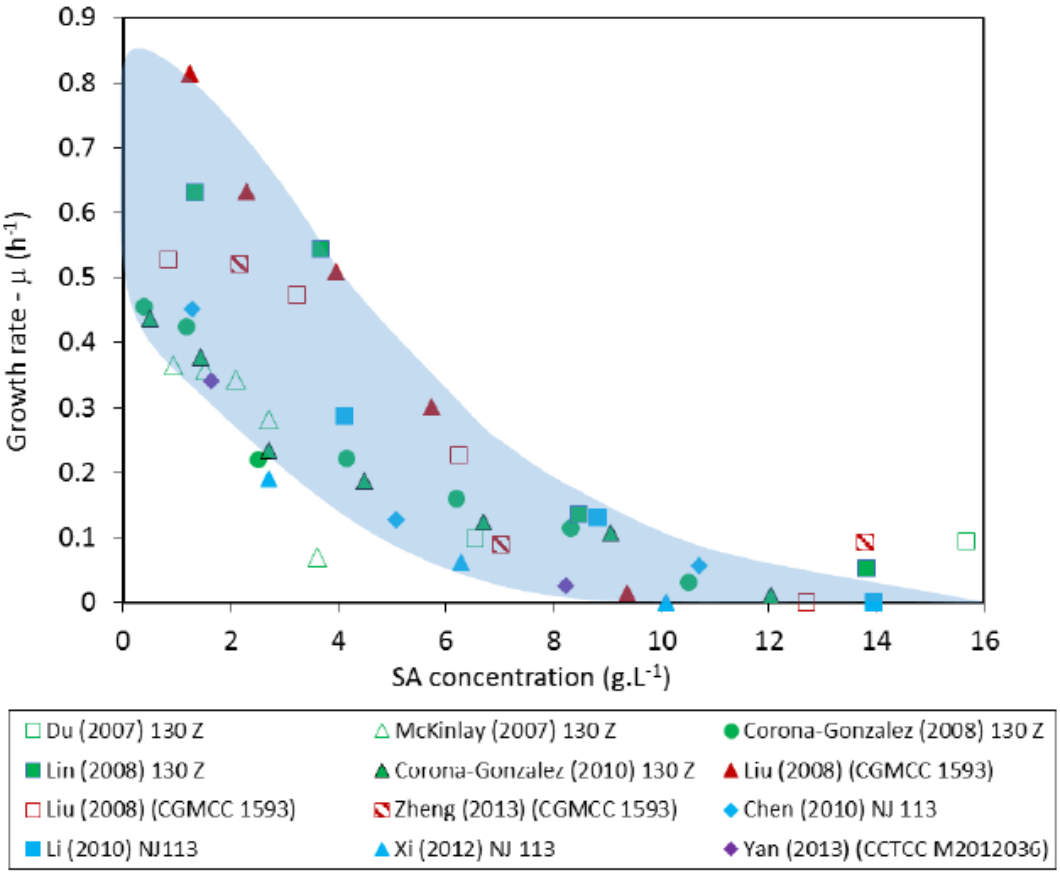

Figure 2-5: Specific cell growth rates of prominent batch studies as a function of SA titres, collated by Brink and Nicol [21]. Severe growth inhibition is shown with increasing SA titres and negligible growth is encountered beyond 10 g L^{-1} SA

Neutralising agents

Maintaining the ideal pH for fermentation requires constant neutralisation of the acid metabolites produced. Several neutralising agents, including $Ca(OH)_2$, NaOH, Na_2CO_3, $NaHCO_3$, $Mg(OH)_2$, KOH, $CaCO_3$ and $MgCO_3$, have been investigated for their efficacy in promoting growth and succinic acid production in *A. succinogenes* fermentation. Sodium-based neutralising agents were found to result in cell flocculation, whereas calcium-based agents caused growth inhibitions as well reduced succinic acid production [64]. Although the fluidity and permeability of the membrane requires the presence of Ca^{2+} ions for energy and transfer

regulation, their elevated levels are known to interfere with cell membrane regulation and acid accumulation [37]. In the same way, although low levels of sodium ions are critical for maintaining intracellular pH, at high levels they cause hyperosmotic stress [65]. Notable studies on neutralising agents [37] concluded that the use of $MgCO_3$ enhanced succinic acid production as well as cell growth (compared with NaOH). Moreover, cell flocculation was prevented when $MgCO_3$ was used in conjunction with NaOH. This is because the cation Mg^{2+} is known to be an important cofactor for the PEP carboxykinase enzyme, which catalyses the first step in the C_4 pathway. Furthermore, it does not cause flocculation as it is does not disrupt the stability of the membrane [64].

2.3.2 SA PRODUCTION FROM MODEL AND INDUSTRIAL FEEDSTOCKS

Table 2-3 shows the fermentation performance of batch studies of *A. succinogenes* on different pure carbohydrate sources. Studies on pure sugar substrate offer a fundamental understanding of the microorganism and its metabolic bottlenecks as pure substrates are free from inhibitors which may be found in industrially relevant streams. Due to the redox-consuming nature of the C_4 pathways through which succinic acid is produced, the use of highly reduced carbon substrates has resulted in higher yield, titre and productivities of SA as compared with the fermentation of less-reduced sugars [66]. To this end, other batch studies have demonstrated the advantage of an external supply of redox in enhancing succinic acid production by addition of H_2 or electrically reduced neutral red [67]. For free cell batch fermentation of wild-type strains, succinic acid titres ranged from 8.3 to 60 g L^{-1}, whereas yield on the carbon substrates reached as high as 0.83 g g^{-1}, while productivities ranged from as low as 0.5 to 2.16 g $L^{-1}h^{-1}$. The use of cell immobilisation greatly improves batch performance as can be seen from the results of Yan et al. [23], with high succinic acid titres of 98.7 g L^{-1} at a yield of 0.89 g g^{-1} and a productivity of 2.77 g $L^{-1}h^{-1}$. Moreover, cell immobilisation allows the strategy of reusing immobilised cells in repeat batches, thereby cutting downtime by avoiding the initial lag phase.

A significant portion of batch studies has focused on exploring the use of cheap and industrially relevant feedstocks for succinic acid production. This is an important undertaking considering the economic feasibility of the biobased succinic acid process. These feedstocks mostly include agricultural residues (e.g. sugarcane bagasse, carob pods, corncob, cotton stalk and corn stalk) and industrial waste streams and byproduct streams (e.g. crude glycerol, sugarcane molasses, sake lees and cheese whey). In a biorefinery context, these feedstocks will first undergo pretreatment to deconstruct the biomass in order to make the sugars accessible to the biocatalyst

for conversion – this is a crucial and often costly step [68]. In most studies the dilute acid and hydrothermal hydrolysis are preferred methods for biomass deconstruction and are currently finding commercial application in the lignocellulosic bioethanol plants. However, microbial inhibitors, such as furfural, hydroxymethylfurfural, acetic acid and low molecular weight phenolics, are often introduced during pretreatments of lignocellulosic biomass and as such duly hamper the fermentation performance [69].

The fermentation performance of *A. succinogenes* on industrial feedstocks is comparable to that on pure sugars with regard to reported SA yields and titres (see Table 2-4). However, the reported productivities can still be improved. Shen at al. [15] achieved high succinic acid titres of 75 g L^{-1} by fermenting duckweed hydrolysate, with a yield of 0.9 g g^{-1} and a productivity of 1.35 g L^{-1} h^{-1}. The fermented duckweed hydrolysate was not detoxified to remove microbial inhibitors which were reported to be present in the hydrolysate. Moreover, in the study by Salvachúa et. al [26] *A. succinogenes* was shown to metabolise furfural and hydroxymethylfurfural microbial inhibitors into furfuryl alcohol and hydromethylfurfuryl alcohol during fermentation, subsequent to which substrate consumption rates improved. This demonstrates the robustness of *A. succinogenes* and thus its industrial promise. Nonetheless, both Salvachúa et. al [26] and Chen et. al [70] reported significant improvements in SA productivity after detoxification of feedstocks, and thus the productivity improvements gained by adding a detoxifying step must be weighed against the required capital and processing costs. Even so, the ability of *A. succinogenes* to perform competitively on industrially relevant feedstocks is encouraging.

Table 2-3: Succinic acid batch production studies on pure carbon substrates

Substrate	Strain	Mode	SA titre ($g\ L^{-1}$)	Yield ($g\ g^{-1}$)	Productivity ($g\ L^{-1}\ h^{-1}$)	Reference
Sorbitol	NJ113	Batch (free)	29.8	0.75	2.13	[66]
Fructose	CGMCC1593	Batch (free)	38.4	0.79	0.64	[71]
Xylose	CGMCC1593	Batch (free)	32.6	0.77	0.54	[71]
Sucrose	NJ113	Fed-batch (free)	60.5	0.83	2.16	[72]
Glucose	130Z	Batch (free)	39	0.79	0.49	[25]
Glucose	CCTCC M2012036	Fed-batch (Immobilised)	98.7	0.89	2.77	[23]
Lactose	CGMCC 1593	Batch (free)	40.1	0.81	0.67	[71]
Cellobiose	NJ113	Batch (free)	38.9	0.66	1.08	[73]
Maltose	CGMCC 1593	Batch (free)	38.8	0.8	0.65	[71]
Glycerol	130Z	Fed-batch (free)	49.6	0.64	0.96	[74]
Gluconate	NJ113	Batch (free)	8.3	0.54	0.59	[66]

Table 2-4: Major fermentation studies on industrially relevant feedstocks by *A. succinogenes*

Feedstock	Strain	Main sugars	Mode	SA titre ($g\ L^{-1}$)	Yield ($g\ g^{-1}$)	Productivity ($g\ L^{-1}\ h^{-1}$)	Reference
Cane molasses	130Z	Sucrose, glucose, fructose	Batch	45.6	0.76	1.27	[75]
Carob pods	130Z	Sucrose, glucose, fructose	Batch	18.9	0.94	0.66	[76]
Corn fibre hydrolysate	NJ113	Glucose, xylose, arabinose	Batch	35.4	0.73	0.98	[77]
Sake lees hydrolysate	130Z	Glucose (reported)	Batch	48	0.75	0.94	[78]
Rapeseed meal	130Z	Glucose, fructose arabinose	Batch	15.5	0.6	0.31	[79]
Straw hydrolysate	CGM CC1593	Glucose, xylose	Fed-batch	53.2	0.83	1.21	[27]
Jerusalem artichoke hydrolysate	130Z	Glucose, fructose	Batch	47.9	0.74	0.99	[80]
Cotton stalk hydrolysate	BE-1	Glucose, xylose, cellobiose	Batch	15.8	1.23	0.62	[81]
Lignocellulosic hydrolysate	NJ113	Xylose, glucose, mannose, arabinose	Fed-batch	67.5	0.73	1.41	[82]
Palm oil	130Z	Glucose, xylose	Batch	23.5	0.33	0.62	[83]
Sugarcane juice	GXA5 137	Glucose, sucrose	Batch	62.1	-	1.29	[84]
Duckweed hydrolysate	GXA5 137	Glucose, xylose, arabinose, galactose	Fed-batch	75.46	0.83	1.35	[15]
Cheese whey	130Z	Lactose	Batch	21.1	0.57	0.44	[85]
Sugarcane bagasse hydrolysate	CIP10 6512	Glucose, xylose	Batch	22.5	0.43	1.01	[86]
Corncob hydrolysate		Xylose, glucose, arabinose	Batch	23.6	0.58	0.49	[87]

2.4 CONTINUOUS PRODUCTION STUDIES

As discussed in Section 2.3, most fermentation studies on *A. succinogenes* have been performed in batch mode, but lately continuous fermentation studies have been gaining attraction. Commodity chemicals such as succinic acid necessitate the production of large volumes of the product. In this respect, continuous fermentation offers the advantage of attaining high productivities (as has been demonstrated for commercial bioethanol and lactic acid bioproduction) [88], consistent product quality compared with batch studies, as well as reduced labour and capital costs. On the other hand, continuous fermentation has disadvantages such as high risk of contamination (due to the open system nature of continuous fermentation), low metabolite titres which increase separation costs, and incomplete substrate consumption. All these trade-offs must be considered for the development of a bulk production process.

A. succinogenes readily and unavoidably self-adheres to available surfaces in the bioreactor to form biofilms in continuous fermentations [20, 89]. Generally, biofilms consist of a structured community of microbial cells embedded in a gel-like matrix of extracellular polymeric substances (EPS) and are often found adhering to surfaces or existing as flocs. Cell concentrations in biofilms become significantly higher than can be attained in suspended cell mode (without using cell-retainment equipment), and consequently this boosts fermentation productivities. Despite the improvement in productivities, the EPS matrix of the biofilm confers on it many beneficial attributes, such as sustained long-term activity and an enhanced tolerance to otherwise toxic environments [90]. The aforementioned properties are indeed ideal for continuous bulk processing where the stability of the biocatalyst is of utmost importance. The suitability of biofilm reactors for specialty and bulk chemical production is reviewed in detail elsewhere [91–93].

2.4.1 BIOFILM GROWTH, STABILITY AND ACTIVITY

The initial phase of any continuous biofilm fermentation is the development of biofilm on the available support in the fermenter prior to switching to a production phase at an ideal dilution rate. Van Heerden and Nicol [89] noted that biofilm development, using Genulite™ packing as support, was rapid at high dilution rates (above 0.35 h^{-1}) which corresponded to low product concentrations in the fermenter. Ultimately, Van Heerden and Nicol [89], using succinic acid concentration as a marker, concluded that above succinic acid concentrations of 10 g L^{-1} there were no observable increases in biofilm formation (i.e. growth halted). Maharaj et al. [20]

further investigated the steady state, stability and reproducibility of biofilm fermentation. The observations of Van Heerden and Nicol [89] were confirmed as rapid biofilm formation was observed at high dilution rates. However, it was difficult to maintain steady-state conditions as the excessive growth resulted in biofilm shedding/sloughing events. followed by regrowth, and thus ultimately caused oscillatory behaviour. Finally, Maharaj et al. [20] concluded that the extent of biofilm growth rate at steady state, which increases with increasing dilution rate, causes instability in the attached biofilm by resulting in sloughing events of significant amounts of biomass; this was more evident at dilution rates of 0.32 h^{-1} and above, whereas below these dilution rates steady-state conditions were maintained for longer periods (more than 72 h).

Regarding biofilm activity, the study by Maharaj et al. [20] showed that specific succinic acid productivities (mass-based SA productivity) decreased with increasing succinic acid titres. To explain this behaviour, it was suggested that either the fraction of metabolically active cells within the biofilm decreased with increasing succinic acid titres as conditions would be increasingly hostile, or that the fraction of cellular material in the biofilm decreased with increased SA titres since biomass composition was not quantified. In a novel homogenous shear biofilm reactor, Brink and Nicol [21] obtained the same results of decreasing succinic acid mass-based productivities, although only the cellular biomass of the biofilm was considered as biofilm composition was quantified. This observation discounted changes in the biofilm composition as the reason for the reported decline in mass-based productivities and suggested that cell death was most probably the cause. Chapter 3 in this study explores these observations by cultivating biofilms in controlled conditions of high succinic acid titres (above 10 g L^{-1} SA) and low succinic acid titres (below 10 g L^{-1} SA) in order to ascribe the impact of product accumulation conditions to both the structure of developed biofilms and their activity, both visually and quantitatively.

Table 2-5: Performance of continuous fermentation studies by *A. succinogenes* under steady-state conditions

Strain	Substrate	Mode	Titre ($g\ L^{-1}$)	Yield ($g\ g^{-1}$)	Productivity ($g\ L^{-1}\ h^{-1}$)	Biomass concentration ($g\ L^{-1}$)	Longest operation	Reference
130Z	Glucose	Continuous; chemostat	7.1	0.61	1.83	2.65	-	[21]
130Z	Glucose	Continuous; biofilm	18.1	0.75	17.1	28.9	-	[21]
130Z	Glucose	Continuous; biofilm	17.6	0.7	15.2	24.4	-	[94]
130Z	Glucose	Continuous; biofilm	48.5	0.91	9.4	-	50 days 15 h	[22]
130Z	Glucose	Continuous; biofilm	32.5	0.9	10.8	27.9	45 days 12 h	[20]
130Z	Glucose	Continuous; biofilm	12.7	0.57	1.7	-	44 days 23 h	[95]
CCTCC M2012036	Glucose	Continuous; biofilm	55.3	0.8	2.77	-	18 days	[96]
130Z	Glucose	Continuous; biofilm	43	1.09	35	-	5 months	[16]
130Z	Xylose hydrolysate	Continuous; biofilm	39.6	0.78	1.77	-	64 days 14 h	[24]
130Z	xylose	Continuous; biofilm	29.4	0.68	3.4	-	32 days	[97]
130Z	Glucose	Continuous; biofilm	10.4	0.72	2.08	-	-	[25]
130Z	Glucose	Continuous; biofilm	13.4	0.5	6.63	-	-	[98]
130Z	Glucose	Continuous; biofilm	11.3	0.69	6.35	-	78 h	[89]

2.4.2 FERMENTATION PERFORMANCE

Table 2-5 summarises the performance of continuous fermentation studies. The succinic acid titres achieved in continuous studies are relatively lower than in batch studies, but the productivities attained in continuous studies are an order of magnitude higher. Because biomass is immobilised in biofilm mode, high dilution rates can be used without cell washout, hence the high productivities attained. High succinic acid titres can be obtained in continuous operation at low dilution rates; however, this results in low productivities and thus there are trade-offs. Ferone et al. [16] achieved productivities as high as 35 g L^{-1} h^{-1} at a dilution rate of 1.9 h^{-1} in a packed bed biofilm reactor with Tygon support. Brink & Nicol [21] employed a novel shear-controlled reactor to compare chemostat operation with biofilm fermentation. It was found that biofilm operation outperformed chemostat operation with regard to yield (0.48 vs 0.74 g g^{-1}), titre (7.1 vs 18.1 g L^{-1}) and productivity (1.83 vs 17.1 g L^{-1} h^{-1}). This was due primarily to the high biomass concentrations achieved in biofilm fermentation (27.4 g L^{-1}) compared with chemostat runs (2.65 g L^{-1}), further accentuating the advantages of biofilm operation.

2.4.3 METABOLIC FLUX DISTRIBUTION

It has been noted that under biofilm conditions *A. succinogenes* shows a unique metabolic behaviour that favours the production of succinic acid. In a study by Bradfield and Nicol [22] biofilms of *A. succinogenes,* immobilised on stainless-steel wool, exhibited increasing distribution of carbon flux towards succinic acid at increasing succinic acid titres (increasing glucose consumption) with a concomitant reduction in by-product formation. This was also observed when xylose was used as the carbon substrate [97]. In this way, both the SA yield and selectivity increased with increasing succinic acid titres. The reported ratio of SA to acetic acid increased from 2.4 g g^{-1} to 5.7 g g^{-1}, which corresponded to a shift in the ratio of formic acid to acetic of 0.77 g g^{-1} to 0 g g^{-1}. The mass ratio changes indicated a metabolic shift from the PFL route to the PDH/FDH route of acetic acid production at the pyruvate node. This affords the C_4 pathways more redox power, hence the increase in succinate yield and selectivity. The study by Maharaj et al. [20] also demonstrated the same metabolic behaviour of *A. succinogenes* under biofilm conditions, although biofilm was immobilized on Poraver® beads.

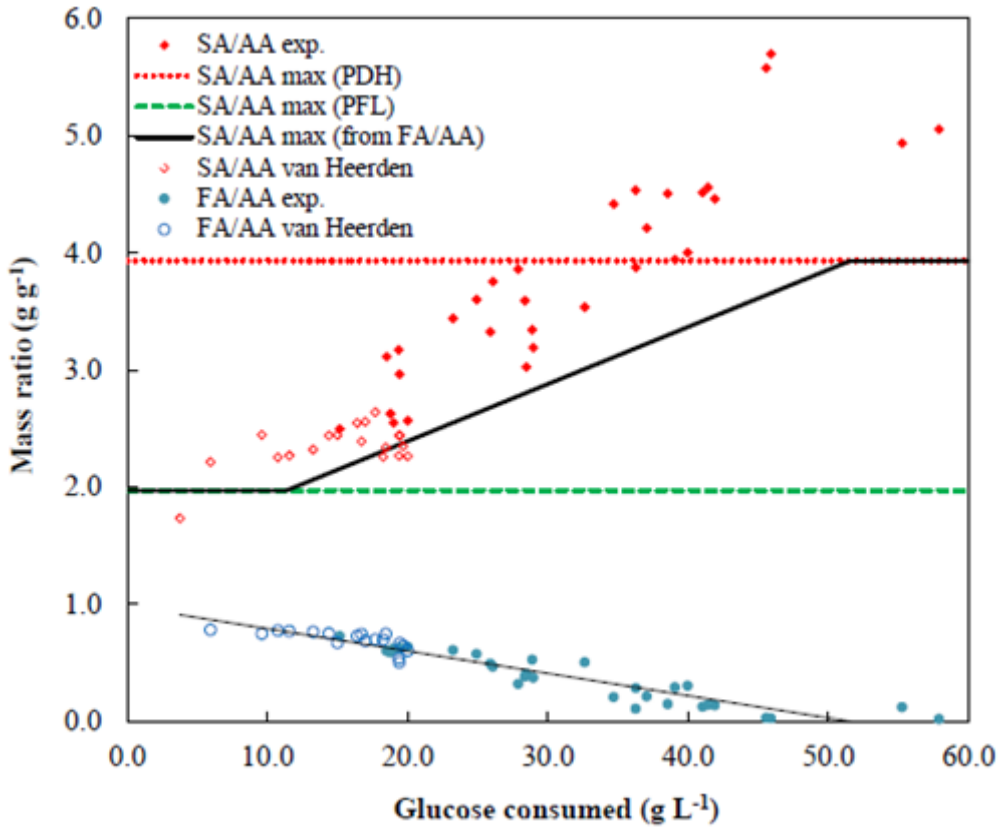

Figure 2-6: Increased succinic acid production with increasing glucose consumption showing a shift in the flux distribution which favours succinic acid selectivity (Source: Bradfield & Nicol [22])

The high SA selectivity noted in the study by Bradfield and Nicol [22] exceeded the theoretical limit of 3.93 g g^{-1} assuming a redox balanced system, and thus the results indicated an additional unknown redox source. Reaching pseudo-steady-state conditions in continuous fermentation allows the analysis of redox balances since cellular metabolic fluxes presumably also reach pseudo-steady-state conditions, which means that there should be no net redox generation or consumption in these conditions. Further studies by Bradfield and Nicol [99] demonstrated that the OPPP pathway supplied additional redox power, which partly helped to explain the high selectivity for SA. The redox power generated by the OPPP pathway is in the form of NADPH and it is assumed that it is readily converted to NADH by the transhydrogenase enzyme to make it available for catabolic functions. The OPPP activity was also shown to increase with increasing SA titres; in this way more redox was supplied by OPPP at high succinic acid concentrations. This propensity of *A. succinogenes* to produce succinic acid at yields and

selectivity beyond its set metabolic limit makes it desirable as a potential biocatalyst for industrial-scale succinic acid production.

2.5 BACKGROUND ON BIOFILMS

Given the importance of biofilm operation in the succinic acid production process of the bovine rumen bacterium *Actinobacillus succinogenes*, this section provides a brief background on biofilms in general as a basis for the ensuing study of *A. succinogenes* biofilms.

Biofilms epitomise the most successful mode of bacterial life. Although bacteria have mostly been studied as free-flowing cells in suspension (planktonic cells), they grow predominantly as sessile communities known as biofilms. Certainly, more than 99% of microbes in nature are estimated to exist as biofilms [100–102]. Costerton [103] describes biofilms as "a structured community of cells (mixed or pure species) embedded in a self-produced matrix of extracellular polymeric substances (EPS) adherent to inert or living surfaces". They may form as communities that are surface attached or as flocs, which are mobile biofilms that form in the absence of any substratum [104]. Biofilm bacteria constitute a coordinated functional community that is more efficient than floating planktonic cells, made possible by the physiological cooperativity of bacterial cells in stable juxtaposition with cells of the same species [105]. Indeed, biofilm thicknesses may vary from as small as a few microns to a few centimetres.

It is the gel-like EPS matrix – also known as the slime – that confers on the biofilm mode many desirable characteristics that are not obtainable in planktonic form. The highly hydrated EPS matrix can reportedly account for up 90% of the dry biomass weight [104]. The EPS matrix consists of an assembly of different types of biopolymer which form the support for the three-dimensional biofilm morphology, and it is reportedly responsible for the adhesion to surfaces and for the cohesiveness of the biofilm [106]. Constituents such as polysaccharides, proteins, external DNA, humic substances and lipids are commonly found in the EPS matrix of most biofilms [106]. However, among these, the extracellular polysaccharides and proteins have been shown to be key components of the biofilm [104]. Collectively, the EPS matrix protects the biofilm from desiccation, grants biofilm cells enhanced tolerance against antimicrobial agents, and acts as a sorbent for nutrients in the liquid phase [104, 106]. Moreover, because the matrix immobilises cells, it allows for synergistic interactions and processes such as horizontal gene transfer. Flemming and Wingender [104, 106] provide a detailed discourse on biofilms [104]

and on the role of the EPS matrix [106]. In summary, the biofilm mode of life provides bacterial cells with emergent characteristics which are superior to those of the suspended mode of life.

Biofilm applications

It must be noted that because of their robustness, their long-term stability and their resistance to toxic environments, biofilms have also been a source of deleterious effects in several industries. In medicine, biofilms cause problems due to their enhanced resistance to treatment by antimicrobial agents, causing infections due to attachment to medicinal equipment such as syringes. Biofilms have also served as sources of industrial biofouling as they are involved in microbially influenced corrosion and biodeterioration of heat exchanger equipment, synthetic polymers, wood and wine materials, among others [107]. On the other hand, the qualities of biofilms have been exploited in various bioprocessing industries.

1. Biofilms are increasingly finding application in bioremediation, whether in soil, subsurface or water media. Although suspended cells can also metabolise pollutants for bioremediation, their survival in polluted environments is less likely due to decreased protection in comparison with matrix-encased biofilm cells [102, 108, 109]. Moreover, the diversity of species that can be harbored in biofilms allows them to complement one another metabolically, thereby giving them the ability to survive in varying nutrient conditions [109].
2. In water and wastewater treatment, various biofilm reactor systems such as rotating biological contactors [110], trickling filters [111] and membrane biofilm reactors [112] find common use. The enhanced biological stability, increased cell concentrations and tolerance to toxic conditions of these biofilm operations mean that these systems often operate for months on end, something that would be hard to come by in suspended cell mode operation.
3. Several review papers have emphasised the potential of single-culture biofilm reactors to produce speciality and bulk chemicals via fermentation and biosynthesis [91–93]. For this purpose, the self-immobilising nature of biofilms is instrumental in obtaining high productivities as a result of high cell density fermentation.

2.5.1 BIOFILM FORMATION AND STRUCTURES

Biofilm formation follows a sequence of events that are characteristically similar for different microorganisms [113, 114]. Initially, suspended cells in the bulk phase are transported to the substratum surface by either diffusion, convection or self-motility, and there they form a weak, reversible adhesion with the surface of the substratum [115]. The initial stage of reversible adhesion is affected by factors such as surface roughness and charge, hydrophilic interactions, as well as the shear environment. It is reported that while adhesion is close to the substratum surface, strong adhesion forces trigger a phenotypic change to a biofilm state – it is this change to a biofilm state that initiates the second stage of biofilm development [115]. Following initial reversible adhesion, bacteria on the substratum surface begin to condition the surface by molecular interactions between the cell and the surface. Subsequently, polymeric substances (such as the EPS matrix) and protein structures are produced on the outside of the cell membrane, which ultimately renders the cell irreversibly attached to the substratum surface. Consequent to irreversible surface colonisation, a biofilm maturation stage ensues which is characterised by an extensive increase in cell density, EPS production and the development of complex biofilm structures. The maturation phase is succeeded by a stage in which sessile cells disperse to recolonise other surfaces; this can occur through various mechanisms, such as by detachment of biofilm clumps, or by "swarming or seeding" where the inner part of the biofilm "liquifies", thereby allowing cells to swim out and recolonise new surfaces [116].

The resultant biofilm structures formed are dictated by a combination of various factors which can be extrinsic or intrinsic. These factors include nutrient availability, the growth rates of microorganisms, hydrodynamic shear forces, adhesive capabilities, and/or environmental conditions (e.g. temperature and pH), among others [117]. According to the literature, biofilm structures can be classified as either structured, flat or a combination of the two [118]. Structured biofilms are those consisting of an interspersed cluster of cell microcolonies with a thin layer of cells evenly distributed on the substratum surface. In this heterogeneous structure, water channels can be formed within the biofilm by the coalescing of closely spaced cell clusters, and these channels assist in the convectional transport of nutrients and metabolite [103]. The shape of cell microcolonies may be mushroom-like structures, filamentous streamers or pillar-like structures [103]. Conversely, flat biofilms are homogenous and without any of the macroscopic structural characteristics observed in structured biofilms, such as protrusions of cell microcolonies and water channels. These resemble the biofilm structures often encountered

in dental plaque [119] and river water biofilms. Lastly, the biofilm morphology that resembles a combination of both structures consists of a basal layer of a dense biofilm with a dispersion of microcolony protrusions that are spread apart.

2.5.2 BIOFILM VISUALISATION AND MEASUREMENT TECHNIQUES

Various microscopic visualisation techniques have been used to study biofilms. These include atomic force microscopy, electron microscopy, confocal scanning laser microscopy (CSLM) and light microscopy. Together these microscopic visualisation techniques have contributed to the current understanding of biofilms as no single technique gives a complete picture of the biofilm. Nonetheless, it is the confocal scanning laser microscope technique that is commonly used by researchers to study biofilms, mainly due to the advantages it offers. This study also primarily used the CLSM for biofilm visualisation.

Confocal scanning laser microscope

The CSLM technique was developed to overcome the challenges of out-of-focus blur encountered in conventional light and fluorescence microscopy. In fluorescence microscopy, 2D images may contain as much as 90% of fluorescence from out-of-focus planes which obscure fluorescence from the focused planes [120]. This out-of-focus blur seriously degrades the image by reducing its sharpness and contrast. Confocal microscopy eliminates background information using point illumination and the placing of a detector pinhole in an optically conjugate plane. In this way, light emanating from out-of-focus planes is rejected by the detector pinhole, which only allows light very close to the point source. CSLM is thus capable of extracting optical sections of specimens without background halos and scatter information, offering improved resolution in the axial and lateral directions as compared with conventional light and fluorescence microscopy [121, 122]. In this way it allows a non-destructive, in situ and accurate examination of the internal detail of fully hydrated biofilms, without the use of harsh chemical fixations and embedding techniques. Coupled with computerised control of the microscope stage in the z direction, a series of digital xy optical sections (a z-stack) can be automatically collected and processed to build a 3D reconstruction of the biofilm. Thus, CSLM allows a four-dimensional (4D) analysis of biofilms (x, y, z, t). Moreover, its episcopic nature allows examination of biofilms cultivated on various non-transparent substrates, thereby broadening the types of analysis that can be performed [123].

The use of CSLM in biofilm studies has significantly advanced the understanding of biofilms [124]. Through CSLM, the general biofilm structure (architecture) with voids and 3D surface topographies can be visualised, showing different morphological structures. Moreover, the distribution of the EPS matrix within biofilms, as well as the identity of the matrix constituents, have been studied with CSLM [124] by the use of EPS staining, and external DNA fluorescent stains. The process of biofilm development can be studied by semi-continuously imaging the temporal changes, from inoculation to maturation, of the biofilm grown in flow cell reactors in CSLM. Moreover, cell activity and overall biofilm activity can also be studied using various Live/Dead bacterial viability staining kits. Environments that exist in the biofilm have been visualised with CSLM using environmentally and chemically sensitive fluorophores, revealing pH gradients, nutrient gradients and metabolite gradients within the biofilm [124]. These capabilities have been brought about using CSLM along with sensors that can extract structural aspects, chemical cues and diffusivity. In this study biofilm structural aspects were investigated by using the DNA staining fluorophores SYTO™ 9 and propidium iodide. These stains are also used to reveal cell activity within the biofilm.

Because CLSM produces accurate images by excluding out-of-focus blur, the digital images it produces are often used in the quantitative analysis of biofilms through image-processing software, enabling the computing of biofilm descriptive parameters such as maximum thickness, thickness distribution and area coverage. The quantification of biofilm descriptive parameters removes subjective analysis of the images based on visual inspection and allows the comparison of research findings by other researchers. In this respect, Kober et al. [125] described a method that determines the minimum sampled biofilm area that would be representative of the biofilm when doing quantitative analysis. Determination of this area ensures that the conclusions arrived have been based on the analysis of enough area that is representative of the biofilm being investigated.

3 THE EFFECT OF PRODUCT ACCUMULATION ON BIOFILM MORPHOLOGY AND PHYSIOLOGY

3.1 BACKGROUND

High cell density fermentation is crucial for obtaining high volumetric productivities and is especially important for the production of bulk chemicals as they require large volumes due to demand. Various cell retention strategies have been employed in efforts to increase cell concentrations in bioreactors. However, these add considerably to processing costs and cause clogging problems. It is in this context that the bovine rumen bacterium *A. succinogenes* is ideal as it is known to self-immobilise readily and unavoidably to available surfaces to form biofilms [20, 89], thereby attaining high cell densities and subsequently increased volumetric productivities. Biofilm fermentation is a key requisite for the successful bulk production of succinic acid by *A. succinogenes*. Although the literature shows that numerous biofilm fermentation studies on *A. succinogenes* have been performed, these have mostly focused on the productive aspects of the biofilm and have neglected characterisation of the biofilm properties and its physiology as dictated by fermenter conditions. Since it is optimistically assumed that the *A. succinogenes* biofilm process will eventually be commercialised, it is imperative that it is understood how best to develop the biofilm and to have insight into how the biofilm biocatalyst is affected by various fermentation conditions, particularly in terms of its stability and activity. This entails a microscopic-level investigation of the biofilm structure and the activity of cells embedded within its matrix, as related to changing conditions in the bioreactor.

The extent of product accumulation in the bioreactor has been shown to affect the rate of biofilm development and cell growth (Sections 2.3.1 and 2.4.1) and subsequently the stability of the developed biofilms. Rapid biofilm formation is reported in low product accumulation (LPA) conditions, marked as below 10 g L^{-1} of SA by Van Heerden and Nicol [89], whereas slowed biofilm formation is witnessed in high product accumulation (HPA) conditions (above 10 g L^{-1} of SA). In addition, the specific cell-based productivity of biofilms is reported to decrease

with increasing product accumulation. Thus, there exists an incontestable interaction between the biofilm and product accumulation conditions in the bioreactor.

This chapter investigates how the accumulation of metabolite products in *A. succinogenes* continuous fermentation interacts with the biofilm on the basis of its development, structure and viability (embedded cell activity) in its early-stage development and within the two regimes of LPA and HPA conditions. A novel biofilm bioreactor was constructed which allows cultivation of biofilm on 12 sample probes that can be aseptically inserted and sampled individually in the reactor space. Biofilm is thus cultivated in controlled conditions of LPA (below 10 g L^{-1} of SA) and HPA (above 10 g L^{-1} of SA), microscopically visualised under a CSLM and further analysed with image processing software to give objective quantitative data relating to its structure and viability. Most of the content in this chapter formed part of the work published by Mokwatlo et al. in *Applied Microbiology and Biotechnology* [126] and a minor portion of the work was published by Mokwatlo and Nicol in *Biochemical Engineering Journal* [127].

3.2 EXPERIMENTAL

3.2.1 THE BIOFILM CULTIVATION REACTOR

A novel custom-designed bioreactor suitable for sterile and multiple biofilm sampling was used. The bioreactor consisted of a middle section of a hollow aluminium cylinder which housed twelve slots, three on each of the four sides, within which cylindrical aluminium rods carrying the biofilm sample coupon could be inserted. Each sample probe rod carried two sample coupons (refer to Figure 3-1). Two 13 mm diameter Thermanox coverslips (Thermo Fisher Scientific, Massachusetts, USA) were temporarily affixed to each sampling probe prior to each run. The top and bottom of the middle hollow aluminium section were connected to a cylindrical glass, which allowed for an aluminium head and an aluminium base to encase it. The aluminium head was fitted at the centre with a shaft holding a Rushton 6 blade impeller for mixing within the bioreactor using an overhead stirrer. Four wooden sticks covered with mutton cloth were reversibly attached to the aluminium reactor base to provide an attachment surface for sufficient and stable biofilm growth within the main fermenter body, only for biofilm cultivation in HPA conditions. An external recycle line was added to the reactor (from reactor head to reactor base) to facilitate measurement of temperature and pH through an in-line aluminium probe holder (Figure 3-2).

The total working volume of the fermenter was 3 000 mL and it was maintained by means of an overflow tube (in the fermenter) connected to the exit pump. Temperature and pH were controlled at 37.0 ± 0.1 °C and 6.80 ± 0.01 respectively. A Liquiline CM442 (Endress+Hauser, Gerlingen, Germany) coupled to a Ceragel CPS71D glass electrode (Endress+Hauser, Gerlingen, Germany) measured both temperature and pH and also controlled pH through on/off dosing of 10 M NaOH by using an internal relay. Temperature was controlled by a feedback PID controller, custom developed in Labview. All gas vents and inlets were fitted with 0.2 µm PTFE membrane filters (Midisart 2000, Sartorius, Göttingen, Germany) to ensure sterility. Mixing in the bioreactor was kept at 300 rpm using a Rushton 6 blade impeller connected to an overhead stirrer. CO_2 flow to the reactor was controlled at 0.1 vvm using a Brooks 5850S mass controller with a maximum flow output of 500 mL min^{-1}. Both CO_2 and NaOH were added to the reactor via the external recycle line. Foaming in the bioreactor was controlled by addition of 10% (v/v) Antifoam SE-15 (Sigma-Aldrich, Germany) solution directly onto the foam formation in a dropwise fashion.

3.2.2 MICROORGANISM AND FERMENTATION MEDIA

Wild-type *Actinobacillus succinogenes* 130Z (DSM No. 22257; ATCC No. 55618) was acquired from the German Collection of Microorganisms and Cell Cultures (Braunschweig, Germany). Stock cultures (1.5 mL) were stored at -40 °C in 66% v/v glycerol solutions. Inoculum was prepared by transferring a stock culture to 100 mL of sterilised tryptone soy broth, which was then incubated at 37 °C and 120 rpm for 16−24 h. High-performance liquid chromatography (HPLC) was used to determine the purity and viability of the inoculum by checking for consistent metabolite distribution prior to inoculation of the system. The presence of ethanol and lactic acid in the inoculum indicated contamination of the inoculum.

The composition of the fermentation medium used was based on that of Bradfield & Nicol [22]. All chemicals were obtained from Merck KGaA (Darmstadt, Germany) unless otherwise stated. The medium was made up of three parts: the nutrient and salts solution, a phosphate buffer and the glucose solution. The nutrient and salt solution was composed of: 10.0 g L^{-1} of clarified corn steep liquor (Sigma-Aldrich, St. Louis, USA), 6.0 g L^{-1} yeast extract, 0.5 g L^{-1} NaCl, 0.2 g L^{-1} $MgCl_2 \cdot 6H_2O$, 0.2 g L^{-1} $CaCl_2 \cdot 2H_2O$ and 10 mL L^{-1} antifoam SE-15 (Sigma-Aldrich, Germany). The phosphate buffer consisted of 3.2 g L^{-1} KH_2PO_4 and 1.6 g L^{-1} K_2HPO_4. The

glucose concentration was kept at 60 g L^{-1}. CO_2 (Afrox, South Africa) was fed to the fermenters at 0.1 vvm.

1. Peristaltic pump
2. Antifoam reservoir
3. NaOH reservoir
4. CO_2 cylinder
5. Feed reservoir
6. Phosphate buffer bottle
7. Glucose bottle
8. Foam trap
9. Product reservoir
10. CO_2 line
11. Signal line
12. Mass flow controller
13. pH and temperature probe
14. DAQ/PC control unit
15. Hot plate
16. Biofilm sample probe
17. Reactor body
18. Overhead stirrer
19. Gas filter
20. Fresh feed transfer couple
21. Stream line

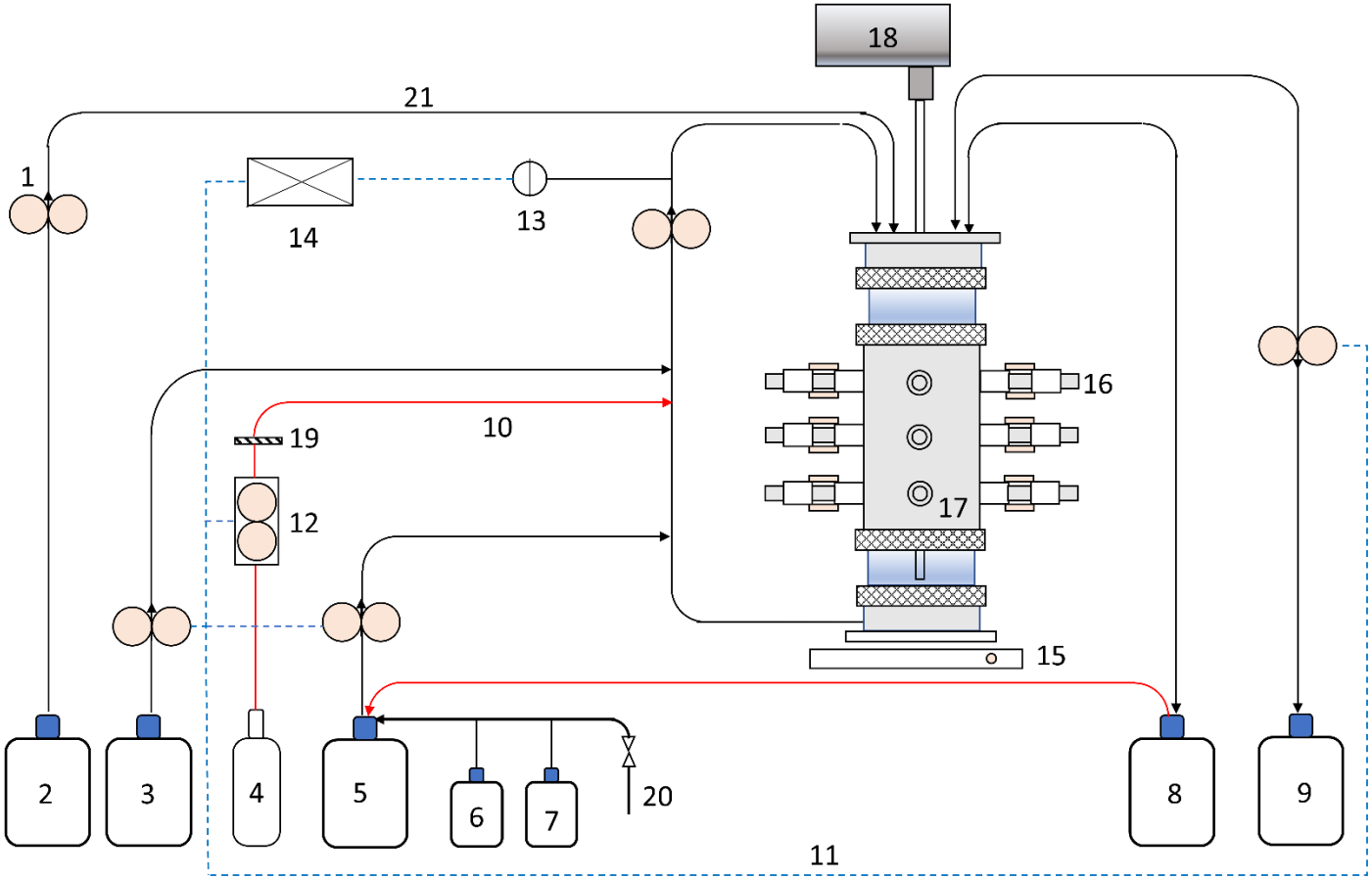

Figure 3-1: Diagrammatic representation of the experimental setup used for continuous biofilm cultivation (not to scale)

Figure 3-2: Photo of the novel biofilm cultivation bioreactor suitable for multiple sterile biofilm sampling on separate events

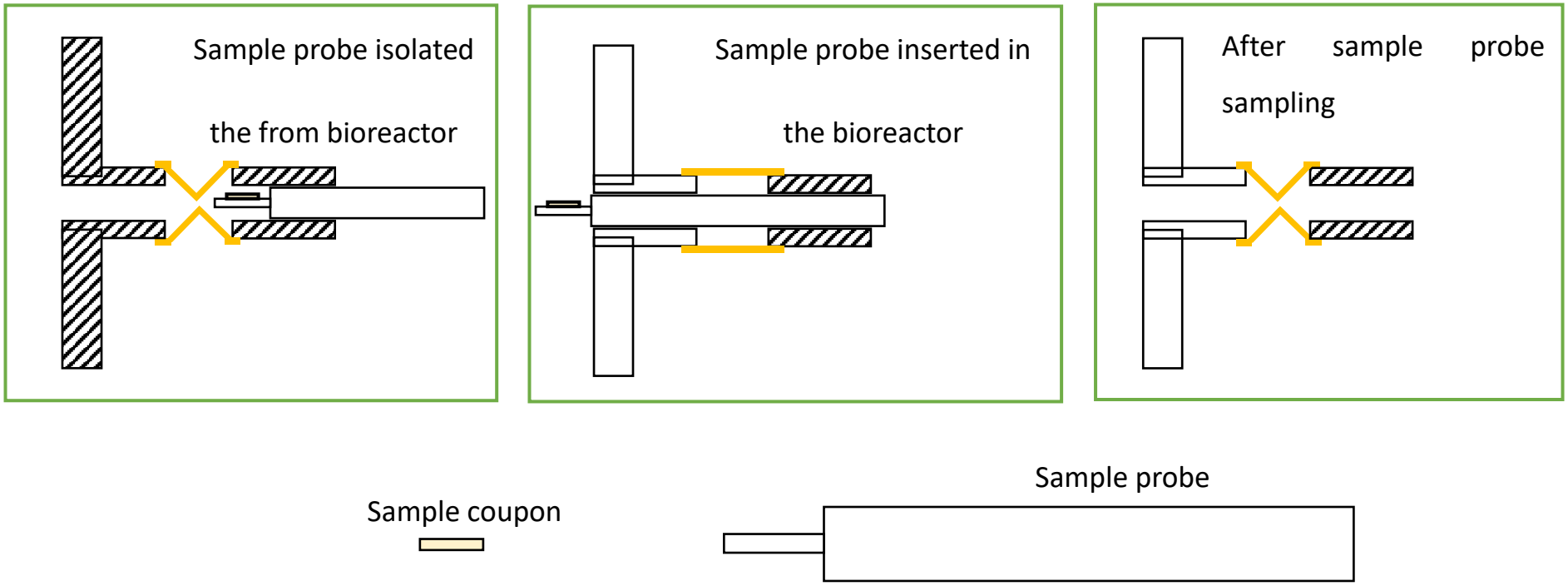

Figure 3-3: Diagrammatic representation of the novel sterile biofilm sampling process using a biofilm probe and a sampling chamber

3.2.3 BIOFILM CULTIVATION

The entire experimental setup was autoclaved at 121 °C for 60 min, excluding the NaOH reservoir. Prior to inoculation, the setup was left to run for a day to confirm sterility. Sample probes were inserted into their slots but isolated from the fermenting medium by clamping the silicon section of the isolation chambers (see Figure 3-3). Sample probes were fully slotted into the bioreactor, aseptically, once the desired acid titre conditions were reached for biofilm cultivation. The bioreactor was operated in batch mode after inoculation (~100 mL inoculum volume). Acid concentrations were monitored during this batch mode and a switch to continuous operation was made at the desired acid titres. A switch to continuous mode was made at 21 g L^{-1} SA for biofilm cultivation in HPA conditions, and a dilution rate of 0.05 h^{-1} was subsequently maintained throughout the run. The sample probes were fully slotted into the bioreactor immediately after switching to continuous mode. Figure 3-4 shows the metabolite titre profiles for the two experiments performed where the biofilm was cultivated in both HPA and LPA conditions. As it was expected that growth would be slow for biofilm cultivation in HPA conditions, biofilm sampling was performed on days 1, 3 and 5 (counting from the day the sample probes were inserted) to extend the period of growth. For biofilm cultivation in LPA conditions a switch to continuous mode was made at 8 g L^{-1} SA titre, and a high dilution rate of 0.3 h^{-1} was maintained. Biofilm sampling was performed on days 1, 2, 3 and 4 as rapid growth of biofilm was anticipated in LPA conditions. In the results section where constant reference to LPA and HPA conditions is made, it should be noted that this refers to the metabolite growth conditions shown in Figure 3-4(a) and Figure 3-4(b) respectively.

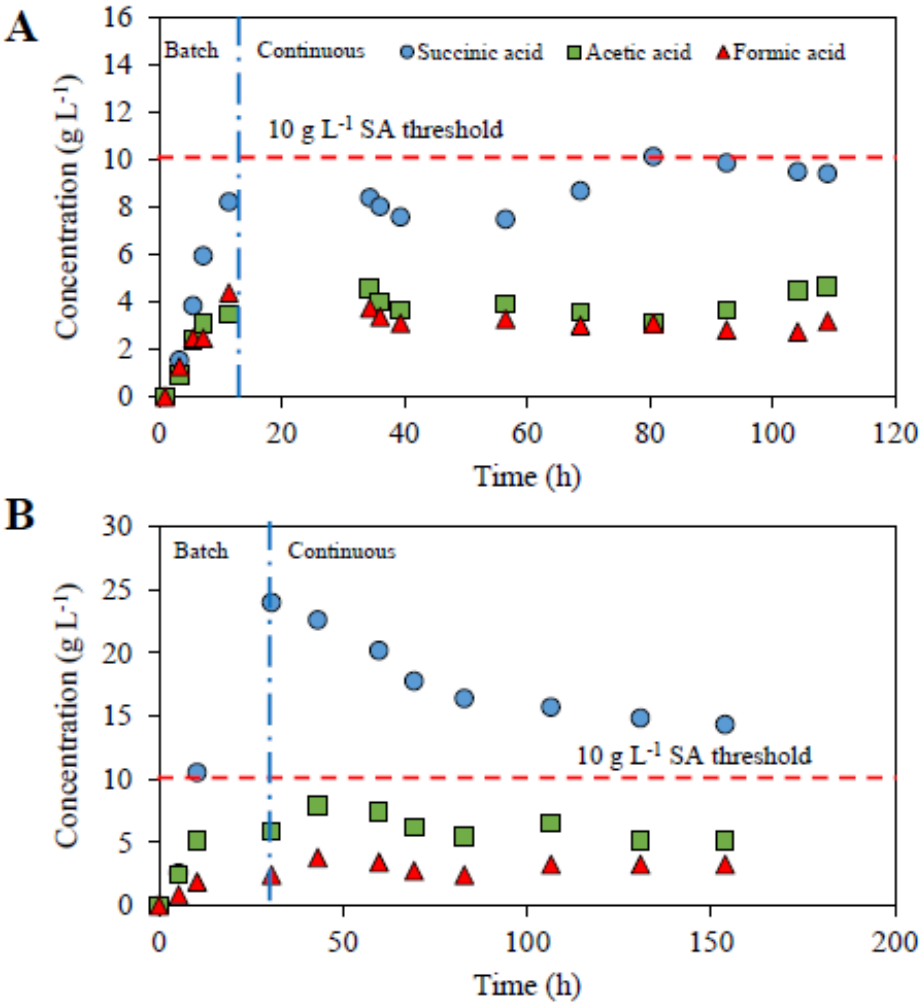

Figure 3-4: Metabolite concentration profiles for biofilm cultivation in low accumulation conditions (A) and in high accumulation conditions (B).

3.2.4 BIOFILM STAINING

After aseptic removal of the sample probes, the coverslip biofilm coupons were gently dislodged from the probes. Subsequently, the coupons were immediately immersed in a phosphate-buffered saline (PBS) solution of pH 7.4 (at 37 °C) inside a six-well plate for 5 min. The coupons were gently rinsed twice with a PBS solution and stained using Baclight LIVE/DEAD bacterial viability stains (Thermo Fisher Scientific, USA) at the recommended concentrations of stains. The sample coupons were then incubated at 37 °C for 30 min in the dark whilst in the dye solution. The stains consisted of SYTO™ 9 and propidium iodide fluorophores, which helps to distinguish between cells with intact membranes and those with compromised membranes, and on this basis ultimately discriminates between "living" and

"dead" cells. SYTO™ 9 stains all cells, giving a green emission fluorescence, whereas propidium iodide only stains cells with compromised membranes, emitting a red fluorescence. After staining, the samples were gently rinsed with distilled water and mounted on glass microscope slides, ready for microscope viewing. All staining was done in a dark room.

3.2.5 DETERMINING THE MINIMUM REPRESENTATIVE BIOFILM SAMPLE AREA

Due to the heterogeneity of biofilm structures, it is important to determine the size of the biofilm area that must be microscopically acquired which will be representative of the biofilm. This will ensure that the results obtained from the quantitative analysis of the biofilm images are accurate and represent the biofilm objectively. Korber et al [125] conducted an experiment in which they plotted a variation of a suitable biofilm parameter, which represented the heterogeneity of the biofilm, against increasing biofilm sampling area. In this way, a biofilm sampling area region where the variation in that parameter was relatively negligible was determined, which meant that the parameter became independent of the sampling area beyond the said region. In this way the minimum sampling area that is representative of the biofilm was determined. Korber et al. [125] found that for *Pseudomonas fluorescens*, when using cell coverage as a determinative parameter, an area of $1x10^6$ μm^2 was representative. Venugopalan et al. [128] determined that a minimum area of $2x10^6$ μm^2 was representative for biofilms of *Sphingomonas* sp. strain L138, when using area coverage as a determinative parameter.

Mokwatlo and Nicol [127] determined the minimum representative biofilm sampling area for *A. succinogenes* using the method described by Venugopalan et al. [128], with the biofilm surface coverage used as the heterogeneity parameter. It was found that a minimum biofilm sampling area of $2x10^6$ μm^2 was representative of the biofilm structure (see Figure 3-5). However, this was later revised to a minimum area of $3x10^5$ μm^2 when using the novel bioreactor described in Section 3.2.1.

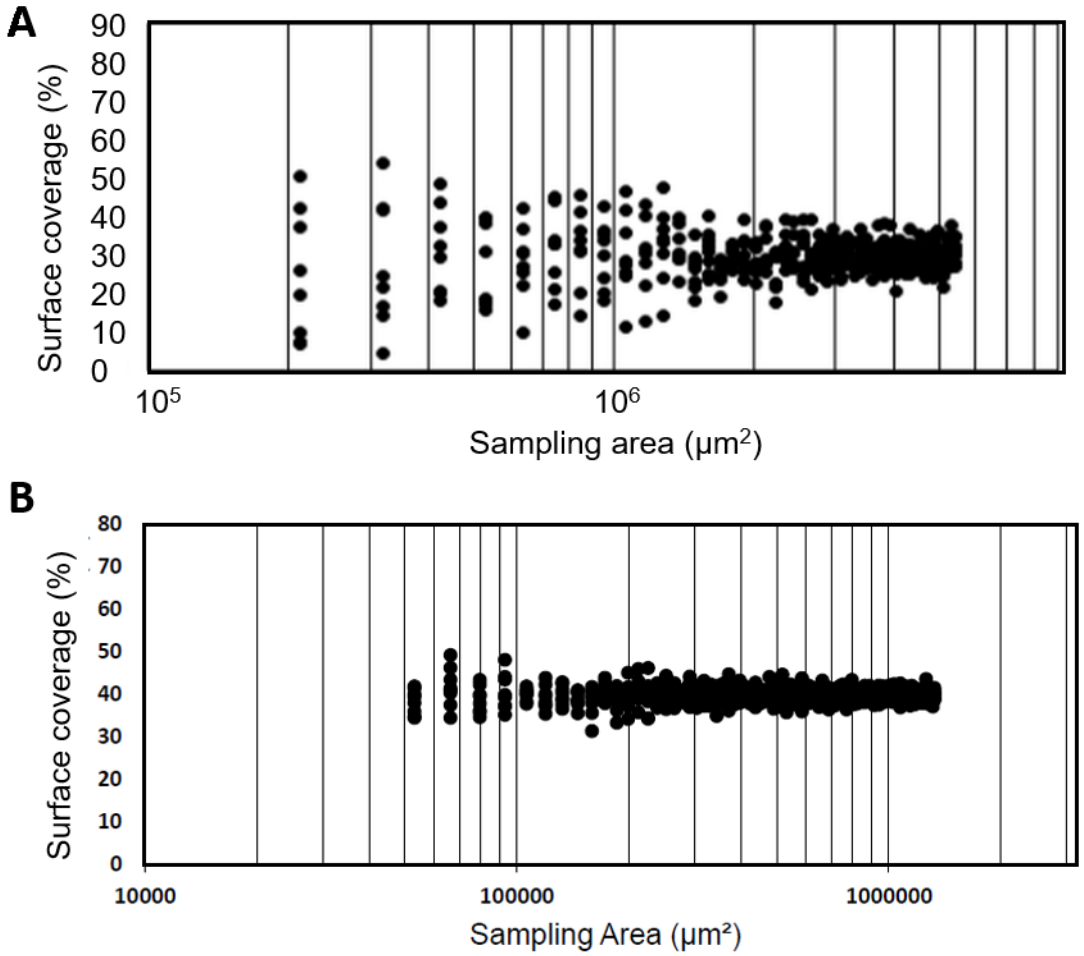

Figure 3-5: Determination of the minimum biofilm sample area that is representative of the biofilm. In (a) the minimum representative biofilm sample area was found to be $2x10^6$ µm^2, but this was later revised to a minimum area of $3x10^5$ µm^2 when using the novel bioreactor (b).

3.2.6 BIOFILM IMAGE ACQUISITION

Biofilm images were acquired using a Zeiss LSM 880 laser scanning confocal microscope (Zeiss, Germany). Biofilm samples were observed with 40× (Plan-Neofluar 40×/1.3 Oil DIC) and 100× (Plan-Apochromat 100×/1.4 Oil DIC) objectives. Image *z*-stacks were acquired by taking a series of horizontal *xy* optical scans from the substratum surface to the top of the biofilm section in set steps of 2 µm. The *z*-stack scans were acquired at random locations on the biofilm coupons. Only the 40× objective lens was used for acquiring *z*-stacks to be used for quantitative analysis. For a 40× objective lens each *z*-stack scanned a biofilm area of $0.45 x10^5$ µm^2. A minimum of 20 image *z*-stacks per day of sampling was acquired, ensuring that descriptive quantitative parameters of the biofilm were computed based on a biofilm sample area that is

three times more than the minimum representative area of the biofilm, as described in Section 3.2.5. An excitation wavelength of 488 nm was used, and the emission fluorescence was collected at 635 nm and 500 nm.

3.2.7 ANALYTICAL METHODS

Image analysis

The acquired biofilm images were post-processed with a ZEN 2.3 Lite Image Processor (Zeiss, Germany) and ImageJ [129] prior to quantitative analysis. Comstat2 digital image analysis software, a plug-in in ImageJ, was used to generate quantitative data of the acquired image *z*-stacks [130]. The mean biofilm thickness (µm), the biomass content of the biofilm (µm biomass voxels per μm^2 surface area), the ratio of biofilm surface to biofilm volume, and the roughness co-efficient parameter were computed for each image stack. The percentage of "live" cells was calculated by assuming that the total number of cells was equal to the sum of the green and red pixels, and further calculating the percentage of green pixels. This calculation was performed for each cross-sectional image scan of each *z*-stack acquired on the day of sampling and finally averaged to give the mean percentage viability for the day. Quantitative biofilm viability results were compared using an unpaired t-test with a confidence level of 95%, using GraphPad Prism software (GraphPad Software, USA).

Metabolite product analysis

The concentrations of glucose, ethanol and organic acids in the fermenter broth were determined by High-Performance Liquid Chromatography (HPLC). An Agilent 1260 Infinity HPLC (Agilent Technologies, USA) equipped with an RI detector and a 300 mm × 7.8 mm Aminex HPX-87H ion exchange column (Bio-Rad Laboratories, USA) was used. Two mobile phases were used for two methods of analysis. The first method consisted of a 5 mM H_2SO_4 mobile phase solution fed at a flowrate of 0.6 mL min^{-1}, and the second method used a 20 mM H_2SO_4 mobile phase at the same flowrate. The second method improved the accuracy of the glucose reading by separating the phosphate, glucose and pyruvic acid peaks.

3.3 Results and Discussion

3.3.1 Impact of product accumulation on cellular morphology

The *Actinobacillus succinogenes* biofilm cells expressed a different morphology according to the respective conditions in which the biofilm was cultivated, as shown in Figure 3-6. The biofilm cells were cocci-shaped with a diameter of approximately 0.4–0.5 µm in a preliminary run, where the average SA titre of cultivation was 6.0 g L^{-1} over 4 days (Figure 3-6(a)). The cells became rod-shaped (width of 0.4–0.5 µm and length of 1–2 µm) when the biofilm was cultivated in LPA conditions where the average SA titre was 8.6 g L^{-1} (over 4 days). Severe biofilm cell elongation (width of 0.4–0.5 µm and length of 5–200 µm) was witnessed in HPA conditions where the average SA titre was 15.9 g L^{-1} (average over 5 days), (**Figure 3-6**(c) and Figure 3-7), although cocci-shaped cells were still observed in the form of cell clusters in this concentration regime. This elongation of cells is known as filamentation, a process that occurs as cells grow continuously yet do not undergo septation and thus do not divide. During this growth, biofilm cells maintain their cell width while increasing in length, causing a reduction in the ratio of their surface area to volume. In this way, *A. succinogenes* cells changed morphology from coccoid to rod-like and eventually to filament-like bacterial cells, according to the severity of the conditions.

There have been reports of bacterial cells undergoing filamentation as a survival strategy under stressful conditions, such as treatment with antimicrobial agents [131], high salinity environments [132] and food starvation conditions [133]. In this study it appears that the accumulation of products during fermentation, together with the associated build-up of the neutralising salts, presented adverse conditions which ultimately caused bacterial cell elongation. This is because cells became increasingly elongated with increasing product accumulation conditions. Various authors have reported increased resistance or tolerance to adverse conditions by filamented cells. For example, the filamented cells of *C. crescentus* showed enhanced resistance to pH fluctuations, hydrogen peroxide and heat treatment compared with normal cells [133]. Therefore, the filamentation of *A. succinogenes* cells in increasingly toxic conditions may be a mechanism that aids in tolerating high acid conditions. Since filamentation causes a decrease in the ratio of surface area to volume of a cell, this means that a higher volume of cell enzymes is available to maintain a relatively smaller surface area of the cell membrane, which is critical at the high osmotic pressures found in HPA conditions due to salt neutralisation.

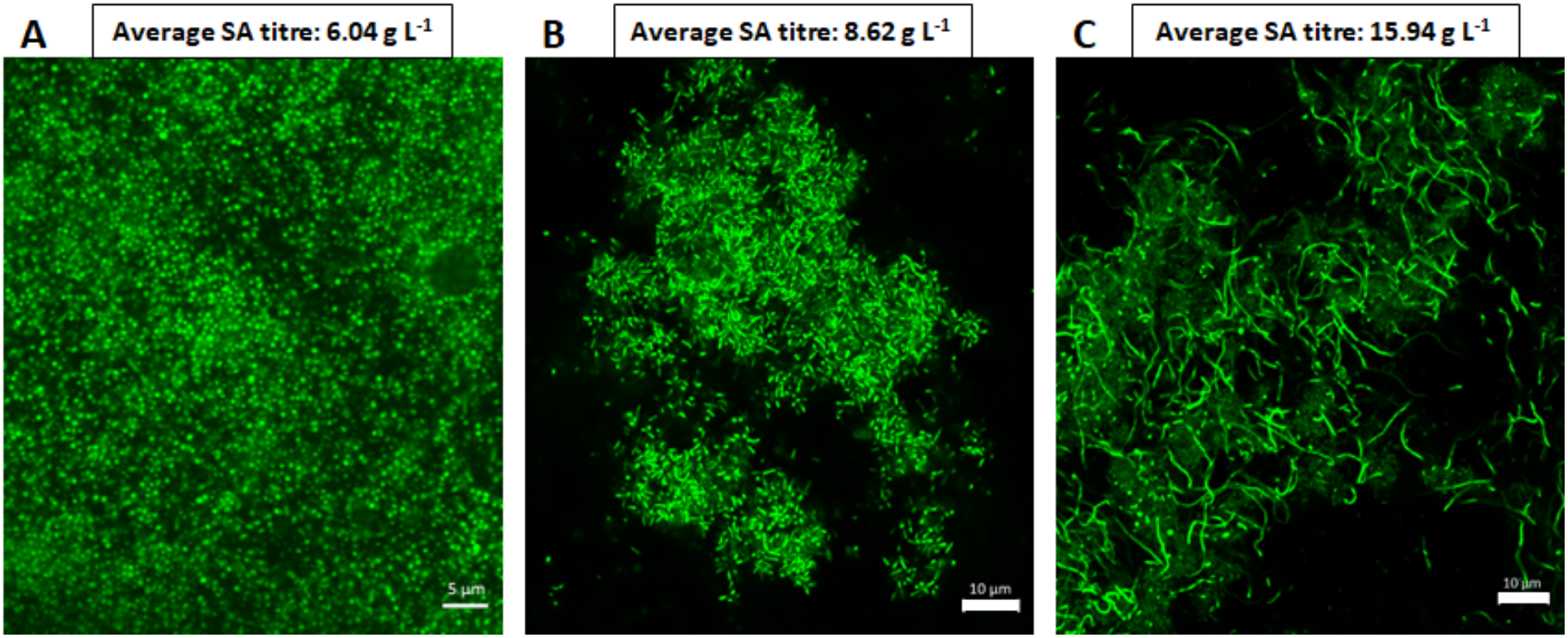

Figure 3-6: The different cell morphologies expressed by *Actinobacillus succinogenes* in biofilms grown under varying succinic acid titre conditions. In (**a**), under lower SA titre conditions, biofilm cells were mostly cocci-shaped, whereas in (**b**) the cells started to exhibit a classic bacillus rod-like shape as the SA growth concentration increased slightly. When biofilm cells were growing at high SA concentrations (**c**) they were drastically elongated, although clumps of cocci-shaped cells were observed. The scale bar indicates 5 µm in (**a**) and 10 µm in (**b**) and (**c**).

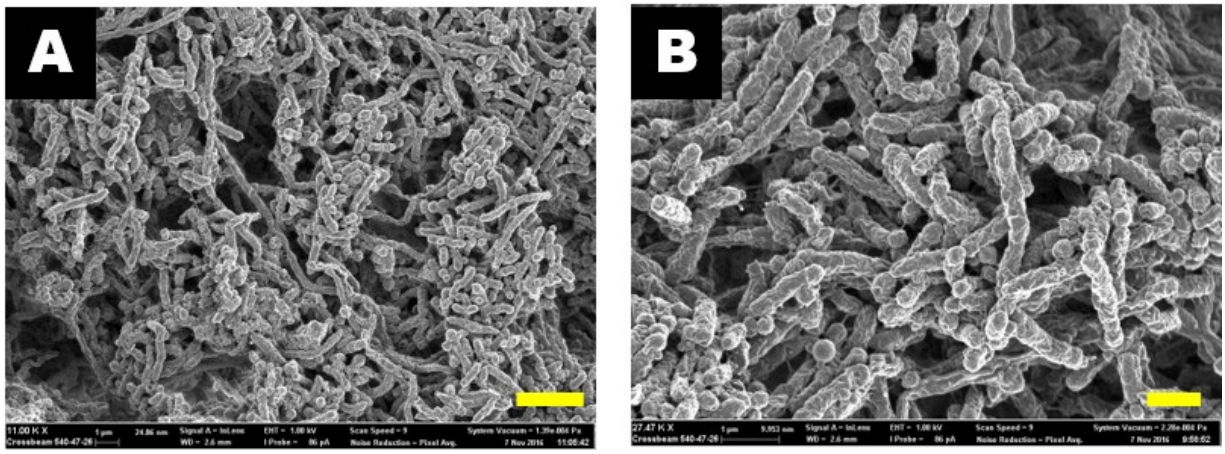

Figure 3-7: Elongated cells were further visualised using SEM (a, b). The scale bar denotes 6 µm. (Source: Mokwatlo & Nicol (127))

3.3.2 BIOFILM DEVELOPMENT AND STRUCTURE

Biofilm development in low accumulation conditions

Representative 3D top-view images profiling the biofilm development in LPA conditions are shown in Figure 3-8, together with the *x-z* plane images showing the biofilm thickness profiles. Growth was rapid when biofilm was cultivated under low product accumulation conditions, confirming that the conditions were favourable for biomass growth. This is consistent with observations by Maharaj et al. [20], Brink and Nicol [21] and Van Heerden and Nicol [89], all of whom reported rapid biofilm development in a continuous bioreactor at high dilution rates where accumulation is low. In keeping with rapid growth, the substratum surface was completely covered by a basal layer of rod-shaped cells (2–4 µm) on the first day, and out of this layer protruded pillars of cell clusters with varying thickness – as can be seen from the uneven thickness profile in Figure 3-8(b) (day 1) – some of which were as thick as 42 µm. The structure observed on the first day at low titre was thus that of a heterogeneous dispersion of amorphous cell clusters. The day 2 and 3 images in Figure 3-8 (a&b) show that the biofilm became thicker and approached homogeneity with regard to thickness across the colonised surface, as cell microcolonies coalesced and became closely spaced. On day 4 there was an overall reduction in the thickness of the biofilm: this was due to an observed shedding of the biofilm as was seen from an increase in the biomass content of the bioreactor broth effluent.

Biofilm development in high accumulation conditions

Although cell growth is regarded as negligible above SA titres of 10 g L^{-1}, there was biofilm development in HPA conditions where the average SA titre was 15.9 g L^{-1}. However, contrary to biofilm development in low product accumulation conditions, the biofilm struggled to grow in high product accumulation environments. After the first day of growth, the biofilm had developed into a patchy distribution of cell clusters which were interconnected by a branched network of long filamentous cells (Figure 3-9a), and thus there was a low coverage of the substratum surface. Cell clusters, made up of cocci-shaped cells, had grown significantly in size and number by the third day and were thus closely spaced, resulting in a biofilm that was fairly uniform with regard to thickness, as is shown in Figure 3-9(b). In addition, more filamentous cells were also observed, and these were mostly located in-between the borders of neighbouring cell clusters (Figure 3-10, indicated by white circles). It was also observed that filamentous cells were protruding out of cell clusters and entering other neighbouring cell clusters (Figure 3-10, indicated by white arrows), giving the impression that they were holding the cell clusters together. This observation was also made by Janissen et al. [134], who reported the filamentation of *Xylella fastidiosa* bacterial cells located on the borders of cell clusters in a biofilm, as well as interconnecting cell clusters. It is possible that the elongated cells connecting the cell clusters play a sensory role as they are much more sensitive to environmental changes around them compared with cells within cell clusters. The interconnection of cell clusters by means of filamentous cells may also provide stability for the resulting biofilm structure because of their tendency to become entangled , as can be seen in Figure 3-7. Moreover, SEM biofilm images revealed extensive cell-to-cell and cell-to-surface cylindrical connection “wires” of constant diameter (20–30 nm) connecting filamentous cells with other cells and with the substratum surface (for those cells near the surface), which further strengthens the biofilm stability (see Figure 3-11). Nonetheless, by the fifth day the biofilm looked patchy again as most of the cell clusters had disintegrated from the biofilm (Figure 3-9(c)). This was expected as the cell clusters were mostly stained red (indicative of cell death) after 3 days of growth, and excessive shedding was witnessed on day 4 as seen from the increased biomass concentration of the broth effluent.

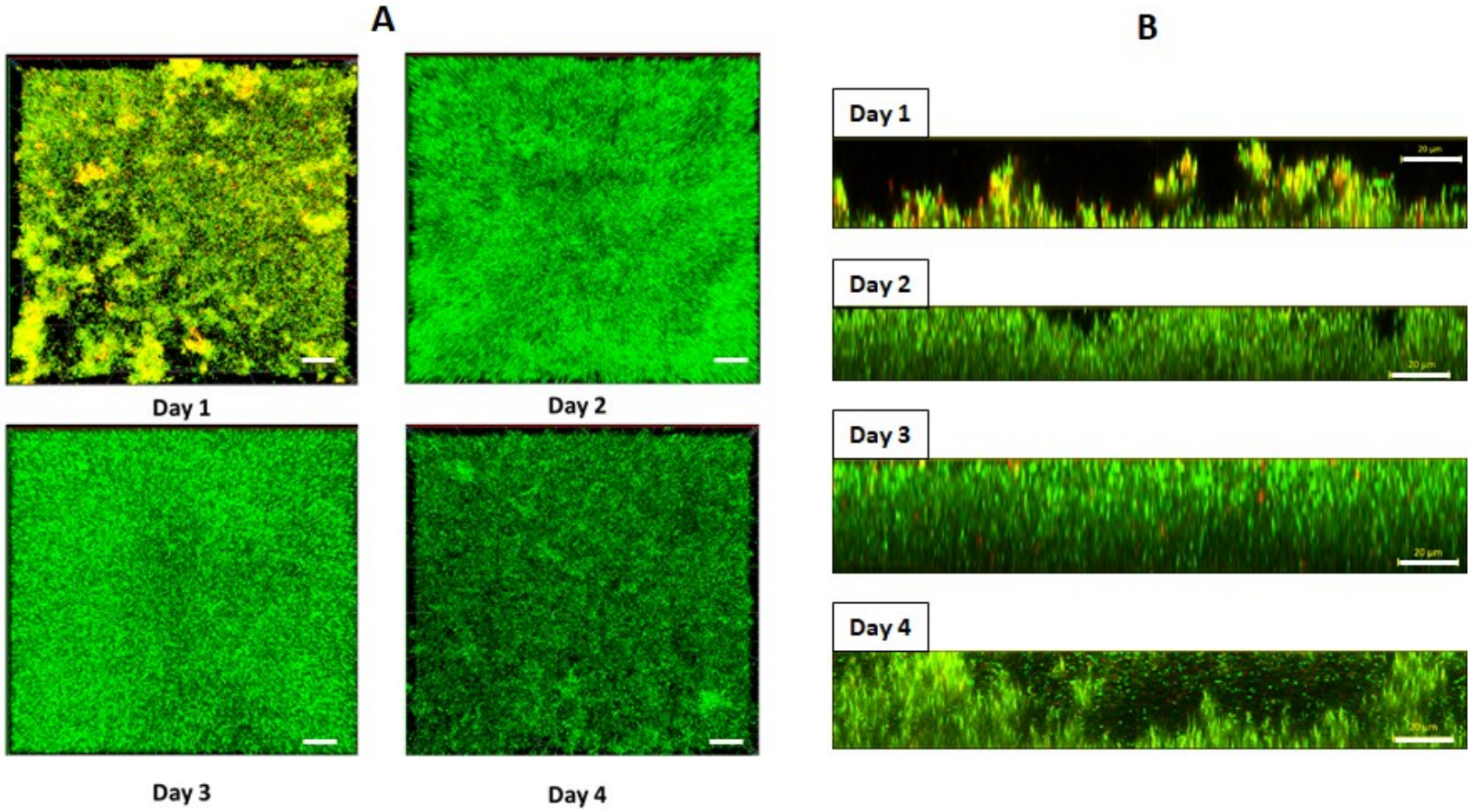

Figure 3-8: Representative *xy-plane* (A) and *xz-plane* (B) views of the biofilm development at low SA titre conditions over a period of four days. The biofilm rapidly achieved a complete basal coverage on the first day although the microcolonies were irregular in height and size. Over the course of the next two days, the biofilm increased uniformly in thickness with minimal voids noticeable between microcolonies throughout the biofilm thickness. The scale bars indicate 20 μm.

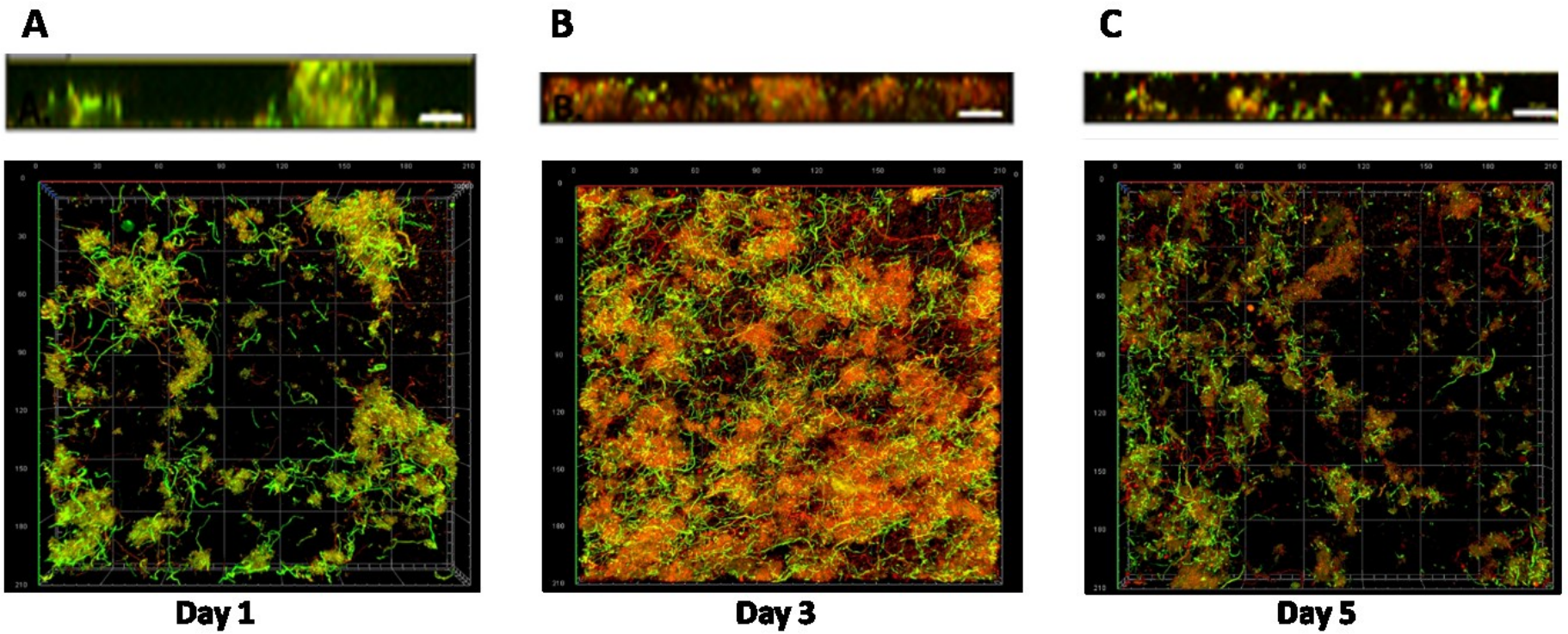

Figure 3-9: Biofilm development at high SA acid titres as represented by *xy*-plane and *xz*-plane images. A patchy biofilm with low surface coverage was observed on the first day with a cluster of cell microcolonies interconnected by a network of elongated cells. On the third day the biofilm was less patchy as the microcolony structures were closely spaced and the network of elongated cells was much denser. Shedding of biofilm resulted in a patchy structure on the fifth day. The scale bars indicate 20 µm.

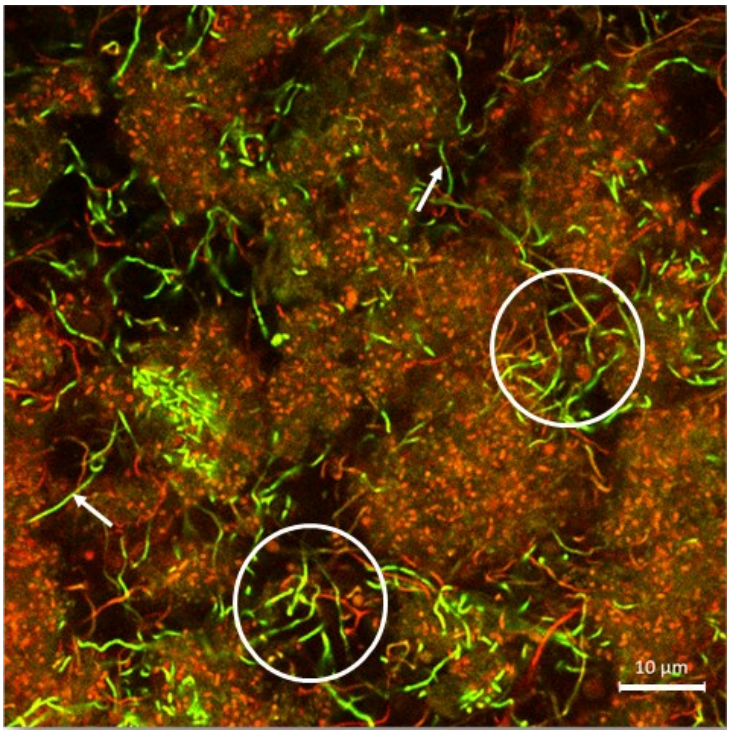

Figure 3-10: Cell clusters surrounded by filamentous cells**.** Filamentous cells were mostly located in-between the borders of neighbouring cell clusters (indicated by white circles) and were protruding out of cell clusters and entering other neighbouring cell clusters (indicated by white arrows) as if interconnecting cell clusters. Filamentous cells were mostly emitting green fluorescence, which was indicative of cell viability. The scale bar indicates 10 µm.

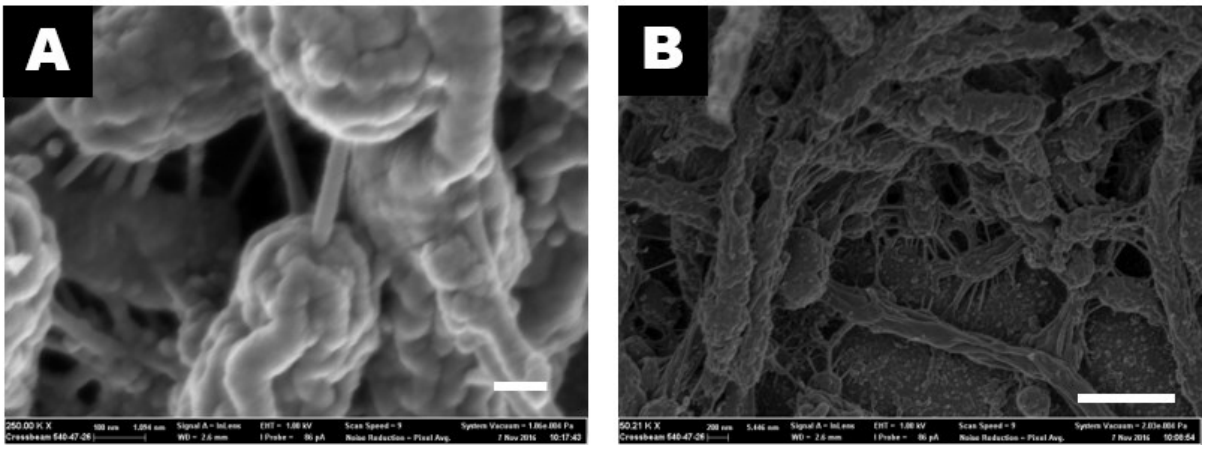

Figure 3-11: Constant diameter (20–30 nm) wire-like structures were observed interconnecting cells to each other (A) and to surfaces (B). (Source: Mokwatlo & Nicol (127))

Quantitative comparison of biofilms cultivated in LPA and HPA conditions

A quantitative analysis of the biofilm *z*-stack images collected during the experiments was performed using COMSTAT for a quantitative comparison of the parameters for biofilm grown in low and high accumulation environments. Exactly the same procedure as for preprocessing of the biofilm images prior to quantitative analysis was followed so as to not introduce variability. The biomass content of the biofilm, the exposed biofilm surface to biofilm volume area, the mean biofilm thickness, and the roughness co-efficient of the biofilm were compared. The results are shown in Figure 3-12. The standard deviations of the computed parameters in Figure 3-12 were quite significant, but this is a common observation in biofilm parameter quantification due to innate biofilm structure variability, and it is to be expected as an extensive biofilm area was sampled (minimum of 20 image *z*-stacks).

The quantitative data were consistent with observations made visually from the microscopic images. The biomass content of LPA-cultivated biofilms increased at a rapid rate compared with that of biofilms cultivated in HPA conditions (a mean rate of 10 $\mu m^3\ \mu m^{-2}\ day^{-1}$ vs 5 $\mu m^3\ \mu m^{-2}\ day^{-1}$), further confirming that high growth rates are encountered below SA titres of 10 g L^{-1} (Figure 3-12(a). LPA-cultivated biofilms were much thicker than HPA-cultivated biofilms with a maximum mean thickness of 30 µm and 15 µm for the LPA and HPA cultivations, respectively. The reduction of biomass content and biofilm thickness after the third day of growth was consistent with the observed shedding of the biofilm for both HPA- and LPA-cultivated biofilms. The roughness co-efficient of LPA-cultivated biofilms stabilised around a low value of 0.2, which is indicative of a homogenous biofilm with a relatively even surface (Figure 3-12(b). High growth rates achieved in LPA conditions allow the biofilm to occupy the entire surface of attachment, thus resulting in the observed homogenous biofilms. For HPA-cultivated biofilms, the roughness co-efficient had an average of 0.71, which is indicative of a patchy biofilm structure as a result of the biofilm struggling to grow under these harsh conditions. Consequently, the patchy biofilm formed in HPA conditions had high exposed surface area per volume of biomass, whereas the uniform biofilm under LPA conditions had the lowest exposed surface area per volume of biomass (Figure 3-12(d).

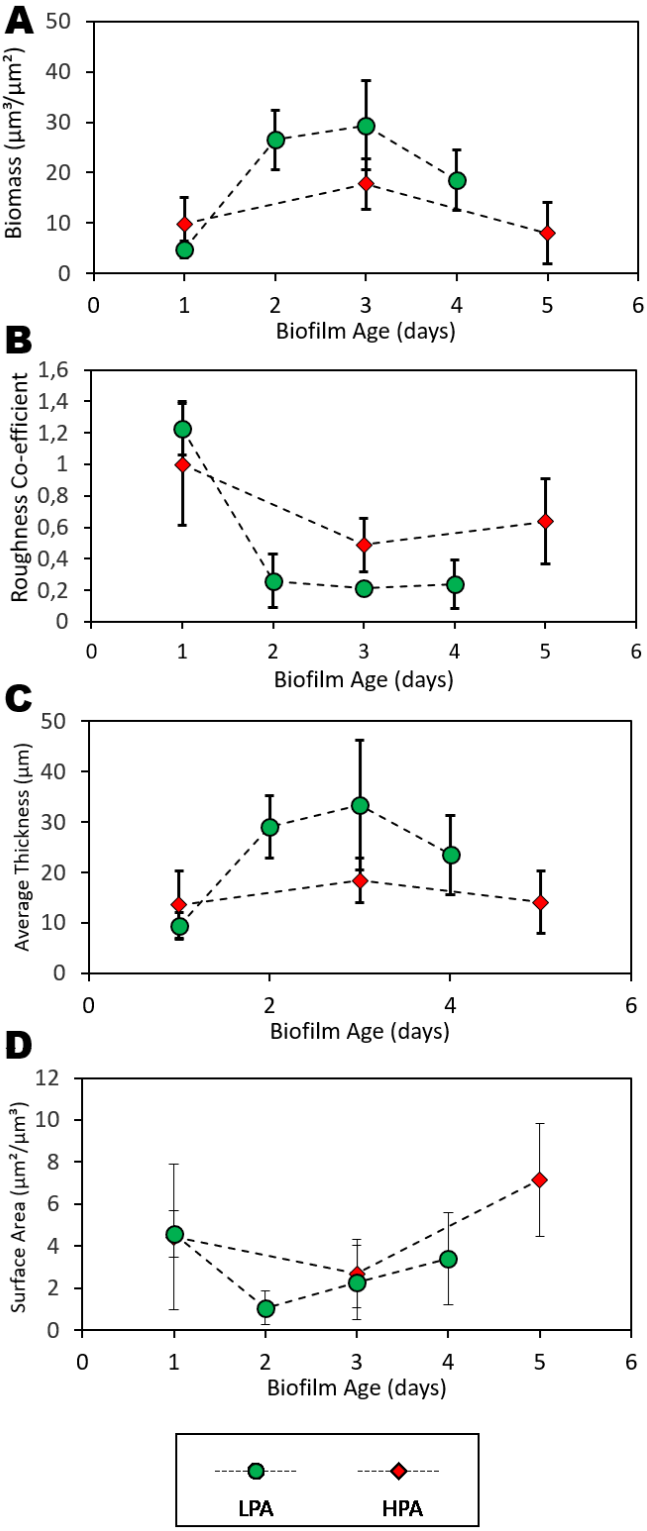

Figure 3-12: A quantitative comparison of biofilm parameters for biofilm grown in low and high SA environments**.** It is apparent that biofilm experiences high growth rates at low SA titres as shown by rapid increases in biomass volume per area (A) and thickness (± 10 µm per day) (C) when compared with growth in high acid conditions in which the biofilm struggles to grow. The patchy structure of the biofilm grown in high acid environments results in a high exposed biofilm surface area per volume, which is needed in these harsh conditions. The quantitative data are consistent with observations from the qualitative image analysis.

3.3.3 BIOFILM VIABILITY

Biofilms cultivated under low product accumulation conditions maintained a high percentage of viable cell content compared with biofilms cultivated in HPA conditions (Figure 3-13). The fraction of viable cell content of LPA-cultivated biofilm increased from 56% after the first day to 74% by the third day, showing that the biofilm became more and more composed of viable cells for the first 3 days of cultivation. HPA-cultivated biofilms experienced a decline in the viable cell content as the biofilm viability decreased from 54% on the first day of cultivation to 46% by day 5 of cultivation. The results show that, in addition to inhibition of cellular growth, HPA conditions also cause significant cell death in biofilms. Therefore, although biofilm development occurs in HPA conditions, it happens at a great cost to biofilm viability. This explains the decrease in specific mass-based SA productivity under increasing product accumulation conditions observed by both Brink and Nicol [21] and Maharaj et al. [20]. The apparent loss in biomass-based SA productivity is due to the fraction of active cells within the biofilm decreasing with increasing metabolite accumulation conditions. Moreover, since biomass growth depends on the number of active cells within the biofilm, it may well be that extensive cell death at high acid titres contributes much to the apparent slow/inhibited growth. A statistical comparison (student's t-test) of viability for LPA and HPA for day 1 and day 3 is given in Table 3-1. The LPA-grown biofilms had significantly higher viability than the HPA-grown biofilms, and this was more pronounced on the third day. Accumulation conditions thus caused a statistical difference in the viability of biofilms.

It was also observed that the branched networks of filamentous cells, expressed in biofilms cultivated in HPA conditions (Figure 3-9(b, c) and Figure 3-10), were mostly stained green. This indicated that filamentous cells were more tolerant towards high metabolite accumulation conditions. As discussed in Section 3.3.1, it has been reported that cells which undergo filamentation due to stressful conditions have shown increased tolerance to those conditions compared with normal cells. Indeed, a high surface area per volume of bacterial cell, such as exhibited by coccoid-shaped cells, is crucial for maximising the transportation of nutrients in high growth rate conditions, whereas a low surface area to volume ratio is beneficial for resisting the osmotic stresses experienced in HPA conditions.

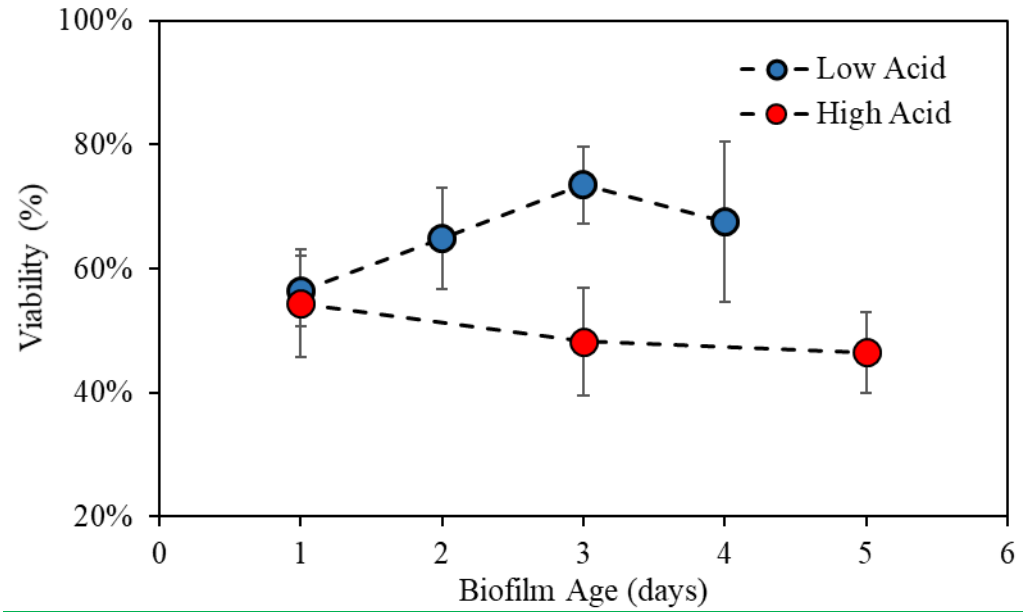

Figure 3-13: The activity of the biofilm during low acid titre and high acid titre biofilm development. A higher green to red colour intensity correlates to images where cells were mostly active (green). Biofilm grown at low acid titres was mostly active throughout its development, whereas that grown in a high acid environment became increasingly inactive, even resulting in excessive shedding.

Table 3-1: A statistical comparison of biofilm viability for growth in low and high accumulation conditions

Biofilm age	Biofilm cultivation conditions				Statistical comparison		
	HPA		LPA				
	Mean viability (%)	Samples	Mean viability (%)	Samples[1]	P value	Difference between means	Comment
Day 1	54.4± 8	203	56.4± 5	347	0.0004	2	Significantly different (P< 0.05)
Day 3	48.3 ± 8	344	73.5 ± 6	358	0.0001	25.2	Significantly different (P< 0.05)

[1] Refers to the number of *xy* plane optical scan images of the biofilm processed for a particular day of biofilm sampling.

3.3.4 DEVELOPMENT OF FILAMENTOUS BIOFILM

Filamentous cells formed in HPA conditions appear to confer on the cell tolerance to the inhibitions encountered in these HPA conditions. To assess this speculation which is based on the visual evidence obtained from images acquired in HPA conditions (Figure 3-9(b, c) and Figure 3-10), an additional experiment was performed with the aim of developing a biofilm composed of filamentous biofilm so that the viability of the biofilm could be analysed. To do this, biofilm was cultivated in LPA conditions (a dilution rate of 0.3 h^{-1}) for 2.5 days without sampling, the dilution rate was decreased to 0.2 h^{-1} for a day, and then the dilution rate was decreased to a final value of 0.05 h^{-1} which was maintained for 4 days. It was hypothesised that with a gradual decrease in the dilution rate, the rod-shaped cells formed at high dilution rates would gradually filament without significant loss in the viability of the cells. The biofilm was therefore sampled after 7.5 days of growth; the metabolite conditions in this experiment are shown in Figure 3-14(a).

A total area of 1.56×10^{6} μm^2 was sampled and visualised after 7.5 days of biofilm cultivation, which is more than the minimum representative biofilm sampling area. As shown in Figure 3-14(a), the LPA-cultivated biofilm was subjected to HPA conditions for 3 days during which the average succinic acid titre was manipulated to approximately 20 g L^{-1}. Visualisation revealed a biofilm composed mostly of filamentous cells, as shown in Figure 3-14(b). Moreover, visual observations indicated that the biofilm had high viability, despite being exposed to HPA conditions for 3 days. To confirm this, the acquired images were used to calculate the average biofilm viability and this was compared against the viability of 3-day-old HPA- and LPA-cultivated biofilms. The viability of the filamentous biofilm was 63%, which was 15% higher than that of the 3-day-old HPA-cultivated biofilm, despite the fact that the filamentous biofilm was exposed to an average SA titre of 20 g L^{-1} for 3 days, whereas the HPA-cultivated biofilms were subject to an average SA titre of 15.6 g L^{-1} (Figure 3-14). The results thus demonstrate the advantages of allowing the developed biofilm to ease slowly into high SA titre operation, as this allows the biofilm cells to transition into a morphology that gives them greater tolerance to high titre operation.

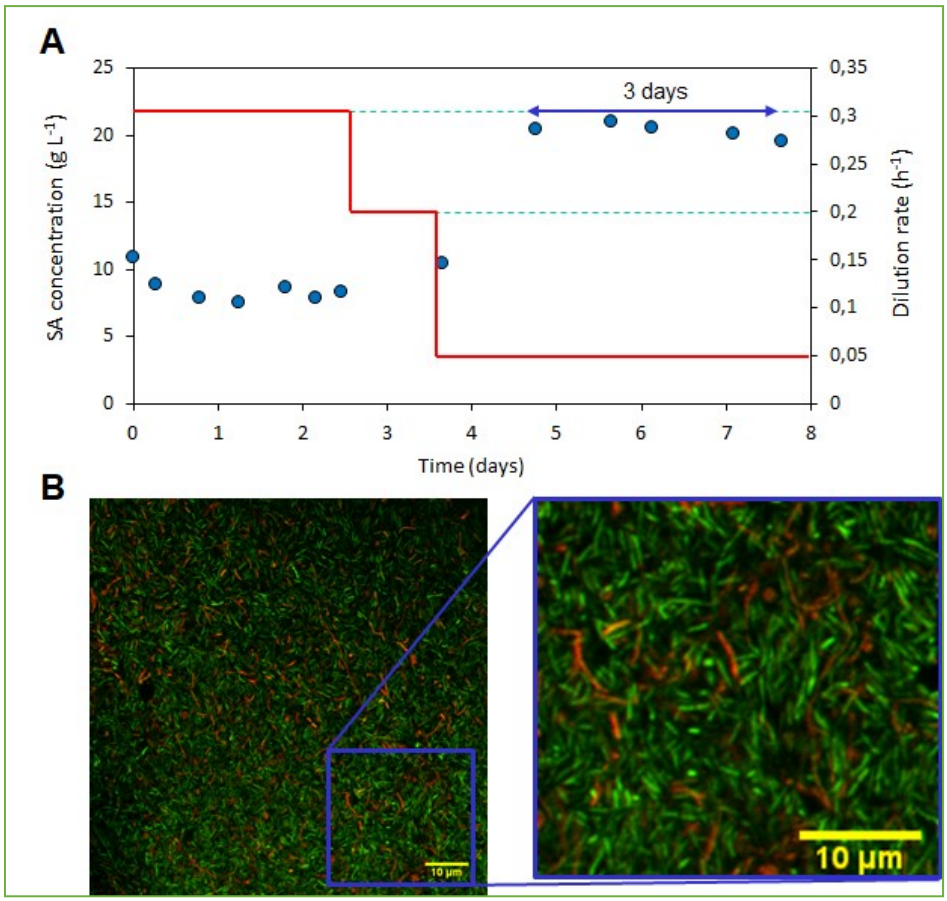

Figure 3-14: The development of a filamentous biofilm. In (A) both the metabolite concentrations and the dilution rates are shown. A filamentous biofilm was successfully developed as shown in (B); it was composed of viable filamented cells. The scale bars indicate 10 µm.

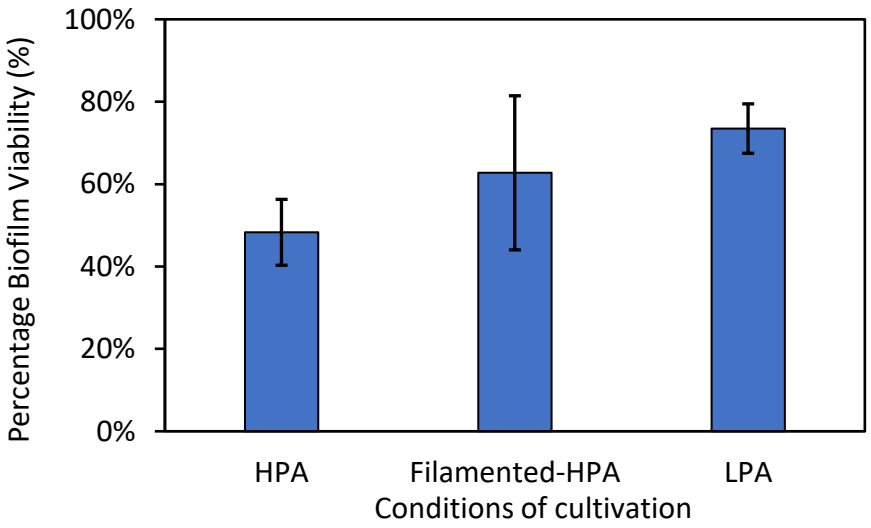

Figure 3-15: Comparison of the viability of 3-day-old HPA- and LPA-cultivated biofilms with the viability of a filamentous biofilm subjected to HPA conditions for 3 days. The filamentous biofilm exhibited high viability after being subjected to HPA conditions, demonstrating its high tolerance to HPA conditions.

3.4 CONCLUSIONS

The stability and activity of the biocatalyst biofilms of *Actinobacillus succinogenes* are critical to the prospect of bulk-scale continuous fermentative production of succinic acid. Unlike physical catalysts, biocatalysts will be impacted by the surrounding environmental conditions. This chapter investigated the impact of the accumulation of product metabolites, together with sodium due to pH control with caustic, on the development of the *A. succinogenes* biofilm by employing microscopic analysis. The findings in this chapter show that biofilms of *A. succinogenes* develop rapidly and with high cellular viability when cultivated under low product accumulation (LPA) conditions. In contrast, very slow growth and low cell viability of biofilms are observed when the biofilm is cultivated in high product accumulation (HPA) conditions. At a cellular level, *A. succinogenes* biofilm cells respond to increasing HPA broth conditions by becoming elongated. The elongated cell morphology confers tolerance on the cell to what would otherwise be harmful conditions as filamentous cells remain active at HPA conditions. It is proposed that by gradually decreasing the dilution rate, after biofilm cultivation at high dilution rates, slow product accumulation can be obtained, thus allowing the rod-shaped cells in the previously developed biofilm to filament. This results in biofilm composed of filamentous cells able to tolerate operation at high metabolite accumulation without significant loss of biofilm viability.

4 THE EFFECT OF SHEAR ON BIOFILM MORPHOLOGY, COMPOSITION AND METABOLIC ACTIVITY

4.1 BACKGROUND

The previous chapter investigated the influence of acid accumulation in the fermenter on the development, structure and viability of *A. succinogenes* biofilms [16]. In summary, it was found that high product accumulation (HPA) conditions (above 10 g L^{-1} SA) impeded biofilm growth and resulted in patchy biofilms with significant cell death, whereas low product accumulation (LPA) conditions (below 10 g L^{-1} SA) favoured biofilm growth with relatively higher cell viability within biofilms. Moreover, it was discovered that cell elongation under HPA conditions confer on the cell tolerance towards what would otherwise be harmful conditions as filamentous cells remained active in HPA conditions. However, the resultant biofilm structure and physiology formed in bulk continuous SA production will not only be a product of accumulation conditions, but will also depend on the hydrodynamic shear conditions caused by mixing in the reactor. Indeed, according to the literature [135–137], it is expected that hydrodynamic shear conditions (HSC) in bioreactors will also influence the characteristics of biofilms formed by *A. succinogenes*. Most literature reports the formation of stronger (dense) and thinner biofilms at high HSC, compared with low HSC where heterogeneous, porous and weaker biofilm structures tend to be formed [138–140]. Moreover, studies in microbial fuel cells have consistently shown that high shear operation resulted in more viable biofilms with increased metabolic activity and high current generation [141]. It follows that shear could potentially impact *A. succinogenes* biofilms in such a way that it improves biofilm viability and ultimately SA productivity. Thus far, no studies have been conducted on the impact of shear variation on the development of *A. succinogenes* biofilms, particularly looking at the possibility of forming more viable biofilms by varying the shear conditions in the fermenter and ultimately increasing total cell-based SA productivity.

The objective of the current chapter was to investigate the role of hydrodynamic shear conditions in the development of *A. succinogenes* biofilms, specifically assessing the biofilm morphology, cellular viability and SA cell-based productivity by employing two custom-

developed bioreactors. The first bioreactor is the one employed in Chapter 3, which allowed visualisation of the impact of shear on the biofilm morphology through microscopic analysis. The second bioreactor allowed for complete removal of all the biofilm that was developed in the reactor and was used to measure biofilm composition and SA cell-based productivity. In this way, the impact of shear was evaluated at a microscopic level in the first bioreactor with respect to the structure and cell activity of biofilms, and it was evaluated at a macroscopic level in the second bioreactor where the SA cell-based productivity of the biofilm and its composition were measured. Succinic acid concentrations were controlled below 10 g L^{-1} in the first bioreactor to favour substantial biofilm growth, in accordance with the results given in Chapter 3. Intensive mixing was used to vary shear in the first bioreactor (250 & 500 rpm), and the liquid linear velocity flowrate (0.36 & 0.64 m s^{-1}) was used to vary shear in the second bioreactor. Both methods have been validated as effective methods for regulating the shear rate [139]. The bulk of this work was published by Mokwatlo et al. [142] in *Bioprocess and Biosystems Engineering*.

4.2 MATERIALS AND METHODS

4.2.1 FERMENTATION MEDIA

The fermentation medium was prepared in a similar manner to that described in Section 3.2.2. The glucose concentration for microscopic visualisation experiments was kept at 60 g L^{-1} and at 40 g L^{-1} for biofilm productivity experiments.

4.2.2 BIOREACTORS

Two types of bioreactor were used in the study. The first bioreactor (bioreactor A) was custom developed for the purpose of microscopic visualisation of biofilm development; the details of this reactor are described in Section 3.2.1. The visualisation and analysis of the microscopic biofilm development was facilitated by the extraction of multiple asynchronous sterile samples of biofilm coupons from the bioreactor volume. These coupons could then be studied under a confocal laser scanning microscope (CSLM) to investigate the microscopic architectural differences caused by variation of hydrodynamic shear conditions (HSC). HSC were varied by altering the rotating speed (rpm) of the Rushton six-blade impeller connected to the overhead stirrer. The maximum speed of the stirrer was 500 rpm. The second bioreactor type (bioreactor B) is a homogenous shear silicone tube bioreactor, presented in the study by Brink & Nicol [21]. The reactor consisted of a 3 mm diameter silicon tubing of approximately 5 m in length, with an active volume that ranged from 50to70 mL depending on the gas hold-up at the time. Bioreactor B, shown in Figure 4-1, was used for testing the biomass-based succinic acid productivity performance of biofilms developed at varying HSC as it allowed the complete removal of the developed biofilm for further analysis and quantification. In bioreactor B, HSC conditions were varied by changing the superficial velocity of the broth within the tube.

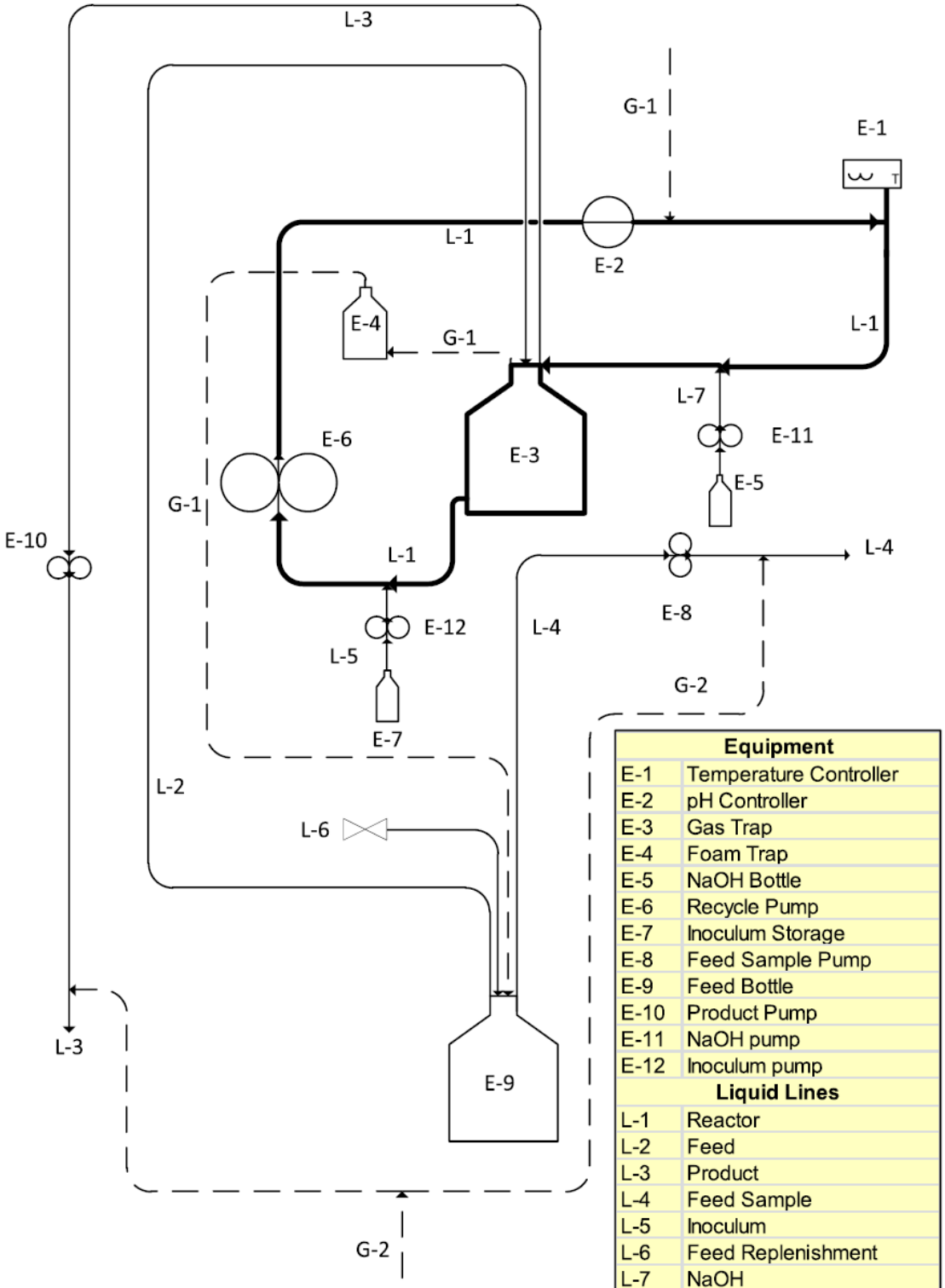

Figure 4-1: Diagrammatic representation of bioreactor B used in the study by Brink & Nicol [21]. The reactor section is shown in bold. The bioreactor allowed for complete removal of all biofilm and was used to analyse biofilm composition and productivity.

In both bioreactors, temperature and pH were controlled at 37.0 ± 0.1 °C and 6.80 ± 0.01 respectively. A Liquiline CM442 (Endress+Hauser, Gerlingen, Germany) coupled to a Ceragel CPS71D glass electrode (Endress+Hauser, Gerlingen, Germany) measured both temperature and pH, and controlled pH by dosing of a 10 M NaOH solution by means of a peristaltic pump connected to an internal relay. Temperature was controlled by a feedback PID controller, custom developed in Labview. All gas vents and inlets were fitted with 0.2 µm PTFE membrane filters (Midisart 2000, Sartorius, Göttingen, Germany) to ensure sterility.

4.2.3 BIOFILM CULTIVATION FOR VISUALISATION

Biofilm was cultivated under LPA conditions (below 10 g L^{-1} SA) in bioreactor A in a manner similar to that described in Section 3.2.3, except that shear conditions were varied by varying the mixing speed from 250 to 500 rpm. In summary, the bioreactor was initially run in batch mode to facilitate the accumulation of substantial suspended cell biomass (1.86 ± 0.3 g DCW L^{-1}), while below 10 g L^{-1} of SA, to avoid cell washout before switching to continuous mode for biofilm cultivation. Subsequently, the biofilm sampling coupons were aseptically inserted into the bioreactor while simultaneously switching to continuous operation mode at a dilution rate of 0.3 h^{-1}. This ensured that the biofilm was cultivated on the coupons (13 mm Thermanox coverslips, Thermo Fisher Scientific, Massachusetts, USA) below the limiting acid concentration from the onset. Acid metabolite concentrations were monitored throughout the biofilm cultivation period to ensure that the LPA conditions were maintained. The concentration profiles are given in Figure 4-2. Mixing was set at 500 rpm (maximum stirrer output) for high shear conditions. This corresponded to an impeller tip velocity of 1.65 m s^{-1} and a local shear velocity of 0.66 m s^{-1} at the biofilm coupon surface on the basis of the study by Madhrani [143] which found that tangential velocities near the wall of stirred tanks were 0.2 to 0.5 of the impeller tip velocity. For low shear conditions, mixing was set at 250 rpm which corresponded to a local shear velocity of 0.33 m s^{-1} at the coupon surface. Biofilm coupons were sampled daily (starting 24 h after insertion of coupon probes) for 3 days and immediately prepared for microscopic viewing. All operational variables were controlled at similar conditions, except for shear conditions.

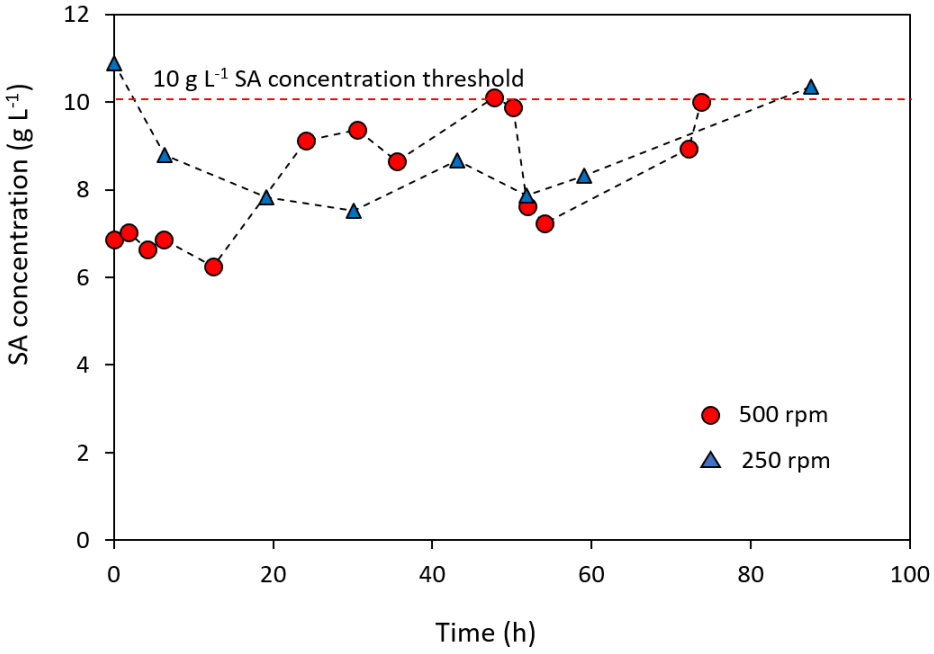

Figure 4-2: Succinic acid concentration profiles in the fermenter during biofilm cultivation for low and high hydrodynamic shear conditions

4.2.4 BIOFILM IMAGE ACQUISITION

The preparation of sampled biofilm coupons and the acquisition of biofilm image stacks was performed in the manner described in Section 3.2.4. Biofilm images were acquired using a Zeiss LSM 880 laser scanning confocal microscope (Zeiss, Germany). A minimum of 20 image *z*-stacks per day of sampling were acquired, ensuring that descriptive quantitative parameters of the biofilm are computed based on a biofilm sample area that is representative of the biofilm, as previously determined in Chapter 3. An excitation wavelength of 488 nm was used and the emission fluorescence was collected at 635 nm and 500 nm.

4.2.5 IMAGE ANALYSIS

A ZEN 2.3 Lite Image Processor (Zeiss, Germany) and the ImageJ [129] software were used to post-process biofilm images prior to quantitative analysis. Post-processing involved determining the surface and top section of the biofilm image stack. Comstat2 digital image analysis software, a plugin to ImageJ, was used to generate quantitative data of the acquired image *z*-stacks [130]. The biomass content of the biofilm (μm^3 biomass voxels per μm^2 surface area), the roughness coefficient parameter and the average biofilm thickness were computed for each image stack. In addition, the volume porosity of the biofilm was computed using Equation

(4-1), as reported by Paramonova et al. [140], where Biovolume is the volume occupied by bacteria in a 3D image, Average Thickness is the average thickness of the biofilm and Area Image is the area of the scanned region.

$$Volume\ Porosity = \left(1 - \frac{Biovolume}{Average\ Thickness \times Area\ Image}\right) \quad (4\text{-}1)$$

The percentage of "live" cells was calculated by assuming that the total cells were equal to the sum of green and red pixels and further calculating the percentage of green pixels. This calculation was performed for each cross-sectional image scan of each *z*-stack acquired on the day of sampling and finally averaged to give the mean percentage viability for the day.

4.2.6 PRODUCTIVITY OF BIOFILMS DEVELOPED AT VARIED SHEAR

Investigation of the mass-based productivity of biofilms developed in different shear conditions was conducted using the homogenous shear silicone tube reactor (bioreactor B). Unlike bioreactor A, bioreactor B allowed for the removal and quantification of the entire developed biofilm, and therefore the global mass-based succinic acid productivity could be determined. Two shear velocities of 0.36 m s^{-1} and 0.64 m s^{-1} were used from the onset of fermentation. The superficial velocities were chosen to mirror approximately the estimated bulk velocities at the surface of the coupons in bioreactor A. Fermentations were initiated by running the bioreactor in batch mode for 24 h after inoculation to increase the cell concentration. The succinic acid concentration at this point ranged from 10 to 12 g L^{-1} for all the runs. At this point a sufficiently high suspended cell concentration was obtained (2.2 ± 0.3 g DCW L^{-1}) to avoid cell washout, and the fermenter was switched to continuous operation at a dilution rate of 0.9 h^{-1} and 0.2 h^{-1}, for both shear velocities of 0.36 m s^{-1} and 0.64 m s^{-1}. Concentrations of metabolites were monitored until steady-state conditions were reached. Steady state was confirmed by a steady average NaOH dosing rate for a period of 6 h.

The entire biofilm developed in the homogenous shear tube reactor (bioreactor B) was sampled once steady-state conditions were achieved. Prior to biofilm sampling, all the reactor flow streams were stopped, the liquid volume of the bioreactor was removed and noted, and the biofilm was rinsed twice with a phosphate buffered saline (PBS) solution at pH 7 to remove any trace of the broth. The removed reactor broth was replaced with the same volume of the PBS solution. The attached biofilm was completely removed by mechanical friction of the

entire length of silicon tubing, both by increasing the liquid superficial velocity and by externally applying pressure.

4.2.7 BIOFILM COMPOSITION QUANTIFICATION

EPS was extracted from the sampled biofilm using the cation exchange resin (Dowex® Marathon® C sodium form, Sigma-Aldrich, Germany) method as it is reported to result in minimal cell lysis [144]. For separation, 10 mL of the harvested biofilm was poured into a 50 mL Duran bottle with 10 g of cation exchange resin (CER) and a magnetic stirrer was inserted. The mixture was then stirred at 600 rpm for 60 min at 4 ºC. After allowing for the decanting of the solid CER, the liquid phase was carefully removed and centrifuged at 20 000 g for 30 min at a temperature of 4 ºC. The cell precipitate was then dried in an oven at 70 ºC until a constant measured mass remained. The EPS concentrate was analysed for protein and polysaccharide content. The carbohydrate concentrations of the EPS were determined with the phenol sulphuric acid method using D-glucose as a standard [145]. The protein content was determined with a Lowry assay method using bovine serum albumin as a standard [146].

4.2.8 MTT ANALYSIS

The metabolic activity of the biofilm cells was quantified using the MTT method described by Wang et al. [147]. Water-insoluble formazan crystals are formed by the reduction of 3-(4,5-dimethylthiazol-2-yl)-2,5-diphenyl tetrazolium bromide (MTT) by the dehydrogenase system of viable cells in the biofilm. The formazan crystals are then dissolved using DMSO (Sigma-Aldrich, USA) and spectrophotometrically quantified at 550 nm to give a measure of metabolic activity. MTT stock solutions of 5 g L^{-1} were prepared using MTT powder (Sigma-Aldrich, St. Louis, MO) and ultra-purified water, filtered with sterile filters into 2 mL cryogenic vials and placed in a dark container at −40 ºC until use.

MTT assays were prepared in triplicate, and 20 µL of the MTT stock solution was pipetted into a cuvette, sealed and incubated in the dark at 37 ºC for 30 min. A 0.2 mL solution of homogenised biofilm sample was added to the cuvettes and further incubated for 60 min at 37 ºC for the reaction to take place, also in the dark. Subsequently, 2 mL of DMSO solution was added to the cuvette solution to dissolve the formazan crystals formed and the dissolution was left for 30 min. Absorbance measurements were then taken at 550 nm to quantify the metabolic activity (T60 UV/VIS Spectrophotometer, PG Instruments, Leicestershire, UK).

4.2.9 METABOLITE ANALYSIS

The concentrations of glucose and organic acids – succinic acid (SA), acetic acid (AA) and formic acid (FA) – in the fermenter broth were determined by the HPLC as described in Section 3.2.7. An Agilent 1260 Infinity HPLC (Agilent Technologies, USA), equipped with an RI detector and a 300 mm × 7.8 mm Aminex HPX-87H ion exchange column (Bio-Rad Laboratories, USA), was used.

4.3 RESULTS AND DISCUSSION

4.3.1 IMPACT OF SHEAR ON BIOFILM MORPHOLOGY

Figure 4-3 shows top views of the biofilm developed in high shear conditions (Figure 4-3, a,b,c) and low shear conditions (Figure 4-3, d-f) from day 1 to day 3 of biofilm cultivation. As expected, biofilm development was rapid since biofilms developed under both low shear and high shear achieved complete surface coverage by the first day of growth (Figure 4-3, a&d). However, after a day of cultivation, a marked difference could already be observed in the surface roughness of the developed biofilms. Biofilms developed under high shear appeared to have a smooth and nearly flat biofilm surface compared with low shear developed biofilms which were rougher, with many protuberances of small-cell microcolony structures (Figure 4-3, a&d). The observations were further confirmed by the quantitative biofilm data; the computed average roughness coefficient decreased from 0.61 on the first day to as low as 0.03 by day 3 for high shear conditions (Figure 4-4 a), whereas for low shear biofilms, roughness varied from 0.84 on the first day to 0.52 on day 3 (Figure 4-4 a). Biofilms cultivated in low shear conditions were at the beginning thicker in comparison with those cultivated under high shear conditions (Figure 4-4 c). This observation agreed with the literature because high shear conditions are often reported to result in thinner biofilms [138–140, 148, 149]. Structurally speaking, the high shear conditions physically impacted *A. succinogenes* biofilms by constantly eroding the biofilm surface, thus resulting in thinner and smoother biofilms compared with low shear conditions. However, by the third day of cultivation the average thickness of low shear biofilms declined to values markedly lower than those of high shear biofilms (22.9 µm vs 15.3 µm). This was caused by biofilm shedding for low shear conditions as slightly increased biomass was observed in the bioreactor effluent.

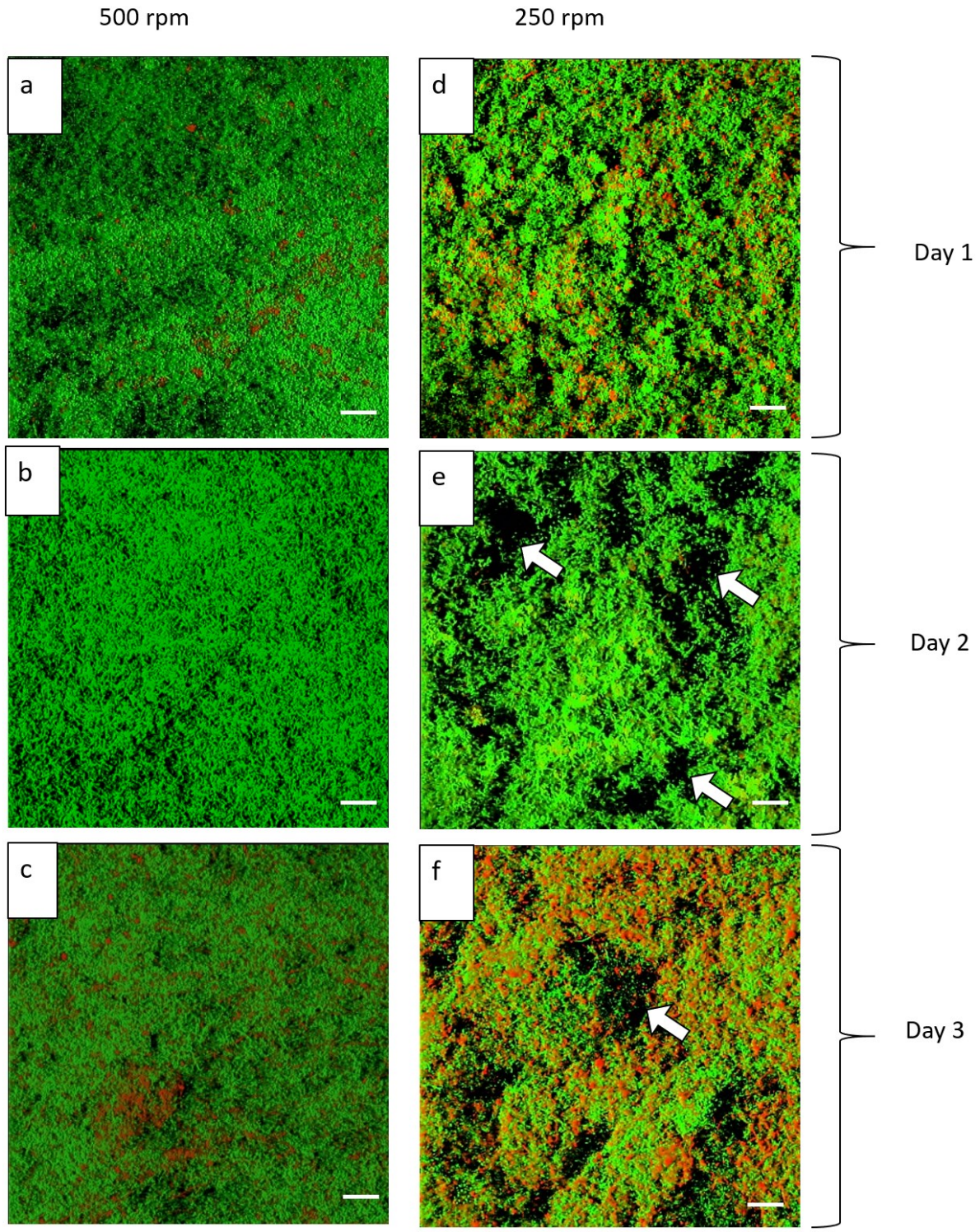

Figure 4-3: Comparison of biofilm morphology for cultivation at high (500 rpm) and low (300 rpm) shear development. Biofilm developed at low shear (LS) formed cell microcolonies, whereas that developed at high shear (HS) appeared much more homogenous (flat-shaped) in comparison. More voids (f & e, white arrows) can be seen at low shear compared with high shear where almost no voids are visible (b & c). The biofilm is mostly stained green on the first 2 days of growth indicating high cell viability, but red stains appear on the third day although red is not the dominant colour. The scale bar indicates 20 µm.

The biofilms developed under low shear appeared more porous (Figure 4-3 e, f) than those developed under high shear (Figure 4-3 b, c). It was further observed that for high shear biofilms, the voids in the biofilms were continually reduced during cultivation so that by day 3 almost no voids could be observed in the structure of the biofilm (Figure 4-3 c). Quantitative data showed that the average volume porosity varied from 0.21 to 0.00 for high shear and from 0.35 to 0.22 for low shear biofilms (Figure 4-4 b). This suggested that the high shear biofilms were becoming denser (more compact) in comparison with the low shear biofilms. Biofilms of *A. succinogenes* thus structurally responded to high shear conditions in a manner that agrees well with the findings in other works [139, 148, 150, 151] by forming smooth, less porous biofilms that are more compact and denser than those developed in low shear conditions. Compact biofilms are desirable considering the stability of the biocatalyst for extended continuous processing as they are less prone to events of biofilm shedding. This is probably the reason why biofilm shedding was observed in the low shear run but not in the high shear run. However, long periods of operation (beyond 3 days) must be employed to substantiate this observation. In contrast, high biofilm densities can be disadvantageous in that they are widely reported to decrease the mass transport of nutrients within the biofilm [139], and thus may cause regions of biofilm inactivity due to substrate unavailability in the deeper regions of the biofilm.

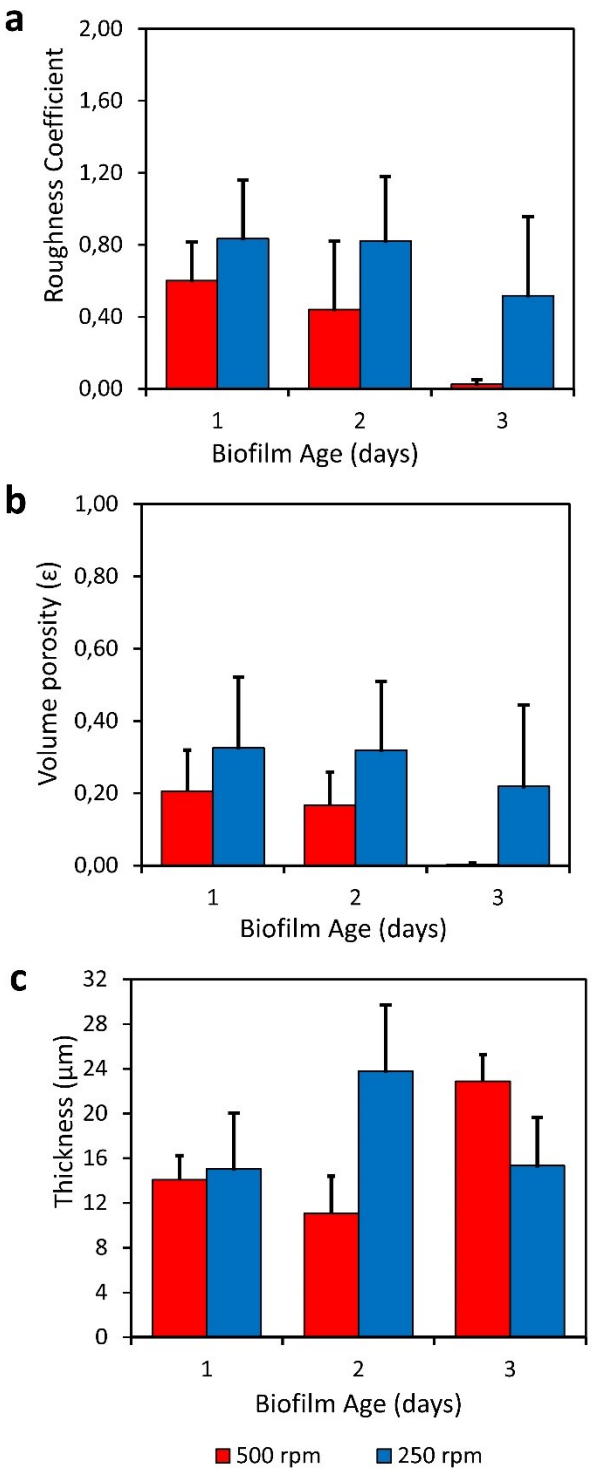

Figure 4-4: Quantitative characterisation of biofilms cultivated for low and high shears. In (A) the surface roughness coefficient of biofilms is compared for 3 days of cultivation. The porosity of biofilms is compared in (B) and biofilm thickness is compared in (C). High shear biofilms were less porous than low shear biofilms (B), demonstrating the compressive effect of high shear which results in compact biofilms. The zero roughness coefficient by the third day (A) shows that high shear biofilms became almost flat by the third day (A). Overall quantitative data agreed well with visual observations.

4.3.2 IMPACT OF SHEAR ON BIOFILM VIABILITY

The biofilm was stained with SYTO™ 9 and propidium iodide from the Baclight Bacterial Viability Kit, which allowed distinction between the "dead" and "live" cells within the biofilm. Dead cells emitted red fluorescence whereas living cells emitted green fluorescence. By counting the green and red pixels on each *xy*-plane image of a *z*-stack, it was possible to compute the percentage of "live cells". The calculation was performed for all the *z*-stacks collected on a sampling day and averaged to give the mean percentage of "live" cells in the biofilm for the day. Figure 4-5 shows the viability results.

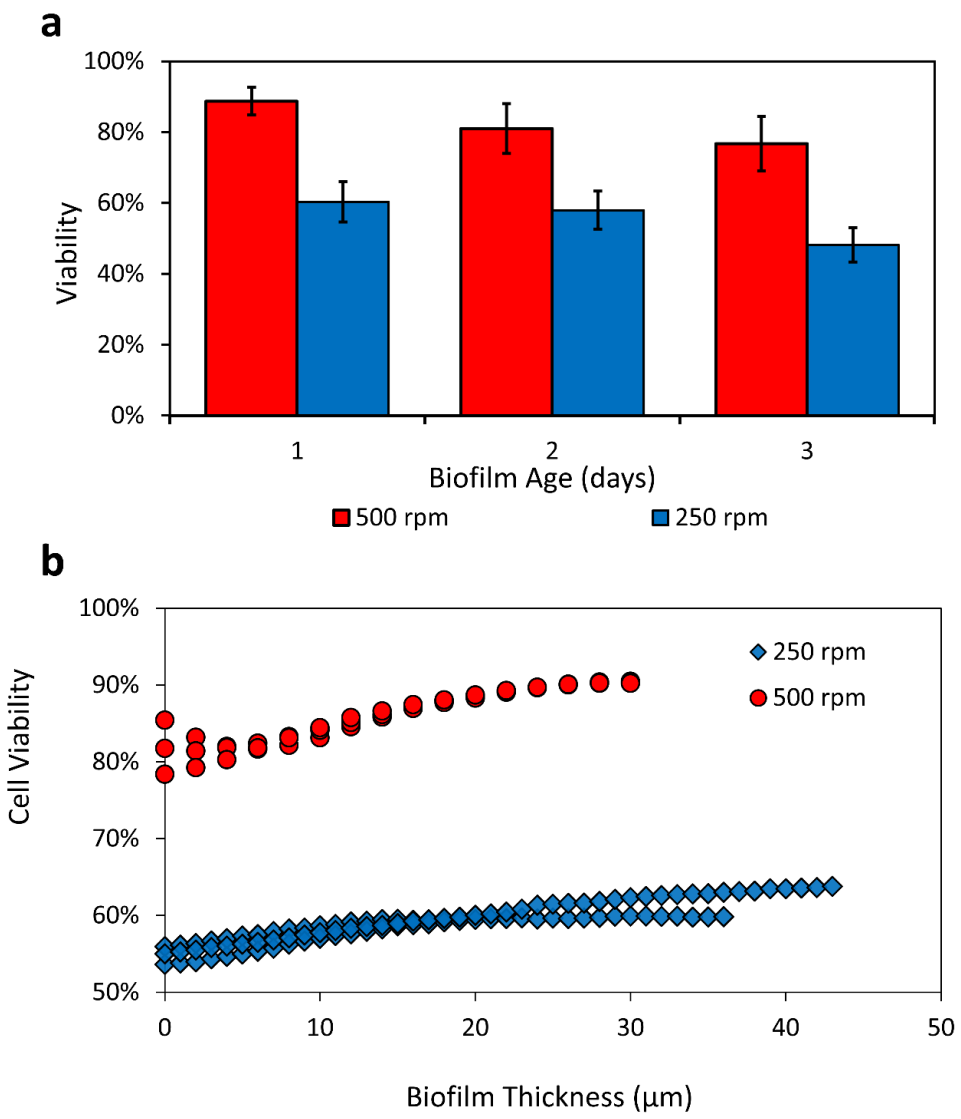

Figure 4-5: Comparison of biofilm viability for high and low shear biofilms for 3 days of cultivation (A). Percentage viability was computed by counting green (living cells) and red (dead cells) pixels for all images sampled on a particular day of biofilm cultivation. In (B), viability variation across biofilm depth is shown for day 2 biofilms for low and high shear conditions, zero thickness represents the substratum surface.

High shear conditions resulted in biofilms with a high percentage of "live" cells throughout the cultivation period (Figure 4-5(a)). The average fraction of active cells (over 3 days) for high shear conditions was 79% compared with 57% for low shear cultivated biofilm, although both experienced a decrease in cell viability as the cultivation period progressed. High shear conditions thus improved the viable cell content in the biofilm and helped to maintain a healthy biofilm. It is likely that increased biofilm viability in high shear conditions is a result of shear constantly eroding dead or inactive cellular material. A profile of the viable cell fraction across the biofilm depth for three randomly selected biofilm *z*-stacks on day 2 of growth is given in Figure 4-5(b) for both low and high shear biofilms. Although high shear biofilms have a markedly higher viability across the biofilm depth compared with low shear biofilms, cell viability decreases slightly (± 10%) towards the deeper layers of the biofilms for both conditions. This may indicate that there were minimal mass transfer effects across the biofilms, even though the high shear biofilms were denser.

Figure 4-6 compares the average viability of biofilms over 3 days for three shear conditions (250, 300 & 500 rpm); this includes data from a 300 rpm run reported in Chapter 3. The results clearly show that increasing the shear conditions in the fermenter leads to the formation of biofilm with a high content of viable cells. The average viable cell content increases from 57% to 65% when mixing intensity is increased from 250 to 300 rpm, and there is a further increase of 14% in viable cell content when mixing is increased from 300 to 500 rpm. This demonstrates that in addition to shaping the biofilm structure, shear may be employed to improve the viable cell content of the developed biofilm. However, it should be noted that increasing shear during biofilm cultivation will at a certain point prevent biofilm formation altogether or result in fewer biomass concentrations, which is undesirable for high SA volumetric productivities which require high cell concentrations. This was observed where the formation of biofilms at high shear conditions was entirely inhibited at high acid titres (unpublished data). It is therefore apparent that there are trade-offs, but these could not be explored in this study due to the mixing limitation of the employed setup at 500 rpm.

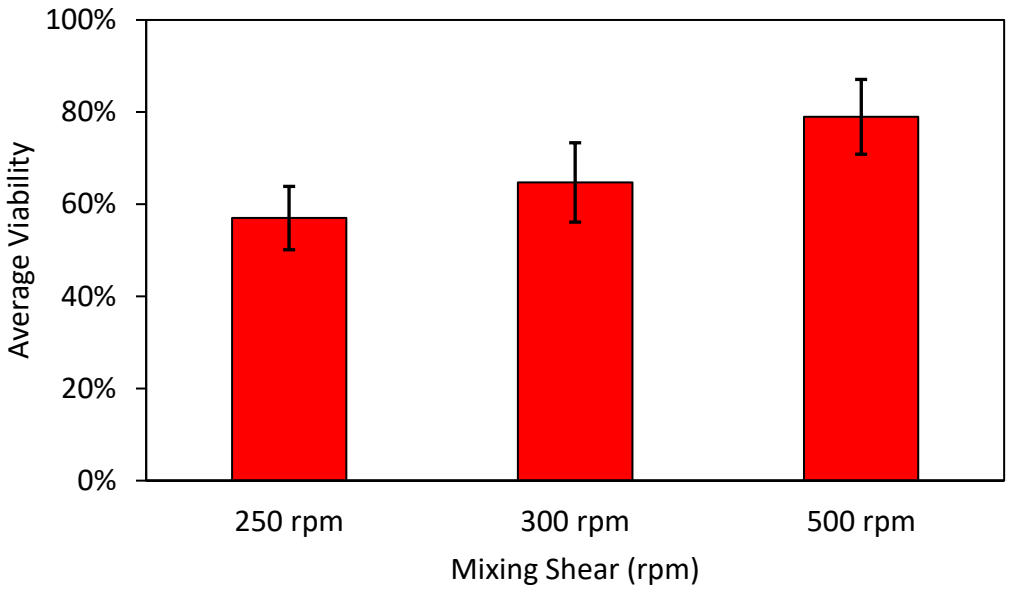

Figure 4-6: Comparison of three day-average biofilm viability for three shear conditions. The 300 rpm shear cultivation data was reported in Chapter 3**.** Increasing shear conditions in the fermenter lead to the formation of biofilm with a high content of viable cells.

Table 4-1 statistically compares computed biofilm porosity, roughness and cell viabilities for the two shear conditions employed in this study using a student t-test. The 3-day means are shown to be significantly different in all cases. This further consolidates the observations that shear impacted both the structure and viability of the biofilms. Overall, from the perspective of microscopic structure, high shear was shown to result in smoother, low-porosity biofilms – characteristics that are reportedly tied to stable biofilms – with a high content of viable cells.

Table 4-1: Statistical comparison of quantitative biofilm descriptive parameters

Parameter	Biofilm cultivation conditions		Statistical comparison		
	500 rpm	250 rpm			
	Mean*	Mean	P value	Difference between means	Comment
Roughness Factor	0.31 ± 0.05	0.755 ± 0.051	2.14×10^{-8}	0.44 ± 0.07	Means are significantly different (P< 0.05)
Porosity	0.11 ± 0.02	0.310 ± 0.027	2.26×10^{-8}	0.20 ± 0.04	Means are significantly different (P< 0.05)
Viability	78.9% ± 0.3%	57.0% ± 0.16%	0	22% ± 0.3%	Means are significantly different (P< 0.05)

* Mean calculated for samples collected over 3 days

4.3.3 IMPACT OF SHEAR ON BIOFILM CONCENTRATION AND COMPOSITION

Reactor B, a tubular reactor, was used to evaluate the effect of shear on the cell-based succinic acid productivity of biofilm structures developed in low shear (0.36 m s^{-1}) and high shear (0.64 m s^{-1}) conditions, as described in Section 4.2.6. In addition, however, the role of shear variation on biofilm composition and viability was also evaluated. Table 4-2 gives a summary of steady-state metabolite and biomass concentrations; steady state was confirmed by a steady average NaOH dosing rate for a 6 h period.

Fermentation runs conducted in low shear conditions (0.36 m s^{-1}) consistently achieved marginally higher total biomass concentrations than high shear (0.64 m s^{-1}) runs at similar dilution rates. For low dilutions of 0.2 h^{-1}, a low shear run achieved a total biomass of 9.5 g L^{-1} compared with 8.7 g L^{-1} for a high shear run, whereas at 0.9 h^{-1}, biomass concentrations of 15.4 g L^{-1} and 11.7 g L^{-1} were achieved for low shear and high shear conditions respectively. Since there is a set surface area within the tubular reactor, which was covered by biofilm, it follows that high shear conditions resulted in thinner biofilms due to lower total biomass concentrations. This ties in well with the microscopic visualisation results. Separating the EPS from the total biomass revealed that low shear runs had a higher fraction of dry cell weight (DCW) than high shear runs (Figure 4-7). The fraction of cells in the total biomass ranged from 0.77 to 0.85 for low shear runs and from 0.46 to 0.75 for high shear runs. Biofilms developed at high flow rates (hence high shear) therefore produced more EPS than low shear biofilms. This was especially evident at a dilution rate of 0.9 h^{-1} in which 6.31 g L^{-1} EPS was produced at high shear compared with 2.43 g L^{-1} EPS produced at low shear. The observation agrees with the study by Celmer et al. [139], which reported that high shear conditions induced the overproduction of EPS in biofilms. Since high detachment forces are experienced at high shear conditions, it appears that the biofilm reacted by producing more EPS to strengthen biofilm attachment.

Table 4-2: Steady-state fermentation results for biofilm fermentation at varied shear velocities

Shear velocity ($m\ s^{-1}$)	Run No.	D (h^{-1})	SA ($g\ L^{-1}$)	AA ($g\ L^{-1}$)	FA ($g\ L^{-1}$)	SA/AA	Total biomass ($g\ L^{-1}$)	Calculated biofilm thickness* (μm)
0.36	1	0.9	11.57 ± 0.35†	4.77 ± 0.06	2.4 ± 0.08	2.43	15.44 ± 0.04	258
	2	0.2	6.84 ± 0.10	4.19 ± 0.01	1.86 ± 0.01	1.63	9.54 ± 0.06	152
0.64	1	0.9	14.85 ± 0.6	5.6 ± 0.4	2.2 ± 0.2	2.65	11.69 ± 0.54	196
	2	0.2	6.75 ± 0.21	3.86 ± 0.02	2.16 ± 0.01	1.75	8.72 ± 0.4	120

* Thickness calculated assuming that dry biomass constitutes 10% of biofilm and uniform biofilm coverage of tubular bioreactor

† Standard deviation calculated for samples taken in triplicate

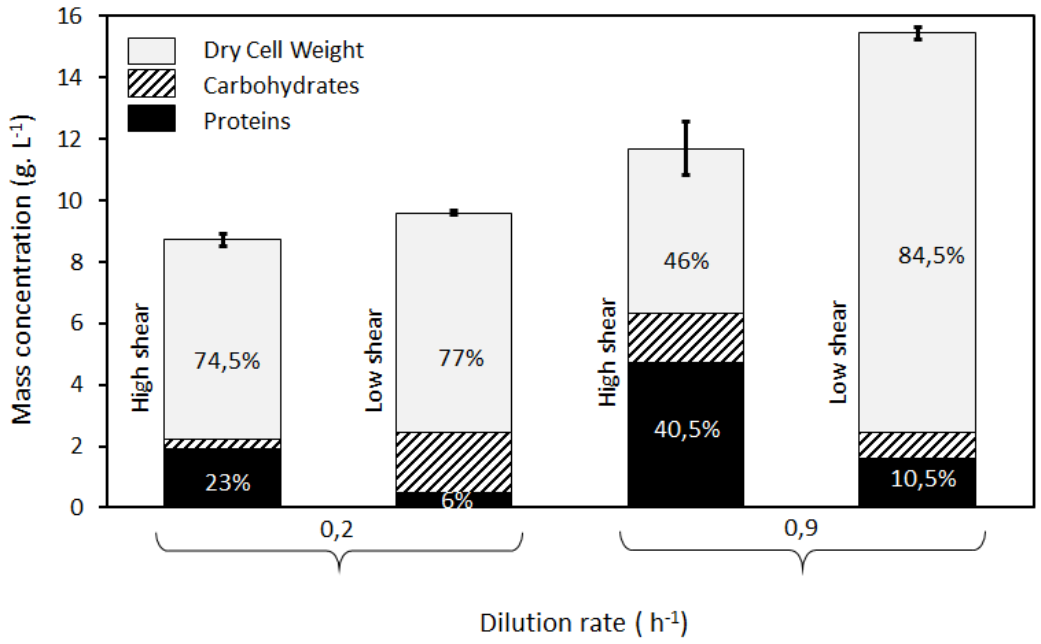

Figure 4-7: Biofilm composition characterisation at different shears and dilution rate. High biomass concentration was consistently achieved in low shear cultivation conditions compared with high shear conditions. High shear conditions resulted in EPS overproduction of which consisted of mostly consisted of proteins.

The composition of the EPS was further analysed for polysaccharides and protein content. High shear biofilm EPS contained comparatively more protein than low shear biofilm EPS (Figure 4-7). Several studies report high protein content in biofilms developed at high shear hydrodynamic conditions [138, 139]. Celmer et al. [139] found that high density biofilms were associated with biofilms with a high protein content. Proteins are said to strengthen the biofilm by providing more binding sites [139]. Assuming that high protein content would have the same impact in *A. succinogenes* biofilms, it can be concluded that shear resulted in denser biofilms, which ties in well with microscopic observations of high shear conditions resulting in low porosity and flat biofilms. Dense biofilms are desirable in continuous biofilm processes as they would result in process stabilities due to reduced biofilm sloughing/shedding. Fermenter stability was not evaluated in this study as biofilm was sampled immediately after steady-state conditions were reached. However, in the study by Maharaj et al. [20], frequent instabilities were reported due to biofilm shedding events when the *A. succinogenes* biofilm was cultivated at high dilution rates (low acid titres) and moderate shears.

4.3.4 IMPACT OF SHEAR ON BIOFILM METABOLIC ACTIVITY AND SUCCINIC ACID PRODUCTIVITY

Estimation of biofilm viability from microscopic images was based only on the sampled biofilm coupons and not on the entire biofilm in the fermenter. To consolidate the global and local cell viabilities, a 3-(4,5-dimethylthiazol-2-yl)-2,5-diphenyltetrazolium bromide (MTT) assay was used to assess the relative metabolic activity levels of the entire biofilm developed in bioreactor B at low and high shear. The levels of metabolically active cells are estimated on the principle of the extent of the conversion of MTT to formazan by the dehydrogenase system of viable cells with active metabolism. The formazan absorbance units per milligram of dry cell biomass was thus used to compare relative biofilm metabolic activity. Figure **4-8**(b) shows that high shear-developed biofilm achieved high metabolic activity per dry cell weight for both dilution rates investigated, as compared with low shear-developed biofilms. This consolidated the microscopic results which also showed that high shear biofilm was composed of a higher fraction of viable cells. Jones and Buie [153] reported increased metabolic activity with increasing shear in electroactive biofilms of *Geobacter sulfurreducens*, whereas Trulear and Characklis [154] and Liu and Taylor [155] reported that high shear also induced high metabolic activity in non-electroactive biofilms. This study thus also demonstrates the improved metabolic activity of *A. succinogenes* biofilms by increased hydrodynamic shearing conditions in line with previous observations [153–155].

Figure 4-8(a) shows the mass-based succinic acid productivity for both the low and high shear runs. The cellular mass in the biofilm was considered when calculating the cell-based SA productivity. Biofilms developed in high shear conditions achieved a three-fold higher succinic acid cell-based productivity (2.4 g g^{-1}DCW h^{-1}) compared with those cultivated in low shear conditions (0.81 g g^{-1}DCW h^{-1}) but at the same dilution rate of 0.9 h^{-1}. At the lowest dilution both low and high shear biofilms achieved comparable productivities, albeit slightly higher for high shear biofilms. The SA volumetric productivity for high shear-developed biofilm (13.3 g $L^{-1}h^{-1}$) was also marginally higher than that of the low shear-developed biofilms (10.4 g L^{-1} h^{-1}) for a 0.9 h^{-1} dilution rate. Even when considering the total biofilm biomass (DCW & EPS), high shear-developed biofilm achieved an almost two-fold higher mass-based productivity than low shear biofilm.

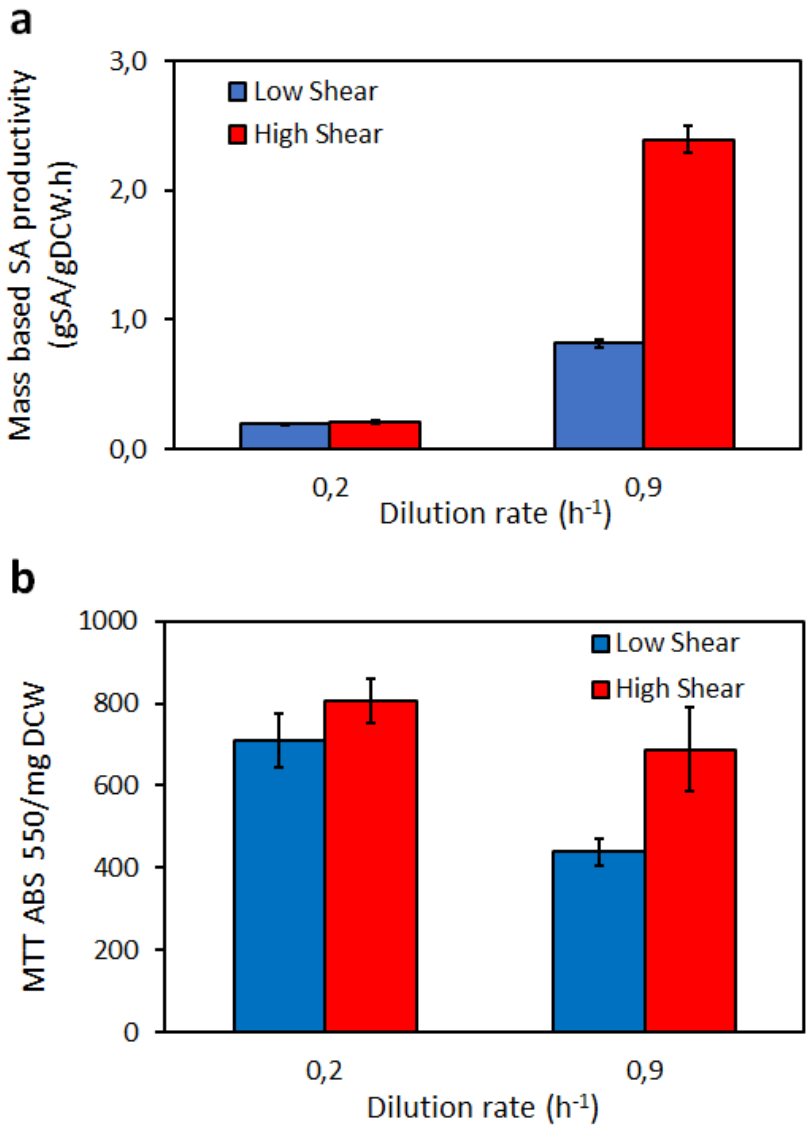

Figure 4-8: Comparison of cell-based succinic acid productivity for low and high shear (A) and metabolic activity for low and high shear (B). Cell-based succinic acid productivity improved with high shear biofilm cultivation (A), which is more evident at a 0.9 h^{-1} dilution rate. MTT assays showed that biofilms developed in high shear conditions were more metabolically active than those cultivated in low shear conditions. This ties in well with the viability results in Figure 4-5.

The results indicate that hydrodynamic shear conditions improved the metabolic activity of the biofilm, which was evidenced by the three-fold higher cell-based SA productivity of biofilms developed in high shear conditions. This result is supported by the microscopic work which showed that biofilms developed in high shear conditions achieved higher cell viabilities (79%, 3-day average) than those developed in low shear conditions (57%, 3-day average), and the

MTT assay results which revealed high metabolic activity in biofilms developed under high shear. The improved cell-based productivities are therefore a result of increased levels of active cells in the biofilm and increased metabolic activities caused by operation at increased shear conditions. This work demonstrates that shear plays an important role in continuous fermentations of *A. succinogenes* biofilms, by impacting biocatalysts both physically and physiologically.

4.4 CONCLUSION

In this chapter hydrodynamic shear conditions in a fermenter were shown to have a significant impact on the morphology, viability and metabolic activity of *A. succinogenes* biofilms. Biofilms developed in high shear environments were flat, smooth and less porous than those cultivated at low shear conditions which tended to be rougher and more porous. The biofilm consisted of a high EPS fraction when cultivated in high shear environments, with the proteins constituting a high fraction of the EPS. Since dense and strong biofilms are reported to have a high protein content, it follows that the biofilms developed in a high shear environment were denser and as a result more stable. Most importantly, however, biofilms developed under high shear conditions were more viable throughout the cultivation period. This translated into biofilms developed in high shear conditions exhibiting high cell-based SA productivity – three-fold higher than biofilms developed in low shear conditions.

5 INTERNAL MASS TRANSFER CONSIDERATIONS IN BIOFILMS OF *ACTINOBACILLUS SUCCINOGENES*

5.1 BACKGROUND

In Chapter 3 and Chapter 4, the role of both product accumulation and hydrodynamic shear conditions in shaping the biofilm morphology, viability and metabolic activity was investigated. The chapters gave insight into how these fermentation parameters can potentially be used as tools for the strategic manipulation of the development of optimised biofilms because of the impact they have on the resultant biofilm properties. However, since biofilms are immobilised catalysts, their performance will also be dependent on the mass transfer characteristics of the developed biofilm. Unlike free-cell fermentations, biofilm fermentations are prone to mass transfer limitation phenomena. Nutrients and substrates must diffuse within the biofilm matrix to be accessed by the biofilm cells [156]. Numerous biofilm fermentation studies on *A. succinogenes* include batch [23], fed-batch [23], repeat batch [25] and continuous [20, 21, 25] bioreactor operation strategies. In most of these studies the aim had been to elevate biomass concentrations and consequently raise volumetric productivities by utilising different biofilm immobilisation approaches. The studies consistently reported significant gains in product volumetric productivities, as compared with planktonic fermentations, but it is uncertain to what extent mass transfer effects were rate-limiting. Increased biomass development inherently causes significant increases in biofilm thicknesses which, as a result of mass transfer limitations, would probably cause substrate-depleted zones and/or SA-saturated zones within these biofilms. Mass transfer limitations not only lead to inefficient use of biocatalysts, but also result in process instabilities due to disintegration of biofilms [156]. This is likely to be one of the reasons why Maharaj et al. [20] reported difficulties in reaching and maintaining steady state at high dilution rates, due to frequent biofilm shedding events.

Internal mass transport limitations in biofilms are largely dependent on biofilm composition and properties, such as porosity and cohesiveness [156]. Dense biofilms are characterised by slow diffusion rates, whereas porous biofilms promote diffusion [157]. In addition, extracellular polymeric substances (EPS) in biofilms impede diffusion, which is a problematic property in

pathogenic biofilms as it increases resistance to antimicrobial treatments [158]. Chapters 3 and 4 have shown how both the composition and properties of *A. succinogenes* biofilms vary depending on the conditions of hydrodynamic shear and accumulated acid. Low shear conditions would result in porous structures and be favourable in terms of mass transfer, but the biofilms tend to be unstable and prone to shedding events [117, 135, 159]. On the other hand, dense biofilms formed in high shear conditions are known to be stable while limiting diffusion rates [117, 135, 159]. Central to the successful implementation of bulk microbial production of SA is the development of biofilms that are stable but do not limit potential productivities.

This chapter investigated internal mass transfer in biofilms of *A. succinogenes* by initially developing a theoretical transient internal mass transfer biofilm model, using intrinsic SA production kinetics estimated from resuspended batch biofilm fermentation experiments (i.e. to eliminate mass transfer limitations), in concert with known *A. succinogenes* biofilm properties from previous chapters. The model was validated by accurate prediction of experimental transient batch biofilm behaviour. Subsequently, the model was extended to pseudo-steady-state continuous operational conditions and used to assess how acid conditions, changes in biofilm density and composition, as well as in biofilm thicknesses, would affect glucose (Glc) availability and SA production effectiveness. Finally, a simplified method was proposed for the evaluation of pseudo-steady-state Glc penetration depth and active biofilm effectiveness – a tool for the design and optimisation of SA-producing *A. succinogenes* biofilm reactors. The bulk of the work in this chapter has been included in the paper submitted by Mokwatlo et al. to *Chemical Engineering Journal.*

5.2 METHODS AND MATERIALS

5.2.1 FERMENTATION MEDIUM

The fermentation medium was prepared in a manner similar to that described in Section 3.2.2. The glucose concentration was kept at 80 g L^{-1} for all batch experiments, except for one fermentation (batch 3) in which 125 g L^{-1} was used. CO_2 (Afrox, South Africa) was fed to the fermenters at 0.1 vvm.

5.2.2 BIOREACTOR

A silicone tube bioreactor presented in Section 4.2.2 and Figure 4-1 was used for all fermentations in this chapter. The reactor consisted of 3 mm diameter silicone tubing approximately 5 m in length, with an active volume that ranged from 50 to 70 mL depending on the gas hold-up at the time. Temperature and pH were controlled at 37.0 ± 0.1 °C and 6.80 ± 0.01 respectively. A Liquiline CM442 (Endress+Hauser, Gerlingen, Germany) coupled to a Ceragel CPS71D glass electrode (Endress+Hauser, Gerlingen, Germany) measured both temperature and pH, and controlled pH by dosing of a 10 M NaOH solution by means of a peristaltic pump connected to an internal relay. Temperature was controlled by a feedback PID controller, custom developed in Labview. All gas vents and inlets were fitted with 0.2 µm PTFE membrane filters (Midisart 2000, Sartorius, Göttingen, Germany) to ensure sterility.

5.2.3 BATCH FERMENTATIONS

All batch fermentations performed were preceded by a continuous fermentation period, during which the biofilm was established. After the biofilm had developed and pseudo-steady-state conditions had been achieved, a switch was made to batch operation. A sample was taken at the onset of the batch fermentation to note initial conditions for a batch run. The product outflow and feed inlet pumps were switched off to initiate batch fermentation operation. For batch 1 to batch 3, the developed biofilm was left intact on the inner walls of the silicone tube reactor during the entire batch fermentation to test for mass transfer effects. For a control run, i.e. “mass transfer-free” conditions, the developed biofilm was mechanically loosened from the inner silicone walls and mixed at high shear velocities until homogenous. In this way, for batches 4 and 5, the biofilm was resuspended to simulate a free-cell environment, and the recirculation velocity of the reactor volume was kept high to prevent biofilm cell re-attachment on the surface throughout the course of the batch fermentation. At the end of each batch fermentation, total

biomass concentration was determined by sampling the entire volume of the reactor, taking care to remove all the attached biomass (batches 1–3). The sampled biomass was further treated to extract extracellular polymeric substances and thus determine the fraction of the biofilm that consisted of cellular biomass. Table 5-1 gives a summary of the steady-state conditions that preceded the onset of batch fermentations for all the runs.

5.2.4 EPS EXTRACTION

The extraction of EPS was performed as described in Section 4.2.7, although the biofilm was only sampled at the end of the batch runs.

5.2.5 ANALYTICAL METHODS

The concentrations of glucose and organic acids in the fermenter broth were determined by High-Performance Liquid Chromatography (HPLC) as described in Section 3.2.7. An Agilent 1260 Infinity HPLC (Agilent Technologies, USA), equipped with an RI detector and a 300 mm × 7.8 mm Aminex HPX-87H ion exchange column (Bio-Rad Laboratories, USA), was used.

Table 5-1: Summary of initial concentration conditions before the start of batch fermentations

	Total biomass ($g\ L^{-1}$)	Biofilm cellular biomass ($g\ L^{-1}$)	Total cellular[i] biomass ($g\ L^{-1}$)	Glucose ($g\ L^{-1}$)	SA ($g\ L^{-1}$)	AA ($g\ L^{-1}$)	FA ($g\ L^{-1}$)
Batch 1	12.01	6.01	7.83	68.24	6.95	3.70	1.78
Batch 2	7.32	7.01	7.64	66.23	9.63	4.80	2.54
Batch 3	10.51	4.83	7.30	113.59	9.35	4.12	1.61
Batch 4[ii]	6.50	2.73	2.73	63.09	5.58	3.40	1.97
Batch 5[iii]	5.93	2.65	2.65	58.46	6.14	4.27	2.89

[i] Includes cellular biomass from the biofilm and suspended cellular biomass
[ii] Free-cell fermentation
[iii] Free-cell fermentation

5.2.6 THEORY AND MODEL DEVELOPMENT

In this section the mathematical equations and assumptions used to model internal mass transport in the biofilm of *A. succinogenes* are presented. A fixed-film biofilm bioreactor system is considered in this study. Since continuous bioreactor operation at steady-state conditions preceded batch operation, both operation modes are considered in the model as the former is necessary to evaluate initial metabolite and substrate concentrations in the biofilm prior to the onset of batch fermentation.

5.2.6.1 *A. SUCCINOGENES* KINETIC MODEL DESCRIPTION

The specific growth rate of *A. succinogenes* was modelled using product inhibition kinetics as described by a Gompertz asymmetrical sigmoid function and reported in the study by Brink and Nicol [21]. Lin et al. [17] reported a low Monod substrate saturation constant, signifying that the specific growth rate of *A. succinogenes* has low dependence on the substrate concentration, thus justifying the choice of product inhibition kinetics.

$$\mu = 0.82\left(1 - e^{-6e^{-0.54C_{SA}}}\right) \tag{5-1}$$

Equation (5-1) incorporates a maximum specific growth rate (μ_{max}) of 0.82 h^{-1} and succinic acid (C_{SA}) as the product inhibition variable. SA concentration is a good proxy variable for inhibition as growth appears to be strongly influenced by the SA concentration. As SA is the major by-product, it is therefore reasonable that it would be the major contributor to inhibition. The cell-based production rate of SA was simulated by a combination of growth-associated (ϕ) and maintenance-associated (θ) production rates, as expressed in Equations (5-2) and (5-3) [17, 21].

$$r'_{SA} = \phi\mu + \theta \tag{5-2}$$

$$\theta = \frac{kC_{SA}}{K_P + C_{SA} + \frac{C_{SA}^2}{K_I}} \tag{5-3}$$

Equation (5-3) shows that the maintenance-associated production rate was not modelled as a constant value but as a decreasing function of increasing SA concentrations by using a modification of the Haldane inhibition model [160]. This is in line with numerous observations of decreasing mass-based SA production rate with increasing SA titres [20, 22]. Figure 5-1 shows the ratio of production rates

of acetic acid (AA) to SA and those of FA to SA as a function of bulk SA concentrations respectively, obtained from prominent continuous fermentation studies of *A. succinogenes* [9, 10, 12, 26, 28]. The mass ratio functions obtained were used to relate the SA production rate to the AA and FA production rates, as given in Equations (5-4) and (5-5 below. Where $Y_{AA/SA}$ is the mass ratio of acetic acid to succinic acid , and $Y_{FA/SA}$ is the mass ratio of formic acid to succinic acid.

$$r'_{AA} = Y_{AA/SA} r'_{SA} \tag{5-4}$$

$$r'_{FA} = Y_{FA/SA} r'_{SA} \tag{5-5}$$

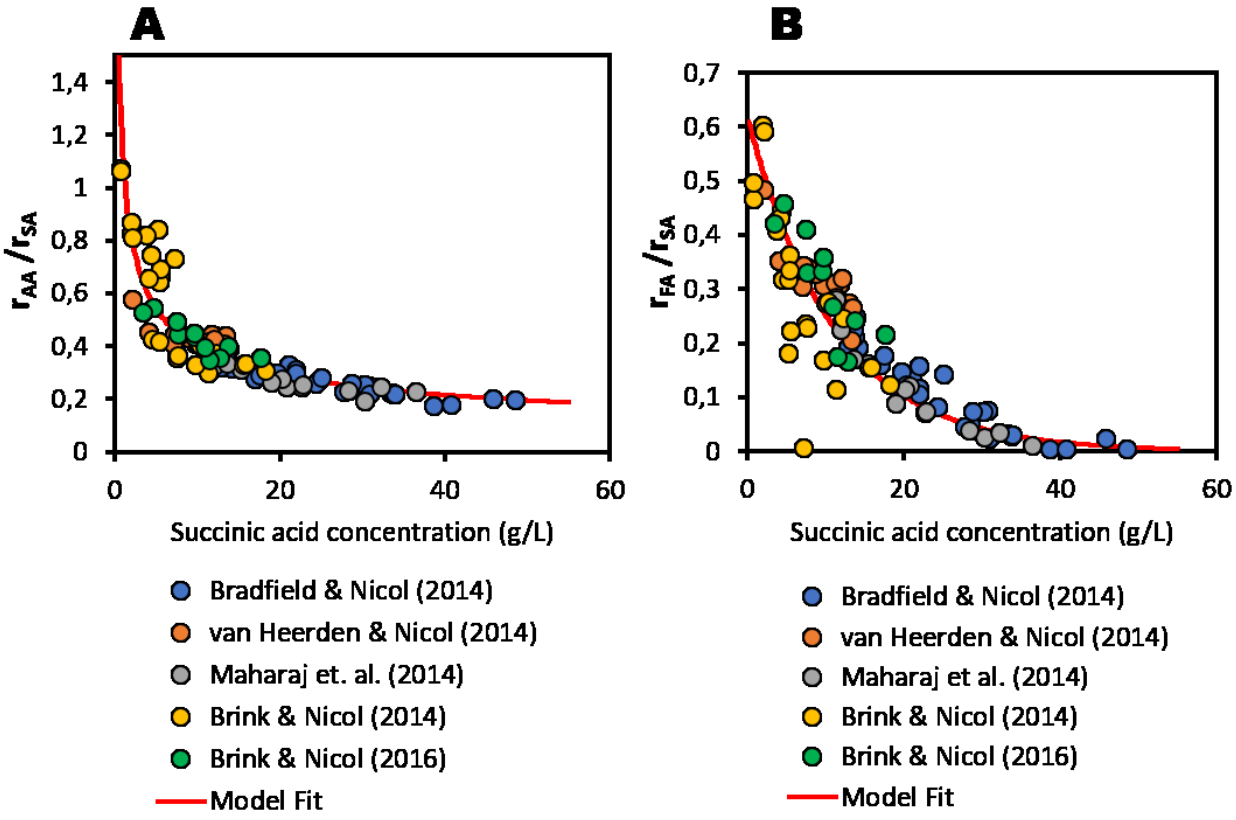

Figure 5-1: Steady-state production rate ratios of acetic acid to succinic acid (a) and formic acid to succinic acid (b). Data were obtained from prominent continuous biofilm fermentation studies.

The mass ratios are a function the succinic acid concentration given in Equations (5-6) and (5-7) (from Figure 5-1).

$$Y_{AA/SA} = 1.112C_{SA}^{-0.445} \quad (5\text{-}6)$$

$$Y_{FA/SA} = 0.6214e^{-0.09C_{SA}} \quad (5\text{-}7)$$

The Glc consumption rates were determined using an electron balance, given the production rates of the by-products (Equations (5-2) to (5-7)). In this balance, the electrons donated by Glc must be captured by the by-products and therefore a degree of reduction balance on a C-mol basis [161] is used to solve for the Glc consumption rate, as shown. To account for minor by-products, specifically pyruvic acid, these were expressed in terms of mass of FA using an equivalent electron base and incorporated into the production rate of FA in Equation (5-8).

$$r'_{Glc}\left(\frac{4}{30}\right) = r'_{SA}\left(\frac{3.5}{29.5}\right) + r'_{AA}\left(\frac{4}{30}\right) + r'_{FA}\left(\frac{2}{46}\right) \quad (5\text{-}8)$$

Combining Equations (5-4) and (5-5 with Equation (5-8) allows a simplified expression of the Glc consumption rate:

$$r'_{Glc} = \left(0.89 + Y_{\frac{AA}{SA}} + 0.33Y_{\frac{FA}{SA}}\right)r'_{SA} \quad (5\text{-}9)$$

5.2.6.2 CONTINUOUS OPERATION PSEUDO-STEADY-STATE CONCENTRATION PROFILES IN THE BIOFILM

To calculate the pseudo-steady-state concentrations of the substrate and the metabolic products in the biofilm layer, the following assumptions were made.

- The geometry of the biofilm is assumed to be a uniformly thick planar slab with one side adjoined to an impermeable substratum surface and the other side exposed to the bulk liquid phase.
- The components of the biofilm, i.e. the cells and the extracellular polymeric substances (EPS) as well as the water in the porous section of the biofilm, are homogenously distributed throughout the biofilm.

- External mass transfer limitation between the biofilm and the liquid interface is neglected.
- Only one-dimensional internal mass transport which obeys Fick's Law is present.

Under pseudo-steady-state conditions, there is no mass accumulation within the biofilm layer, and therefore the rate of reaction equals the rate of diffusion at any point in the biofilm. Equation (5-10) gives the general mass balance used to solve for the concentration profiles. Where D_{e_j} is the effective diffusivity of metabolite j in the biofilm, and C_{XB} is cell concentration in the biofilm phase.

$$D_{e_j} \frac{d^2 C_j}{dz^2} = r_j' C_{XB} \tag{5-10}$$

with the following boundary conditions:

$$\begin{cases} for\ z = \mathrm{L}, & C_j = C_{j-aq} \\ for\ z = 0 & \dfrac{dC_j}{dz} = 0 \end{cases}$$

The system of second-order differential equations describing the concentrations of products and the substrate was solved numerically with an iterative procedure using a finite difference method. More detail regarding the discretisation of the system is presented in the Appendix.

5.2.6.3 BATCH OPERATION MODEL DESCRIPTION

The batch system consists of the bulk liquid phase and the biofilm phase. In the liquid phase suspended cells grow and convert the substrate to products, and there is diffusion of metabolic products and the substrate out of and into the biofilm phase, respectively. Equations (5-11) and (5-12) give a generic mass balance in the liquid phase.

$$\frac{dC_{j_{aq}}}{dt} = r_j' C_{X,aq} + J_j \tag{5-11}$$

$$J_j = D_{e-j} A_p \frac{dC_j}{dz}|_{z=L} \tag{5-12}$$

In the biofilm phase, the general mass balance is presented as in Equation (5-13).

$$\frac{dC_j}{dt}|_z = -D_{e-j} \frac{d^2 C_j}{dz^2} + r_j' C_{XB} \tag{5-13}$$

The batch system of equations was simulated using numerical methods by discretising the system of equations. A detailed description of the discretised system used is given in Appendix b.

5.2.6.4 ESTIMATION OF THE EFFECTIVE DIFFUSIVITY, DE

The parameter $D_{e\text{-}j}$ represents the effective diffusion constant of compound j in the biofilm as related to the aqueous diffusion constant. Effective diffusivity constants were estimated for each metabolic product and for the substrate using the mathematical model proposed by Hinson and Kocher [162] specifically developed for determining effective diffusivities in biofilms (Equation (5-14)). The model uses the biofilm volume fractions of the cells (ε_{cells}), extracellular polymeric substances (ε_{EPS}) and water (ε_W) to estimate diffusivities ($\varepsilon_{cells} + \varepsilon_{EPS} + \varepsilon_W = 1$). It was assumed that wet biofilm consisted of 90% water on a volume basis.

$$\frac{D_{e-j}}{D_{aq-j}} = \left(\frac{D_{e-j}}{D_{eo-j}}\right)\left(\frac{D_{eo-j}}{D_{aq-j}}\right)$$

$$\frac{D_{e-j}}{D_{eo-j}} = \left[\frac{\frac{2}{D_{cr}} + \frac{D_{aq-j}}{D_{eo-j}} - 2\varepsilon_{cells}\left(\frac{1}{D_{cr}} - \frac{D_{aq-j}}{D_{eo-j}}\right)}{\frac{2}{D_{cr}} + \frac{D_{aq-j}}{D_{eo-j}} + \varepsilon_{cells}\left(\frac{1}{D_{cr}} - \frac{D_{aq-j}}{D_{eo-j}}\right)}\right] \tag{5-14}$$

$$\frac{D_{eo-j}}{D_{aq-j}} = \varepsilon_W\left[\frac{\varepsilon_{EPS}}{D_{pr}} + \varepsilon_W\right]^{-1}$$

5.3 RESULTS AND DISCUSSION

5.3.1 BATCH FERMENTATIONS

Figure 5-2 presents the batch profile results for SA, Glc, AA and FA attained in the free-cell batch fermentation experiments (batches 4 & 5). Initial batch conditions for these runs can be found in Table **5-1**. Since biomass measurements were only taken at the end of each fermentation, the initial biomass concentrations for all batch fermentations is uncertain, but as all fermentations operated at a C_{SA} greater than 10 $g.L^{-1}$ for more than 90% of the runs, it is assumed that negligible biomass growth took place due to severe product inhibition [21]. Repeatable results were obtained for all the metabolic products as well as the Glc profile, as seen in Figure 5-2 . No lag phases were observed since batch fermentation was preceded by continuous fermentation operation, during which the biofilm was developed. Prior to the beginning of the batch operation of batches 4 & 5, however, biofilm cells were mechanically loosened from the inner silicon walls and mixed at high shear velocities until they were homogenous in order to emulate free-cell batch fermentation. The concentration profiles in Figure 5-2 were used to estimate the intrinsic "mass transfer-free" kinetic model parameters for Equations (5-2)

and (5-3). The fitted parameters are presented in Table 5-2. As can be seen in Figure 5-2(e), the kinetic model gave a good prediction of the Glc, SA, AA and FA curves – estimated $R^2 = 0.984$ and RMSE = 2.12.

Table 5-2: Estimated model parameters for equations

Parameters	Value	Units	Equation
ϕ	3.60	g. g^{-1}	(5-2)
K	3.00	g. g^{-1} h^{-1}	(5-3)
Kp	13.15	g. L^{-1}	(5-3)
Ki	7.52	(g. L^{-1})^2	(5-3)

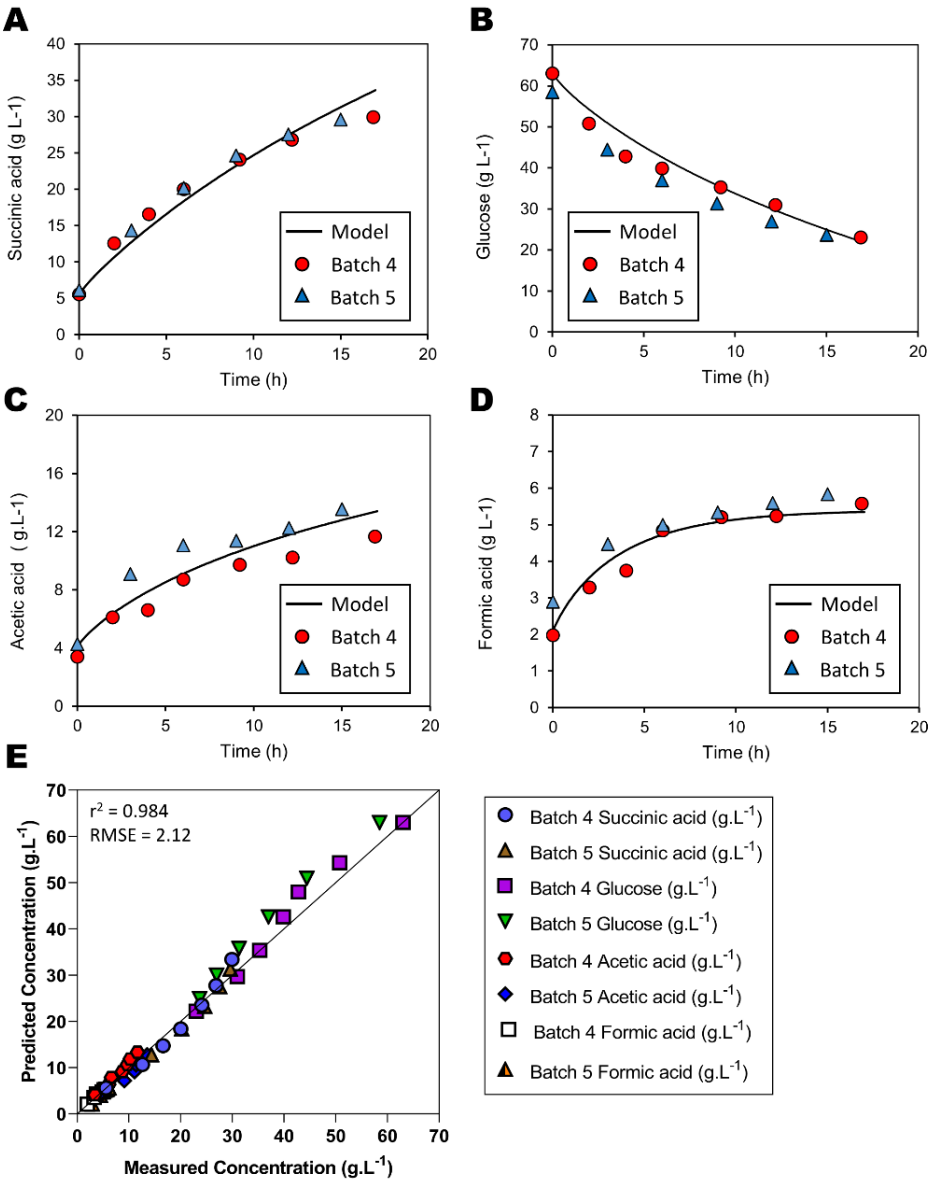

Figure 5-2: Resuspended biofilm "free-cell" batch fermentation concentration profiles for (A) SA, (B) Glc, (C) AA and (D) FA. The solid line shows the predicted concentrations according to the intrinsic kinetic model. (E) shows the parity plot of the predicted metabolite and substrate concentrations vs the measured concentrations.

The batch model presented in Section 5.2.6.3, which considers internal mass transfer, was used to simulate mass transfer effects in batches 1, 2 and 3. To do this, the final total dry biofilm biomass measurements (Table 5-1) were used to estimate the biofilm thickness (L) by assuming that dry biomass constituted 10% of the wet biofilm weight, with a homogenous distribution of biofilm across the entire inner silicone tube area with a fixed thickness. The initial concentrations within the biofilm were solved by using the model presented in Section 5.2.6.2, in pseudo-steady-state conditions. The

results for the simulation are shown in Figure 5-3 as solid lines in the Glc and SA graphs for batches 1, 2 and 3. It can be seen that by accounting for internal mass transfer effects within the biofilm, good predictions were attained (r^2 = 0.981 and RMSE = 3.57 in Figure 5-3 (g)), which closely followed the observed measured concentration profiles. In contrast, significantly poorer prediction was observed when mass transfer effects were ignored (r^2 = 0.947 and RMSE = 6.11 in Figure 5-3 (h)). The same trend was observed for AA and FA profiles. This confirmed the presence of mass transfer effects in batches 1 to 3. Figure 5-3 further shows both models with and without the inclusion of mass transfer effects – demonstrating the impact of mass transfer on the SA and Glc measured in the bulk phase.

In addition, SA reached maximum titres of between 62 $g.L^{-1}$ and 72.1 $g.L^{-1}$ for batches 1, 2 and 3 compared with maximum titres of 29.9 g L^{-1} and 29.6 g L^{-1} SA for free-cell batch fermentations (Figure 5-2). Low total cellular biomass in free-cell batch fermentations (2.73 $gDCW.L^{-1}$ and 2.65 $gDCW.L^{-1}$) as compared with higher total cellular biomass in the biofilm batch runs (7.83 $gDCW.L^{-1}$, 7.64 $gDCW.L^{-1}$ and 7.3 $gDCW.L^{-1}$) caused distinct differences in the observed maximum SA titres. Moreover, as can be seen in Figure 5-3, according to the intrinsic "mass transfer-free" kinetic model, the simulated batch profiles for biofilm batches 1, 2 and 3 predict faster rates than those experimentally observed.

The simulated biofilm batch profiles reached the final titre conditions 2 h earlier for batch 1 (Figure **5-3**(a)), 1 h earlier for batch 2 (Figure 5-3 (c)) and 9 h earlier for batch 3 (Figure 5-3(e)) than measured in the bulk of the reactor. These results clearly indicated mass transfer effects, resulting in limited volumetric productivity rates.

The internal mass transfer batch model appeared to describe the mass transfer effects of the modelled reactor system adequately, using the Hinson and Kocher [162] mathematical model to predict the effective diffusivities of the metabolic products and the substrate within the biofilm.

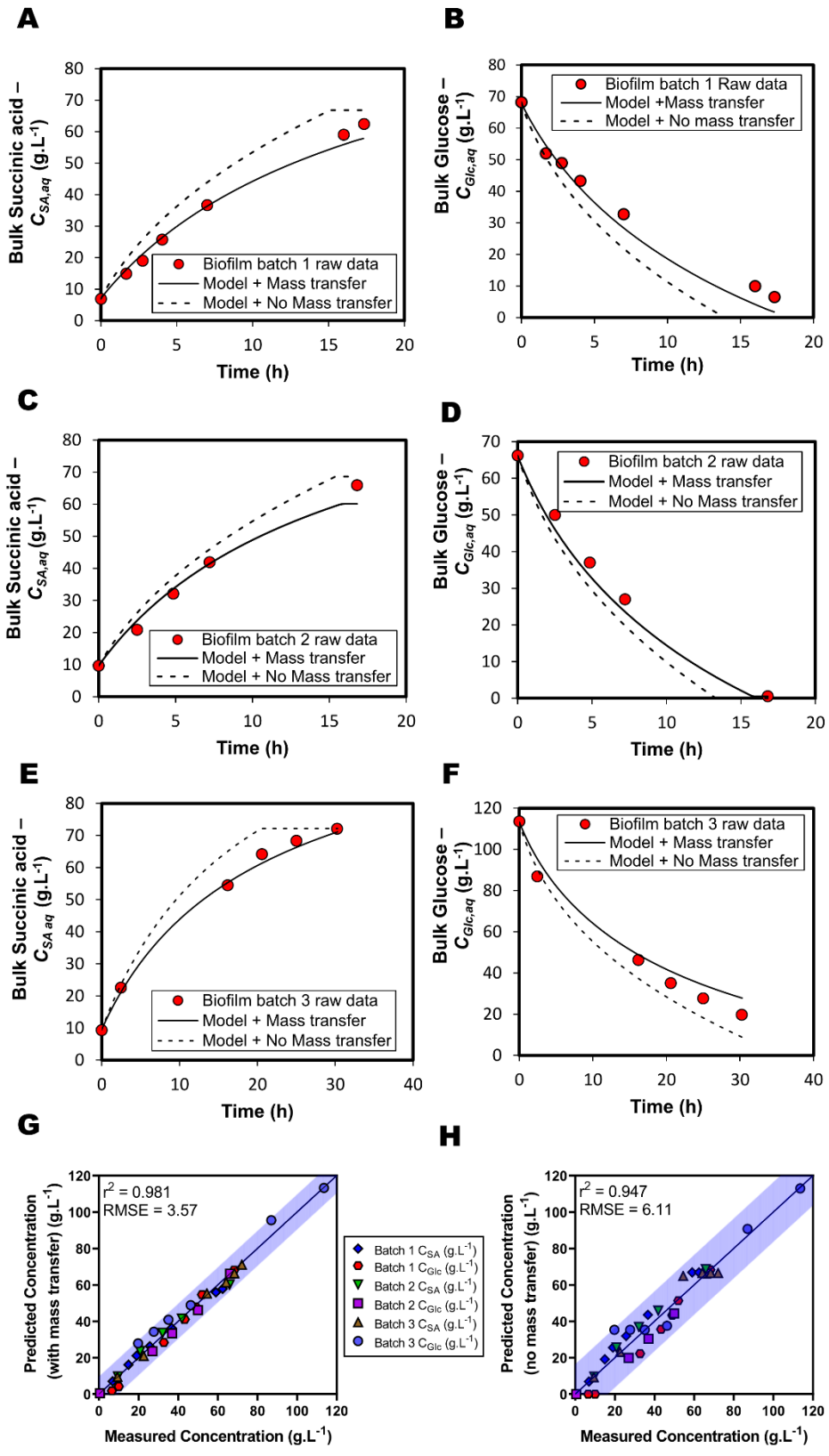

Figure 5-3: Biofilm batch concentration profiles for SA (A, C and E) and Glc (B, D and F) for batches 1 to 3. The dotted lines show the predicted concentration profiles according to the developed intrinsic kinetic model. The solid lines show the concentration profiles obtained when internal mass transfer in the biofilm is accounted for. (G) Parity plot of the Model + Mass transfer vs experimental data. (H) Parity plot of the Model + No Mass transfer vs experimental data.

5.3.2 INTERNAL MASS TRANSFER IN BIOFILM BATCH FERMENTATION

In Figure 5-4(A), the intrinsic cell-based SA productivity according to the kinetic model (fitted from free-cell fermentation results) is compared with the cell-based SA productivities of biofilm batches 1, 2 and 3, all as a function of SA titre. For the batch 1 and batch 3 runs, the cell-based SA productivity was consistently lower than the intrinsic cell-based productivities throughout most of the fermentation period, whereas for batch 2, lower cell-based SA productivities were attained only until an SA titre of 30 $g.L^{-1}$ was reached, after which the productivities were equal to the intrinsic productivities throughout. This suggested that batch 2 experienced mass transfer effects only in the beginning stages of the batch fermentation (first 5 h), after which intrinsic kinetics were observed.

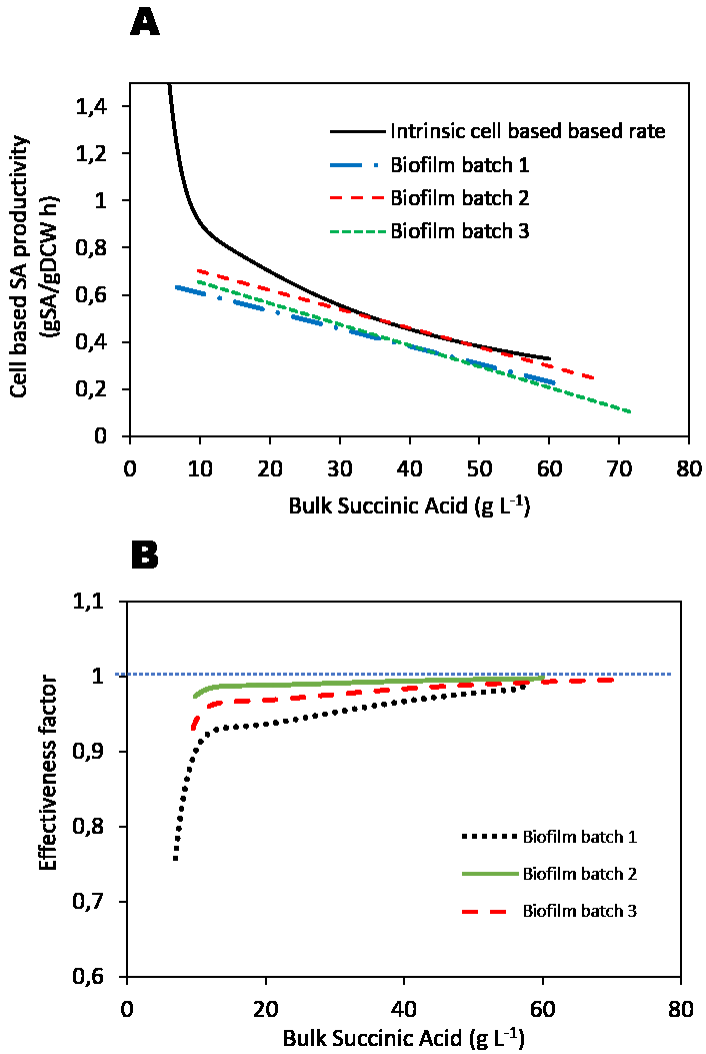

Figure 5-4: Comparison of cell-based SA productivity as a function of SA titres in bulk phase for biofilm batches with the intrinsic rates (a). Biofilm effectiveness factor during batch operation as a function of bulk SA titres (b).

The concentration profiles of Glc and metabolic products throughout the biofilm thickness were predicted for each time point in the batch simulations. Figure 5-5 shows the C_{SA} and C_{Glc} profiles in the biofilm depth at selected time points; the dashed lines indicate the bulk concentrations in the reactor, i.e. at a biofilm depth of 0 µm. The gradients of both C_{Glc} and C_{SA} within the biofilm are higher at the start of fermentation and subsequently decrease with time for all batches. The metabolite gradients were steeper in batch 1 followed by batch 3, and significantly low gradients were observed in batch 2. It is fitting that less mass transfer effects were observed in batch 2 as it attained the lowest estimated biofilm thickness (120 µm) as well as the lowest fraction of EPS in the biofilm (0.03). Moreover, mass transfer effects were dominant in batch 1 where the maximum estimated biofilm thickness of 205 µm was observed. Decreasing gradients within the biofilm with time make sense as increasing C_{SA} decreases cell-based rates due to product inhibition, and thus the difference between diffusion rates and reaction rates is reduced.

An effectiveness factor (η) was computed as the ratio of the r'_{SA} at the average C_{SA} in the biofilm to the r'_{SA} in bulk SA conditions (Equation (5-15)). The η parameter quantifies the mass transfer effects present in the biofilm. The closer to unity, the less the mass transfer limitations experienced by the biofilm and vice versa.

$$\eta = \frac{r'_{SA}\,|_{C_{SA_{avg}}}}{r'_{SA}\,|_{C_{SA_{aq}}}} \tag{5-15}$$

The C_{SA} profiles shown in Figure 5-5 were used to calculate the effectiveness factors of the biofilm throughout the batch fermentations and are shown Figure 5-4(B). The effectiveness factor of the biofilm in batch 1 ranged from 75% at the beginning of the batch to 99% at the end of fermentation, from 97% to 100% for batch 2, and from 92% to 100% for batch 3. Mass transfer effects were nearly negligible in batch 2. In batch 1, however, the biofilm began with a low effectiveness factor of 75% which was most likely caused by low initial SA titres of 6.95 $g.L^{-1}$, whereas for batches 2 and 3, SA titres started at 9.63 and 9.35 $g.L^{-1}$ respectively. The subsequent rapid increase in the effectiveness factor at the early stages of batch 1 is due to the rapid change in acid conditions which reduces reaction rates as a result of product inhibition.

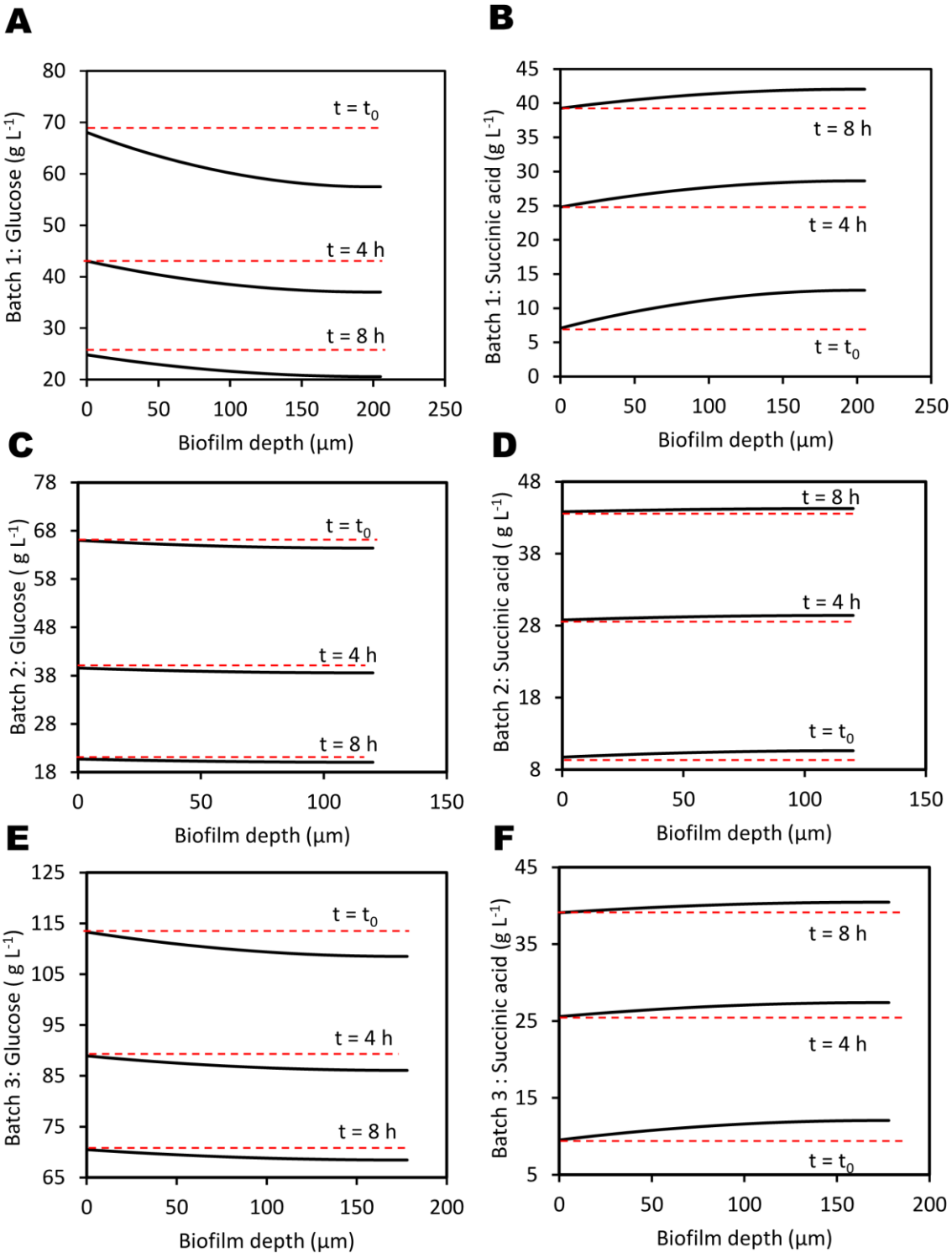

Figure 5-5: Concentration profiles of SA (B, D and F) and Glc (A, C and E) in the biofilm at selected times

5.3.3 EXPANDED ANALYSIS OF THE MODEL AT PSEUDO-STEADY-STATE CONDITIONS

In this section the pseudo-steady-state model (Section 5.2.6.2) was used to gain insight into the influence of the biofilm properties and reaction conditions on the overall effectiveness of the biofilm during continuous pseudo-steady-state fermentations. The complex nature of the model required a method to combine the interactions of the various parameters in a mechanistically interpretable way. A data set of pseudo-steady state biofilm results was obtained by combining results for pseudo-steady state fermentation studies by Maharaj et al. [20], Brink & Nicol [21, 165], and from Chapter 4 (Table 5-3), and a generated set of realistic pseudo-steady state biofilm conditions (Appendix – Table A-1). The data were chosen specifically because it included a significant variation in the shear conditions, biofilm biomass composition, total biomass concentrations (which affects thicknesses), and pseudo-steady state SA titres.

The conditions for each pseudo-steady state was modelled using the pseudo-steady state model from Section 5.2.6.2. The individual interactions between the system variables (L^*, D_e, C_{SA}, C_{XB}) and the overall biofilm effectiveness (η),), as predicted by the pseudo-steady state model (Section 5.2.6.2), are shown in Figure 5-6. The Pearson correlation coefficient heat map in Figure 5-6 show that poor correlation was observed between η and. the system variables. Note: The η values indicate the effectiveness of the L^* depth therefore ignoring any additional biologically inactive biofilm.

Traditionally, catalyst effectiveness is related by a Thiele modulus, which is a dimensionless factor reflecting the ratio of reaction rate to the rate of diffusion in the catalyst [163, 164]. Thiele moduli are derived by non-dimensionalising the component balance under pseudo-steady-state conditions [163, 164]. To obtain the equivalent of the Thiele modulus for the *A. succinogenes* biofilm (α^2), SA was used as a proxy variable in the pseudo-steady-state internal mass transfer balance given in Equation (5-10) due to its impact on *A. succinogenes* kinetics. In addition, Equation (5-10) was further simplified by neglecting growth-associated SA production; the range of SA titres of industrial interest is $\gg 10$ g.L^{-1} and growth is negligible above 10 g L^{-1}[21]. The pseudo-steady-state component balance in Equation (5-10) was therefore simplified to Equation (5-16).

$$D_{e-SA}\frac{d^2C_{SA}}{dz^2} = \frac{kC_{SA}}{K_P + C_{SA} + \frac{C_{SA}^2}{K_I}}\mathrm{C}_{XB} \tag{5-16}$$

Equation (5-16) was subsequently non-dimensionalised to Equation (5-17).

$$\frac{dC_{SA}^{*}}{dZ^{2}} = \frac{\alpha^{2} C_{SA}^{*}}{1 + \beta C_{SA}^{*} + \gamma\beta C_{SA}^{*2}} \tag{5-17}$$

where the non-dimensional SA – C_{SA}^{*} is defined by $\frac{C_{SA}}{C_{SA_{aq}}}$ and the non-dimensional biofilm thickness Z is z/L^{*}. The non-dimensional parameters α^{2}, β and γ are given by $\alpha^{2} = \frac{kL^{*2}C_{XB}}{D_{e-SA}K_{P}}$, $\beta = \frac{C_{SA_{aq}}}{K_{P}}$ and $\gamma = \frac{C_{SA_{aq}}}{K_{I}}$.

It is interesting to note the similarity between the dimensionless parameter α^{2} and the traditional Thiele modulus for a first-order reaction system. It can be concluded that at sufficiently low concentrations of SA, the system will behave as a first-order system. As SA increases, the system will experience significant product inhibition as quantified by the dimensionless inhibition parameters β and γ, thereby deviating from first-order behaviour. To account for this inhibition on the system, a new dimensionless parameter (m) was defined (Equation (5-18))

$$m = \sqrt{\frac{\alpha^{2}}{1 + \beta + \gamma\beta}} \tag{5-18}$$

Equation (5-18) requires knowledge of the dimensionless parameter α^{2} and consequently L^{*} preferably without the need to solve the overall mass transfer model. Stewart [156] defined pseudo-steady state Equation (5-19) in which biofilm penetration can be calculated as the depth at which the rate of diffusion of Glc into the biofilm equal the rate of consumption of the Glc in the biofilm, therefore at full Glc depletion.

$$L^{*} = \begin{cases} \sqrt{\frac{2D_{e-Gluc}C_{Gluc_{aq}}}{\overline{r'_{Glc}}C_{XB}}} ; \sqrt{\frac{2D_{e-Gluc}C_{Gluc_{aq}}}{\overline{r'_{Glc}}C_{XB}}} < L \\ L ; \sqrt{\frac{2D_{e-Gluc}C_{Gluc_{aq}}}{\overline{r'_{Glc}}C_{XB}}} \geq L \end{cases} \tag{5-19}$$

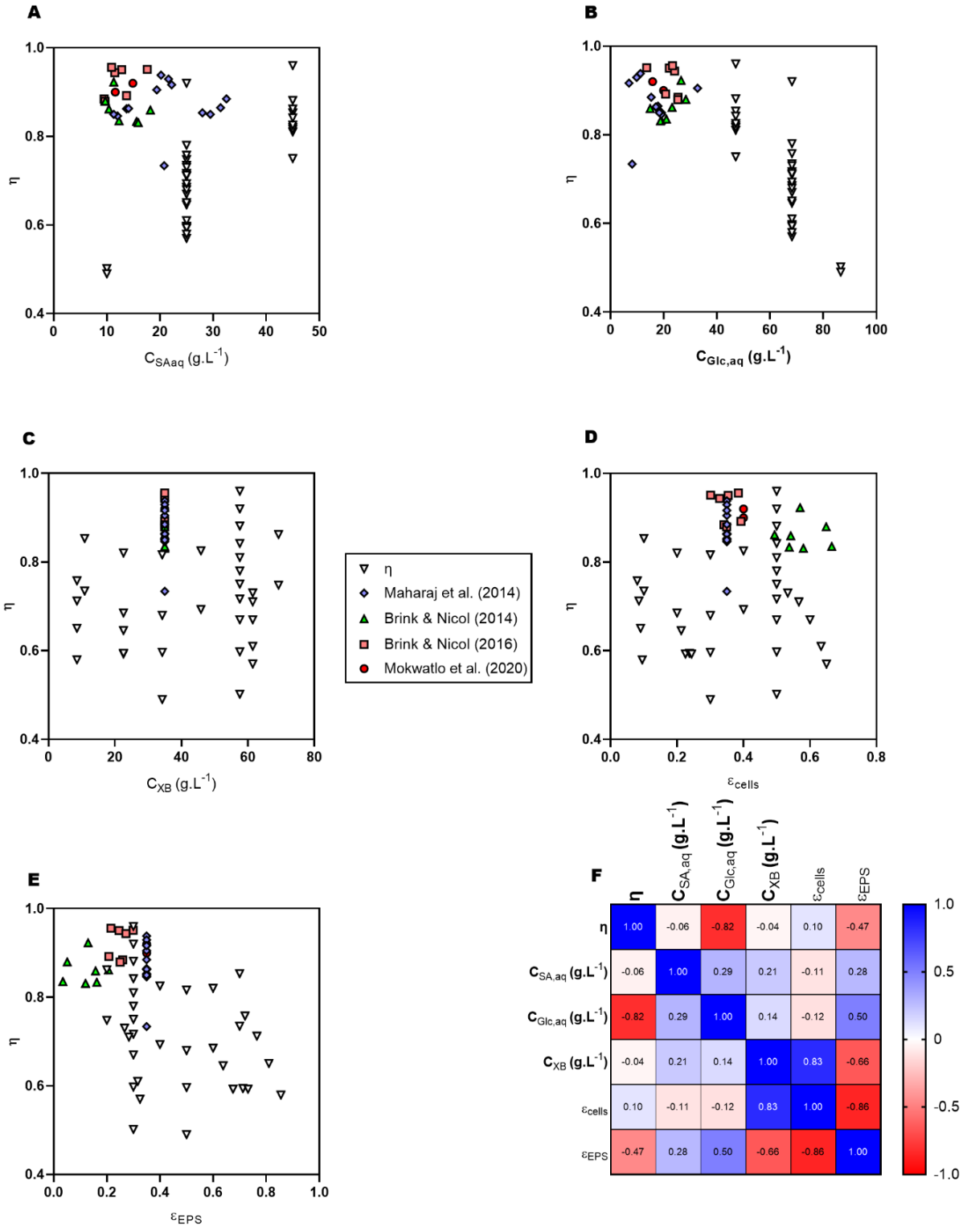

Figure 5-6: Interaction between system variables (L^*, $D_{e\text{-}SA}$, C_{SA}, C_{XB}) and biofilm effectiveness (η)

Table 5-3: Continuous fermentation pseudo-steady-state data used to analyse internal mass in the tubular biofilm reactor (Sources: Maharaj et al. [20], Brink & Nicol [21, 165] and Chapter 4)

Dilution rate (h^{-1})	Glc out ($g.L^{-1}$)	ΔGluc ($g.L^{-1}$)	SA ($g.L^{-1}$)	AA ($g.L^{-1}$)	FA ($g.L^{-1}$)	Total dry Biomass ($g.L^{-1}$)	Total dry cell biomass ($g.L^{-1}$)	Total dry EPS ($g.L^{-1}$)	Estimated biofilm thickness (μm)	Shear velocity ($m.s^{-1}$)	Source
0.054	15.3	36.1	32.5	5.6	2.3	23.8	11.9	11.9	575.4	0.04	[20]
0.11	17.8	37.4	31.4	5.1	2.4	27.9	14.0	14.0	674.5		
0.11	18.5	31.5	28.0	5.3	2.5	23.8	11.9	11.9	575.4		
0.11	19.1	32.8	29.5	3.4	1.3	23.8	11.9	11.9	575.4		
0.31	11.2	23.8	20.2	4.6	3.0	23.8	11.9	11.9	575.4		
0.31	9.8	25.1	21.6	6.3	3.8	23.8	11.9	11.9	575.4		
0.31	32.7	23.4	19.4	5.5	3.3	23.8	11.9	11.9	575.4		
0.32	6.9	26.7	22.2	3.2	1.6	23.8	11.9	11.9	575.4		
0.32	8.1	25.7	20.8	4.2	2.9	23.8	11.9	11.9	575.4		
0.52	17.1	17.3	13.7	4.6	2.1	23.8	11.9	11.9	575.4		
0.71	17.0	17.6	14.1	4.2	3.2	23.8	11.9	11.9	575.4		
0.72	19.1	15.6	12.0	4.0	2.0	23.8	11.9	11.9	575.4		
0.72	18.3	13.8	11.3	4.4	3.5	23.8	11.9	11.9	575.4		
0.51	14.9	26.1	18.2	5.56	2.26	26.1	13.1	13	309	0.09	[21]

0.55	19	21.9	15.6	5.12	2.44	28.9	18.9	10	347		
0.61	18.8	22.8	15.9	5.29	2.47	28.3	16.7	11.6	338		
0.71	26.5	15.1	11.3	3.4	1.29	15.5	8.8	6.7	175		
0.93	28.3	13.1	9.72	3.23	1.64	15	8.2	6.8	169		
0.98	23.1	15.2	10.4	4.21	2.86	17	9.9	7.1	193		
1.0	21	17.1	12.3	4.59	3.01	27.3	17.5	9.8	325		
0.44	13.6	26.7	17.6	6.31	3.79	14.2	11	3.2	159	0.36	[165]
0.75	20.7	19.6	13.7	5.48	3.32	22	16.9	5.1	255		
0.77	22.1	18.6	12.8	4.56	2.13	15.2	12.6	2.6	171		
1.0	25.4	16.4	9.5	4.18	3.19	18.9	15.4	3.5	216		
1.2	24.1	17.1	11.5	4.01	2.02	17.8	16.5	1.3	203		
1.2	25.3	15.5	9.65	4.36	3.46	16.6	11.7	4.9	188		
1.4	23.3	18	10.9	4.31	2.93	14.2	13.5	0.7	159		
0.9	19.9	20.1	11.6	4.77	2.4	15.4	13.1	2.39	258	0.36	Chapter 4
0.9	15.8	24.2	14.9	5.6	2.2	11.7	5.38	6.31	196	0.64	

To solve Equation (5-19) D_{e-Gluc} values were calculated using Equation (5-14). $\overline{r'_{Glc}}$ values were calculated using Equations (5-2) to (5-9), assuming an average SA concentration represented by the logarithmic mean concentration difference between the bulk SA concentration and SA concentrations within the depths of the biofilm, i.e. at full Glc conversion. Chilton and Colburn [166] reported that the mass transfer driving force can be estimated by the logarithmic mean concentration difference, analogous to heat transfer in heat exchangers. The parity plot of the Predicted L^* (Equation (5-19)) and the L^* as obtained from the mass transfer model is shown Figure 5-7(a). It is clear from the correlation parameters (r^2 = 0.993, RMSE = 14.37) and the narrow 99% prediction band (± 38.107 µm), a very good prediction for L^* was obtained from Equation (5-19).

The comparison of the parameter m (Equation (5-18)) and η (Equation (5-15)) for the pseudo-steady state data set (Table A-1 and Table 5-4) is shown in Figure 5-7(b). It was found that the m vs η data fit a segmental linear regression, i.e. two consecutive linear regressions described by Equation (5-20). Any deviation from a perfect fit can be attributed to possible numerical errors resulting from the solution of the biofilm model. However, considering the significant variability between the individual system parameters and η as shown in Figure 5-6, the quality of the linear regression was highly significant.

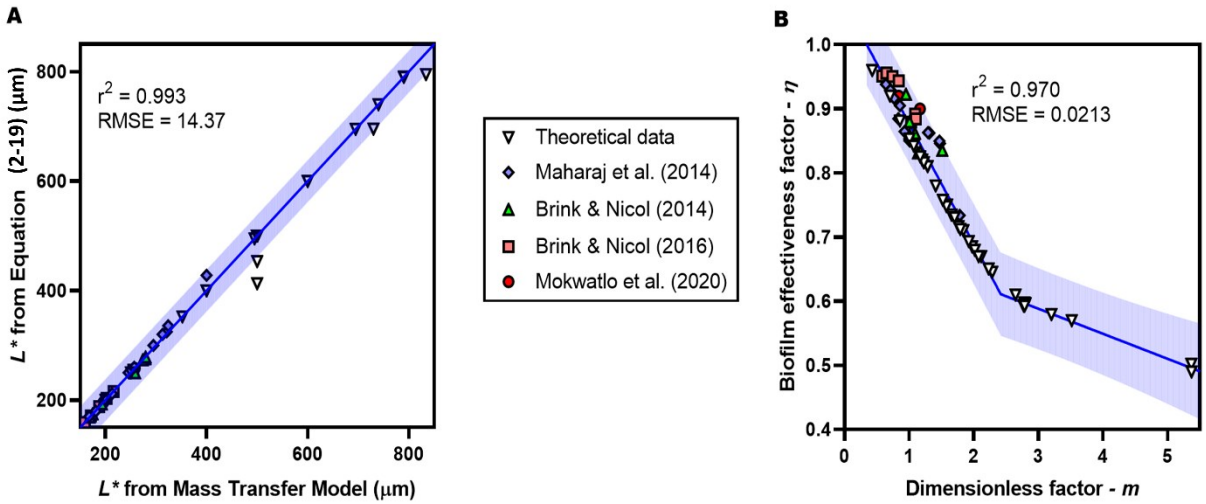

Figure 5-7: A: Parity plot of the L^* calculated using equation (5-19) vs L^* calculated using the internal mass transfer model for the pseudo-steady state data set. B: Effectiveness factor (η) as a function of dimensionless factor m showing a segmental linear regression for the pseudo-steady state data set. The shaded areas in in both A and B show the 99% prediction bands.

$$\eta = \begin{cases} a_1 m + c_1; 0.4 < m \leq m_o \\ a_2(m - m_0) + \eta(m_o)\,; m > m_o \end{cases} \quad (5\text{-}20)$$

Table 5-4: Optimised model parameters and fitting parameters for Equation (5-20).

Parameter	Value
a_1	-0.188
c_1	1.07
m_o	2.42
a_2	-0.0391
Degrees of Freedom	63
R^2	0.970
RMSE	0.0222

Following the derived relationships presented in Equations (5-20) and (5-19), a simplified algorithm – shown diagrammatically in Figure 5-8 – is proposed for determining the impact of mass transfer on pseudo-steady state *A. succinogenes* biofilms. The inputs to the algorithm are $C_{SA,aq}$, $C_{Glc,aq}$, ε_W, ε_{EPS}, and C_{XB} (shown in the clear blocks). The shaded blocks indicate the calculated variables and the arrows show the interactions between different inputs and calculated variables. The most important outputs from the system are L^* and η which give a measure of the mass transfer effects on the biofilm system.

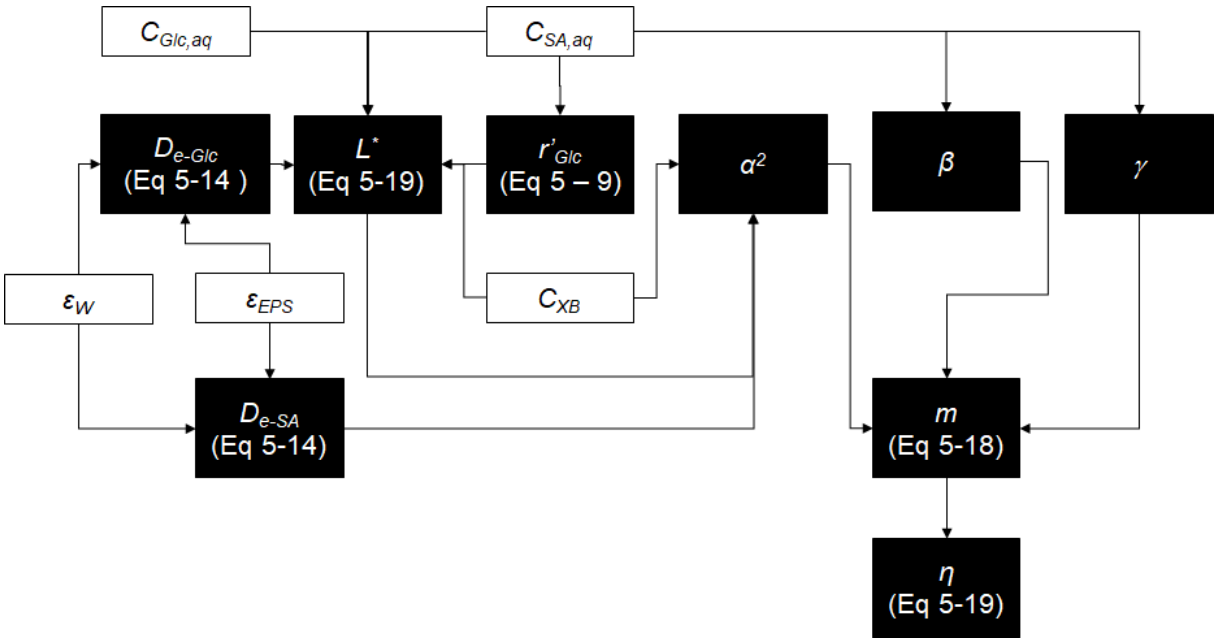

Figure 5-8: The proposed simplified algorithm for quantifying the mass transfer effects in a pseudo-steady state biofilm of *A. succinogenes*. The clear blocks represent inputs to the system and the shaded blocks show the calculated variables.

To illustrate, selected data from Table 5-3 were chosen and analysed to assess the impact of the operational conditions on mass transfer in the biofilm. Within a biofilm system, the biofilm properties are a strong function of the history of the biofilm. Results from Chapter 3 and Chapter 4 showed that metabolite accumulation, specifically C_{SA} and external shear, are major factors in the development of *A. succinogenes* biofilms. The data for Maharaj et al. [20] were obtained in a packed bed system under very low shear conditions (0.04 $m.s^{-1}$) and for dilution rates between 0.054 and 0.72 h^{-1}, corresponding to SA titres between 32.5 $g.L^{-1}$ and 11 $g.L^{-1}$. The data for Brink & Nicol (2014) [21] were obtained at intermediate shear conditions (0.09 $m.s^{-1}$) and for dilution rates between 0.51 and 1.0 h^{-1} (C_{SA} between 18.2 $g.L^{-1}$ and 12.3 $g.L^{-1}$), while those for Brink & Nicol (2016) [165] were obtained under intermediate high shear conditions (0.36 $m.s^{-1}$) at dilution rates between 0.44 and 1.4 h^{-1} (C_{SA} between 17.6 $g.L^{-1}$ and 10.9 $g.L^{-1}$). The data from Chapter 4 were obtained at the high shear conditions investigated (0.64 $m.s^{-1}$) and at a dilution rate of 0.9 h^{-1} (C_{SA} at 14.9 $g.L^{-1}$). In each of these cases the two extreme dilution rates were selected, thereby providing the extreme cases in terms of C_{SA} for each shear condition (except for the data from Chapter 4 as the lowest dilution there was at a titre below 10 g L^{-1}). Table 5-5 shows the selected conditions as well as the applicable calculated values.

Table 5-5: Supplementary analysis of selected pseudo-steady-state results taken from the results reported in Table 5-3 [20, 21, 165]

Shear velocity (m s^{-1})	Dilution rate (h^{-1})	C_{SA} ($g.L^{-1}$)	L^* (Eq (5-19)) (μm)	L^*/L (μm/μm)	η (Eq (5-20))	q_{SA} ($g.L^{-1}.h^{-1}$)	Source
0.04	0.054	32.5	295	0.51	0.91	1.76	[20]
	0.72	11.3	246	0.42	0.79	8.14	
0.09	0.51	18.2	258	0.83	0.88	9.28	[21]
	1.0	12.3	279	0.86	0.79	12.3	
0.36	0.44	17.6	159	1.00	0.96	7.74	[165]
	1.4	10.9	159	1.00	0.95	15.3	
0.64	0.9	14.85	196	1.00	0.91	13.4	Chapter 4

The results summarised in Table 5-5 show that for the lowest shear conditions (Maharaj et al. [20]) the high SA titre conditions translated to a significantly higher L^* than the low SA titre conditions (295 μm vs 246 μm), a result of reduced Glc consumption rate in relation to Glc diffusion rate in the high SA titre biofilm. The active biofilm depth only covered 51% and 43% of the overall depth of the biofilm in the high and low SA titre systems respectively. This implies that significant sections of the biofilm were Glc depleted.

The intermediate shear conditions (Brink & Nicol (2014) [21]) showed a significantly lower L^* for the high SA titre as compared with the low SA titre (258 μm vs 279 μm), the opposite of the effect seen by Maharaj et al. [20]. This observation was probably a result of the much lower SA titres than those observed by Maharaj et al. [20], resulting in a much greater Glc consumption rate in the biofilm and a concomitantly lower L^*. In this case the active layer of the biofilm was approximately equal for both dilution rates (83–86%), indicating a much healthier and more stable biofilm.

At the relatively high shear conditions (Brink & Nicol (2016) [26], 0.36 $m.s^{-1}$), the biofilm L^* was at its lowest value, and full Glc penetration was observed for both SA titre conditions. Further analysis of the full set of results reported by Brink & Nicol (2016) [26] (Table 5-3)

showed complete glucose penetration for all dilution rates (results not shown). Although the high shear run from Chapter 4 did not result in the lowest L^* observed (it was the second lowest L^* observed), full Glc penetration was still observed.

To interpret these results fully requires analysis of Equation (5-19), which shows that L^* is dominated by the ratio of the diffusion rate of Glc through the biofilm to the consumption rate of Glc within the biofilm. This means that the greater the diffusion rate into the biofilm, the greater the L^*. However, this would in turn lead to greater biomass growth rates and therefore a greater C_{XB} and $\overline{r'_{Glc}}$. The interplay between biomass growth and Glc diffusion would eventually lead to Glc depletion in the depths of the biofilm, resulting in biofilm shedding events due to loss of biofilm structural integrity; merely increasing the amount of biomass in the reactor, the usual objective in biofilm reactors, does not necessarily translate into the optimal bioreactor design and operation. For stable long-term operation it is imperative that L^* be maximised within the total biofilm.

To elucidate the complex nature of η required more in-depth analysis of Equation (5-20). This equation shows a direct negative proportionality between η and m; as m increases, the mass transfer effects increase linearly (η decreases linearly). The m parameter has a positive dependence on α^2, while being inhibited by increasing C_{SAaq}. The α^2 parameter is in turn directly proportional to the L^* and C_{XB}, and indirectly proportional to the SA diffusivity. From this it can be observed that the greater the active biofilm length and/or biomass concentration, the greater the mass transfer impact, while an increased SA titre and SA diffusivity reduce the mass transfer impact.

Considering the η values reported in Table 5-3, it is interesting to note that for the lowest shear conditions (Maharaj et al. [20]) a significantly improved η value under low dilution rather than the high dilution conditions (0.89 vs 0.77) were observed. This indicates that the elevated SA titre (low dilution) countered the significantly larger L^*, which consequently resulted in a much larger η value. For the intermediate shear conditions (Brink & Nicol (2014) [21]), the η values followed the same trend as that observed by Maharaj et al. [20], with a significantly greater biofilm effectiveness observed at higher SA titres than with the lower values. In this case the lower L^* also contributed to lower mass transfer effects, resulting in similar η values. In the high shear biofilm experiments (Brink & Nicol (2014) [21]) much greater η values were observed for both SA titres (0.92–0.93), a consequence of the reduced L^*. This meant that the SA titres measured were comparable to those of Brink & Nicol (2014 [21]), even though much

thinner biofilms with correspondingly lower biomass were observed under these elevated shear conditions.

The most striking impact of the high shear conditions can be seen when comparing the volumetric SA production rates (q_{SA}) at similar SA titres for the low- [20] and high shear [165] conditions. In these studies, SA titres of 11.3 g.L^{-1} and 10.9 g L^{-1}, and q_{SA} values of 8.14 g L^{-1} h^{-1} and 15.3 g L^{-1} h^{-1} were measured, respectively. This translates to an 88% increase in q_{SA} when comparing the high shear biofilm [165] to the lowest shear [20], even though the biofilm depths – and consequently biocatalyst present – were 36% lower. A very clear illustration of the effect of η on the production characteristics.

Overall, these results can be interpreted as follows: Since substrate gradients within biofilms grown at low SA titres are expected to be steep due to high reaction rates and excessive growth, biofilm starvation zones would probably result. As the biofilm matures, the SA titres increase and the system tends to pseudo-steady state and frequent biofilm shedding events due to biofilm starvation at the base. High shear operation in these biofilm systems would prevent shedding events due to the high eroding forces encountered therein, which result in thinner and more stable biofilms [139]. The results from Chapter 4 indicated that increased EPS production in dense biofilms developed at high shear conditions would act as a mechanism for strengthening the biofilm. However, the increased diffusional resistance due to higher EPS content would be countered by the thinner biofilm and consequently the negative effect on the biofilm effectiveness is negated.

It would be tempting to consider developing biofilm under high SA titre conditions to benefit from the high biofilm effectiveness discussed earlier. However, Chapter 3 showed that biofilms grown in consistently high SA titre conditions (i.e. batch followed by low dilution rates) were intrinsically limited in terms of thickness and viability due to the severe inhibitory effect of SA on *A. succinogenes*. This resulted in highly unstable biofilms, even under low shear conditions.

Considering that bulk SA fermentation production in industry will preferably occur at high SA titres for lower downstream processing costs [167], mass transfer effects would inherently be significantly reduced. This means that the development of thin and dense biofilms grown under initially low SA titres and high shear conditions will grant more stability to the process while simultaneously increasing the biofilm effectiveness.

5.4 CONCLUSIONS

The results achieved in this study suggest that internal mass transfer has a significant impact on *A. succinogenes* biofilm fermentations. The interplay between metabolite removal and substrate supply to the biofilm interior, on the one hand, and between metabolite production and substrate consumption on the other hand, results in significant gradients within the biofilms. These gradients cause elevated metabolite inhibition and substrate depletion effects that have major impacts on the initial biofilm formation, as well as on the long-term stability of these biofilms. To quantify the effects of these complicated interactions on the active biofilm depth and biofilm effectiveness, a simplified algorithm is proposed, which will be useful for design and optimisation purposes. Further analysis of the interactions of process variables showed that thinner biofilms developed under elevated shear conditions, when compared with thicker biofilms developed under low shear conditions, exhibited improved substrate penetration throughout the biofilm, and also higher biofilm effectiveness, due to diminished mass transfer effects. The improved substrate supply resulted in better biofilm stability, while the biofilm effectiveness resulted in more efficient bioreactor operation. This implies that focusing exclusively on augmenting the biomass concentrations within *A. succinogenes* biofilm reactors could be rendered superfluous due to mass transfer effects.

6 CONCLUSIONS

The biofilm process of *Actinobacillus succinogenes* has demonstrated industrial promise due to the high titre, yield and productivity of succinic acid encountered in the biofilm mode of production. In this respect it has become clear that the biofilm mode of fermentation is a key requisite for the successful bulk production of succinic acid by *A. succinogenes*. Although a considerable number of biofilm fermentation studies on *A. succinogenes* have been reported in the literature, these have mostly focused on the productive aspects of the biofilm and have neglected characterisation of the properties and physiology of the biofilms as dictated by fermenter conditions. For this reason it was the objective of this study to investigate the development of *A. succinogenes* biofilms. More specifically, this thesis aimed (i) to characterise how the accumulation of acid metabolites in continuous operation impacts *A. succinogenes* biofilms with respect to biofilm development, biofilm structure and cell activity within the biofilm, (ii) to show how shear conditions in the fermenter can be used to manipulate the biofilm structure and viable cell content of biofilms, leading to improved cell-based succinic acid productivities, and lastly (iii) to investigate the internal mass transfer effects on biofilm performance, further showing the role played by differences in shear and acid accumulation conditions in this respect.

This thesis demonstrated that biofilms of *A. succinogenes* develop rapidly and with high cell viability when cultivated under low product accumulation (LPA) conditions (< 10 g L^{-1} SA). High product accumulation (HPA) conditions considerably slowed down biofilm development and increased cell mortality. An average cell viability of 65% was achieved for LPA-cultivated biofilms over the growth period, whereas a 50% average cell viability was achieved for HPA-cultivated biofilms. Under HPA conditions some cells exhibited severe elongation while maintaining a cross-sectional diameter like the rod-shaped or cocci-shaped cells predominantly found in LPA conditions. The elongated cells formed in HPA conditions were found to be more viable and thus more resistant to hostile HPA conditions than the clusters of rod-shaped or cocci shaped cells. The gradual increase of accumulation conditions in LPA-cultivated biofilms resulted in biofilms composed of filamentous cells with a high cellular viability of 63%. The global microscopic structure of the HPA biofilms also differed significantly from that of the

LPA biofilms. Although both exhibited shedding after 4 days of growth, the LPA biofilms were more homogenous (less patchy), thicker and with high viability throughout the biofilm depth.

Hydrodynamic shear conditions in a fermenter were also shown to have a significant impact on the morphology, viability and metabolic activity of *A. succinogenes* biofilms. The smooth, low-porosity biofilms obtained under high shear had an average cell viability of 79% (over a 3-day cultivation period) compared with 57% at the lowest shear used. The maximum cell-based succinic acid productivity for the high shear biofilm was 2.4 g g^{-1}DCW h^{-1} compared with the 0.8 g g^{-1}DCW h^{-1} for the low shear biofilm. Furthermore, MTT assays confirmed higher cell metabolic activities for high shear developed biofilm compared with biofilm developed at low shear conditions. This threefold increase in succinic acid productivity obtained from high shear developed biofilm corresponds to the cell viability differences observed from microscopic results. The biofilm contained a high EPS fraction when cultivated in high shear environments with the proteins constituting a high fraction of the EPS. Since dense and strong biofilms are reported to have a high protein content, it follows that the biofilms developed in a high shear environment were denser and as a result more stable. The results clearly indicated that high shear biofilm cultivation has considerable morphological, viability and cell-based productivity benefits.

Finally, internal mass transfer effects within biofilms were considered. The interplay between metabolite removal and substrate supply to the biofilm interior to the one hand, and between metabolite production and substrate consumption on the other hand, results in significant gradients within the biofilms. These gradients cause elevated metabolite inhibition and substrate depletion effects that have major impacts on the initial biofilm formation, as well as on the long-term stability of these biofilms. To quantify the effects of these complicated interactions on the active biofilm depth and biofilm effectiveness, a simplified algorithm is proposed, which will be useful for design and optimisation purposes. Further analysis of the interactions of process variables showed that thinner biofilms developed under elevated shear conditions, when compared with thicker biofilms developed under low shear conditions, exhibited improved substrate penetration throughout the biofilm, and also higher biofilm effectiveness, due to diminished mass transfer effects. The improved substrate supply resulted in better biofilm stability, while the biofilm effectiveness resulted in more efficient bioreactor operation. This implies that focusing exclusively on augmenting the biomass concentrations within *A. succinogenes* biofilm reactors could be rendered superfluous due to mass transfer effects.

Overall, this thesis gave insights into how fermentation parameters, such as product accumulation levels and hydrodynamic shear conditions, can potentially be used as tools for the strategic manipulation of the development of optimised biofilms for successful bulk succinic acid bioproduction considering internal mass transfer effects. To further advance the work, future work must consider performing the experiments for a much longer period to assess the behaviour of biofilm under extended production period, and how this is affected by fermenter conditions.

7 REFERENCES

[1] M. Geissdoerfer, P. Savaget, N.M.P. Bocken, E. J. Hultink, The circular economy–a new sustainability paradigm? J. Clean. Prod. 143 (2017) 757–768. https://doi.org/10.1016/j.clepro.2016.12.048.

[2] G.D.A. Galvão, J. de Nadae, D.H. Clemente, G. Chinen, M.M. de Carvalho, Circular economy: overview of barriers, Procedia CIRP. 73 (2018) 79–85. https://doi.org/10.1016/j.procir.2018.04.011.

[3] S. VijayaVenkataRaman, S. Iniyan, R. Goic, A review of climate change, mitigation and adaptation, Renew. Sustain. Energy Rev. 16 (2012) 878–897. https://doi.org//10.1016/j.rser.2011.09.009.

[4] M. FitzPatrick, P. Champagne, M.F. Cunningham, R.A. Whitney, A biorefinery processing perspective: Treatment of lignocellulosic materials for the production of value-added products. Bioresour. Technol. 101 (2010) 8915–8922. https://doi.org/10.1016/j.biortech.2010.06.125.

[5] H.R. Ghatak, Biorefineries from the perspective of sustainability: Feedstocks, products, and processes. Renew. Sustain. Energy Rev. 15 (2011) 4042–4052. https://doi.org/10.1016/j.rser.2011.07.034.

[6] M.F. Demirbas, Biorefineries for biofuel upgrading: A critical review, Appl. Energy. 86 (2009) S151–S161. https://doi.org/10.1016/j.apenergy.2009.04.043.

[7] P.C.A. Bruijnincx, Y. Román-Leshkov, Sustainable catalytic conversions of renewable substrates, Catal. Sci. Technol. 4 (2014) 2180. https://doi.org/10.1039/c4cy90025a.

[8] H. Dhamankar, K.L. Prather, Microbial chemical factories: recent advances in pathway engineering for synthesis of value-added chemicals, Curr. Opin. Struct. Biol. 21 (2011) 488–494. https://doi.org/10.1016/j.sbi.2011.05.001.

[9] Y. Chen, J. Nielsen, Advances in metabolic pathway and strain engineering paving the way for sustainable production of chemical building blocks, Curr. Opin. Biotechnol. 24 (2013) 965–972. https://doi.org/10.1016/j.copbio.2013.03.008.

[10] T. Werpy, G. Petersen, A. Aden, J. Bozell, J. Holladay, J. White, A. Manheim, D. Eliot, L. Lasure, S. Jones, Top Value Added Chemicals From Biomass. Volume 1. Results of Screening for Potential Candidates From Sugars and Synthesis Gas, DTIC Document, 2004.

[11] P.C. Lee, S.Y. Lee, S.H. Hong, H.N. Chang, Isolation and characterization of a new succinic acid-producing bacterium, *Mannheimia succiniciproducens* MBEL55E, from bovine rumen., Appl. Microbiol. Biotechnol. 58 (2002) 663–668. https://doi.org/10.1007/s00253-002-0935-6.

[12] N. Samuelov, R. Datta, M. Jain, J. Zeikus, Whey fermentation by *Anaerobiospirillum succiniciproducens* for production of a succinate-based animal feed additive, Appl. Environ. Microbiol. 65 (1999) 2260–2263.

[13] E. Scholten, T. Renz, J. Thomas, Continuous cultivation approach for fermentative succinic acid production from crude glycerol by *Basfia succiniciproducens* DD1, Biotechnol. Lett., 31 (2009) 1947–1951. https://doi.org/10.1007/s10529-009-0104-4.

[14] J.J. Beauprez, M. De Mey, W.K. Soetaert, Microbial succinic acid production: Natural versus metabolic engineered producers, Process. Biochem. 45 (2010) 1103–1114. https://doi.org/10.1016/j.procbio.2010.03.035.

[15] N. Shen, H. Zhang, Y. Qin, Q. Wang, J. Zhu, Y. Li, M.G. Jiang, R. Huang, Efficient production of succinic acid from duckweed (*Landoltia punctata*) hydrolysate by *Actinobacillus succinogenes* GXAS137, Bioresour. Technol. 250 (2017) 35–42. https://doi.org/10.1016/j.biortech.2017.09.208.

[16] M. Ferone, F. Raganati, A. Ercole, G. Olivieri, P. Salatino, A. Marzocchella, Continuous succinic acid fermentation by *Actinobacillus succinogenes* in a packed-bed biofilm reactor, Biotechnol. Biofuels. BioMed Central. 11(2018) 1–11. https://doi.org/10.1186/s13068-018-1143-7.

[17] S.K.C. Lin, C. Du, A. Koutinas, R. Wang, C. Webb, Substrate and product inhibition kinetics in succinic acid production by *Actinobacillus succinogenes*, Biochem Eng. J. 41

(2008) 128–135. https://doi.org/10.1016/j.bej.2008.03.013.

[18] S. González-García, L. Argiz, P. Míguez, B. Gullón, Exploring the production of bio-succinic acid from apple pomace using an environmental approach, Chem. Eng. J. 350 (2018) 982–991. https://doi.org/10.1016/j.cej.2018.06.052.

[19] M. Ferone, F. Raganati, G. Olivieri, P. Salatino, A. Marzocchella, Continuous succinic acid fermentation by *Actinobacillus Succinogenes:* Assessment of growth and succinic acid production kinetics. Appl. Biochem. Biotechnol. 187 (2018) 782–799. https://doi.org/10.1007/s12010-018-2846-8.

[20] K. Maharaj, M.F.A. Bradfield, W. Nicol, Succinic acid-producing biofilms of *Actinobacillus succinogenes*: Reproducibility, stability and productivity, Appl. Microbiol. Biotechnol. 98 (2014) 7379–7386. https://doi.org/10.1007/s00253-014-5779-3.

[21] H.G. Brink, W. Nicol, Succinic acid production with *Actinobacillus succinogenes* : Rate and yield analysis of chemostat and biofilm cultures, (2014) 1–12. https://doi.org/10.1186/s12934-014-0111-6.

[22] M.F.A. Bradfield, W. Nicol, Continuous succinic acid production by *Actinobacillus succinogenes* in a biofilm reactor: Steady-state metabolic flux variation, Biochem. Eng. J. 85 (2014) 1–7. https://doi.org/10.1016/j.bej.2014.01.009.

[23] Q. Yan, P. Zheng, J.J. Dong, Z.H. Sun, A fibrous bed bioreactor to improve the productivity of succinic acid by *Actinobacillus succinogenes*. J. Chem. Technol. Biotechnol. 143 (2013) 405–412. https://doi.org/10.1002/jctb.4257.

[24] M.F.A. Bradfield, A. Mohagheghi, D. Salvachúa, H. Smith, B.A. Black, N. Dowe, G.T. Beckham, W. Nicol, Continuous succinic acid production by *Actinobacillus succinogenes* on xylose-enriched hydrolysate, Biotechnol. Biofuels. (2015) 1–17. https://doi.org/10.1186/s13068-015-0363-3.

[25] S.E. Urbance, A.L. Pometto, A. Dispirito, Y. Denli, Evaluation of succinic acid continuous and repeat-batch biofilm fermentation by *Actinobacillus succinogenes* using plastic composite support bioreactors, Appl. Microbiol. Biotechnol. 65 (2004) 664–670. https://doi.org/10.1007/s00253-004-1634-2.

[26] D. Salvachúa, A. Mohagheghi, H. Smith, M.F.A. Bradfield, W. Nicol, B.A. Black, M.J. Biddy, N. Dowe, G.T. Beckham, Succinic acid production on xylose-enriched biorefinery streams by *Actinobacillus succinogenes* in batch fermentation., Biotechnol. Biofuels. BioMed Central, 9 (2016) 28–39. https://doi.org/10.1186/s13068-016-0425-1.

[27] P. Zheng, J.J. Dong, Z.H. Sun, Y. Ni, L. Fang, Fermentative production of succinic acid from straw hydrolysate by *Actinobacillus succinogenes*., Bioresour. Technol. 100 (2009) 2425–2439. https://doi.org/10.1016/j.biortech.2008.11.043.

[28] J.H. Clark, F.E.I. Deswarte, T.J. Farmer, The integration of green chemistry into future biorefineries, Biofuels, Bioprod. Biorefining. 3 (2009) 72–90. https://doi.org/10.1002/bbb.119.

[29] Kirk-Othmer Encyclopedia of Chemical Technology, Wiley, 2000. https://doi.org/10.1002/0471238961.

[30] N. Nghiem, S. Kleff, S. Schwegmann, Succinic acid: Technology development and commercialization, Fermentation. 3 (2017) 26. https://doi.org/10.3390/fermentation3020026.

[31] Markets and Markets, Succinic acid market by type (bio-based succinic acid, petro-based succinic acid), End-use Industry (industrial, food & beverage, coatings, pharmaceutical), and Region (APAC, Europe, North America, South America, Middle East & Africa) – Forecast to 2023. Accessed: 24 February 2020, https://www.marketsandmarkets.com/Market-Reports/succinic-acid-market-402.html?gclid=EAIaIQobChMIqKbaj5eu6QIVj-vtCh3kEQoUEAAYASAAEgJ4c_D_BwE

[32] J.G. Zeikus, M.K. Jain, P. Elankovan, Biotechnology of succinic acid production and markets for derived industrial products, Appl. Microbiol. Biotechnol. 51 (1999) 542–552. https://doi.org/10.1007/s002530051431.

[33] S.R.O. Weastra (Ed.), WP 8.1 Determination of market potential selected platform chemicals: Itaconic acid, succinic acid, 2,5-furanicarboxylic, 2011.

http://www.bioconsept.eu/wp-content/uploads/BioConSepT_Market-potential-selected-platform-chemicals_report1.pdf.

[34] H. Song, S.Y. Lee, Production of succinic acid by bacterial fermentation, Enzyme Microbe. Technol. 39 (2006) 352–361. https://doi.org/10.1016/j.enzmictec.2005.11.043.

[35] M.L.A. Jansen, W.M. van Gulik, Towards large scale fermentative production of succinic acid, Curr. Opin. Biotechnol. 30C (2014) 190–197. https://doi.org/10.1016/j.copbio.2014.07.003.

[36] Y. Cao, R. Zhang, C. Sun, T. Cheng, Y. Liu, M. Xian, Fermentative succinate production: An emerging technology to replace the traditional petrochemical processes, Biomed. Res. Int. 2013 (2013) 723412. https://doi.org/10.1155/2013/723412.

[37] C. Pateraki, M. Patsalou, A. Vlysidis, N. Kopsahelis, C. Webb, A.A. Koutinas, M. Koutinas, *Actinobacillus succinogenes*: Advances on succinic acid production and prospects for development of integrated biorefineries, Biochem. Eng. J. 112 (2016) 285–303. https://doi.org/10.1016/j.bej.2016.04.005.

[38] G.N. Vemuri, M.A. Eiteman, E. Altman, Succinate production in dual-phase *Escherichia coli* fermentations depends on the time of transition from aerobic to anaerobic conditions, J. Ind. Microbiol. Biotechnol. 28 (2002) 325–332.

[39] S. Okino, R. Noburyu, M. Suda, T. Jojima, M. Inui, H. Yukawa, An efficient succinic acid production process in a metabolically engineered *Corynebacterium glutamicum* strain, Appl. Microbiol. Biotechnol. 81 (2008) 459–464.

[40] L.H. Christensen, C.M. Henriksen, J. Nielsen, J. Villadsen, M. Egel-Mitani, Continuous cultivation of *Penicillium chryogenum.* Growth on glucose and penicillin production, J. Biotechnol. 42 (1995) 95–107. https://doi.org/10.1016/0.168-1656(95)00056-V.

[41] G. Stephanopoulos, Metabolic fluxes and metabolic engineering, Metab. Eng. 1 (1999) 1–11. https://doi.org/10.1006/mben.1998.0101.

[42] Y.J. Wee, J.S. Yun, K.H. Kang, H.W. Ryu, Continuous production of succinic acid by a fumarate producing bacterium immobilised in a hollow-fiber bioreactor, Appl. Biochem. Biotechnol. 98–100 (2002) 1093–1104.

[43] L. Agarwal, J. Isar, G.K. Meghwanshi, R.K. Saxena, Influence of environmental and nutritional factors on succinic acid production and enzymes of reverse tricarboxylic acid cycle from *Enterococcus flavescens*, Enzyme Microb. Technol. 40 (2007) 629–636. https://doi.org/10.1016/j.enzmictec.2006.05.019.

[44] O.D. Rotstein, C.L. Wells, T.L. Pruett, J.J. Sorenson, R.L. Simmons, Succinic acid production by *Bacteroides fragilis*. A potential virulence factor, Arch. Surg. 122 (1987) 93–98. https://doi.org/10.1001/archsurg.1987014001300990.

[45] K.-K. Cheng, J. Wu, G.-Y. Wang, W.-Y. Li, J. Feng, J.-A. Zhang, Effect of pH and dissolved CO_2 level on simultaneous production of 2,3-butanediol and succinic acid using *Klebsiella pneumoniae*, Bioresour. Technol. 135 (2013) 500–503. https://doi.org/10.1016/j.biortech.201208.100.

[46] S.M. O'herrin, W.R. Kenealy, Glucose and carbon dioxisw metabolism by *Succinivibrio dextrinosolvens*, Appl. Environ. Microbiol. 59 (1993) 748–755.

[47] R.R. Gokarn, M.A. Eiteman, S.A. Martin, K.E. Eriksson, Production of succinate from glucose, cellibiose, and various cellulosic materials by the ruminal anaerobic bacteria *Fibrobacter succinogenes* and *Ruminococcus flavefaciens*, Apppl. Biochem. Biotechnol. 68 (1997) 69–80. https://doi.org/10.1007/BF02785981.

[48] H. David, M. Åkesson, J. Nielsen, Reconstruction of the central carbon metabolism of *Aspergillus niger*. J. Dairy Sci. 270 (2003) 4243–4253.

[49] E.T.M. Ling, J.T. Dibble, M.R. Houston, L.B. Lockwood, L.P. Elliot, Accumulation of 1-trans-2,3-epoxysuccinic acid and succinic acid by *Paecilomyces varioti*, Appl. Environ. Microbiol. 35 (1978) 1213–1215.

[50] M. Gallmetzer, J. Meraner, W. Burgstaller, Succinate synthesis and excretion by *Penicillium simplicissimum* under aerobic and anaerobic conditions, FEMS Microbiol. Lett. 210 (2002) 221–225. https://doi.org/10.1111/j.1574-6968.2002.tb11184.x.

[51] J.M. Otero, D. Cimini, K.R. Patil, S.G. Poulsen, L. Olsson, J. Nielsen, Industrial systems biology of *Saccharomyces cerevisiae* enables novels succinic acid cell factory, PLoS One. 8 (2013) 1–10.

[52] J. Becker, J. Reinefeld, R. Stellmacher, R. Schäfer, A. Lange, H. Meyer, M. Lalk, O. Zelder, G. Von Abendroth, H. Schröder, S. Haefner, C. Wittmann, Systems-wide analysis and engineering of metabolic pathway fluxes in bio-succinate producing *Basfia succiniciproducens*. Biotechnol. Bioeng. 110 (2013) 3013–3023.

[53] M.V. Guettler, M.K. Jain, D. Rumler, Method for making succinic acid, bacterial variants for use in the process and methods for obtaining variants. (1996) US Patent 5,573,931.

[54] S.J. Lee, H. Song, S.Y. Lee, Genome-based metabolic engineering of *Mannheimia succiniciproducens* for succinic acid production. Appl. Environ. Microbiol. 72 (2006) 1939–1948.

[55] S.Y. Lee, P. Cheon, H.N. Chang, Kinetic study of organic acid formations and growth of *Anaerobiospirillum succiniciproducens* during continuous cultures, J. Microbiol. Biotechnol. 19 (2009) 1379–1384. https://doi.org/10.4014/jmb.0905.05026.

[56] M.V. Guettler, D. Rumler, M.K. Jain, *Actinobacillus succinogenes* sp. nov., a novel succinic-acid-producing strain from the bovine rumen. Int. J. Syst. Bacteriol. 49 (1999) 207–216.

[57] J.B. McKinlay, Y. Shachar-Hill, J.G. Zeikus, C. Vieille, Determining *Actinobacillus succinogenes* metabolic pathways and fluxes by NMR and GC-MS analyses of 13C-labeled metabolic product isotopomers. Metab. Eng. 9 (2007) 177–192.

[58] J.B. McKinlay, M. Laivenieks, B.D. Schindler, A.A. McKinlay, S. Siddaramappa, J.F. Challacombe, S.R. Lowry, A. Clum, A.L. Lapidus, K.B. Burkhart, V. Harkins, C. Vieille, A genomic perspective on the potential of *Actinobacillus succinogenes* for industrial succinate production. BMC Genomics. 11 (2010) 680–696.

[59] J.B. McKinlay, J.G. Zeikus, C. Vieille, Insights into *Actinobacillus succinogenes* fermentative metabolism in a chemically defined growth medium. Appl. Environ. Microbiol. 71 (2005) 6651–6656.

[60] J.B. McKinlay, C. Vieille, 13C-metabolic flux analysis of *Actinobacillus succinogenes* fermentative metabolism at different NaHCO3 and H2 concentrations. Metab. Eng. 10 (2008) 55–68.

[61] R.I. Corona-Gonzalez, A. Bories, V. González-Álvarez, C. Pelayo-Ortiz, Kinetic study of succinic acid production by *Actinobacillus succinogenes* ZT-130. Process Biochem. 43 (2008) 1047–1053.

[62] R.I. Corona-Gonzalez, A. Bories, V. González-Álvarez, R. Snell-Castro, G. Toriz-González, C. Pelayo-Ortiz, Succinic acid production with *Actinobacillus succinogenes* ZT-130 in the presence of succinic acid. Curr. Microbiol. 60 (2010) 71–77.

[63] Q. Li, D. Wang, Y. Wu, M. Yang, W. Li, J. Xing, Z. Su, Kinetic evaluation of products inhibition to succinic acid producers *Escherichia coli* NZN111, AFP111, BL21, and *Actinobacillus succinogenes* 130Z. J. Microbiol. (Seoul, Korea). 48 (2010) 290–296.

[64] C.C. Wang, L.W. Zhu, H.M. Li, Y.J. Tang, Performance analyses of a neutralizing agent combination strategy for the production of succinic acid by *Actinobacillus succinogenes* ATCC 55618. Bioprocess Biosyst. Eng. 35 (2012) 659–664.

[65] E. Padan, Functional and structural dynamics of NhaA, a prototype for Na+ and H+ antiporters, which are responsible for Na+ and H+ homeostasis in cells. Biochim. Biophys. Acta. 1837 (2014) 1047–1062.

[66] J. Li, M. Jiang, K. Chen, L. Shang, P. Wei, H. Ying, Q. Ye, P. Ouyang, H. Chang, Enhanced production of succinic acid by *Actinobacillus succinogenes* with reductive carbon source. Process Biochem. 45 (2010) 980–985.

[67] D.H. Park, J.G. Zeikus, Utilization of electrically reduced neutral red by *Actinobacillus succinogenes*: physiological function of neutral red in membrane-driven fumarate reduction and energy conservation. J. Bacteriol. 181 (1999) 2403–2410.

[68] S.P. Chundawat, G.T. Beckham, M.E. Himmel, B.E. Dale, Deconstruction of lignocellulosic biomass to fuels and chemicals, Annu. Rev. Chem. Biomol. Eng. 2 (2011) 121–145.

[69] E. Palmqvist, B. Hahn-Hägerdal, Fermentation of lignocellulosic hydrolysates. I: Inhibition and detoxification. Bioresour. Technol. 74 (2000) 17–24.

[70] K.Q.Q. Chen, H. Zhang, Y.L.L. Miao, M. Jiang, J.Y.Y. Chen, Enhanced succinic acid production from sake lees hydrolysate by dilute sulfuric acid pretreatment and biotin supplementation. J. Sustain. Bioenergy Syst. 2 (2012) 19–25.

[71] Y.P.P. Liu, P. Zheng, Z.H.H. Sun, Y. Ni, J.J.J. Dong, L.L.L. Zhu, Economical succinic acid production from cane molasses by *Actinobacillus succinogenes*. Bioresour. Technol. 99 (2008) 1736–1742.

[72] M. Jiang, W. Dai, Y. Xi, M. Wu, X. Kong, J. Ma, M. Zhang, K. Chen, P. Wei, Succinic acid production from sucrose by *Actinobacillus succinogenes* NJ113. Bioresour. Technol. 153 (2014) 327–332.

[73] M. Jiang, R. Xu, Y.L. Xi, J.H.H. Zhang, W.Y.Y. Dai, Y.J.J. Wan, K.Q.Q. Chen, P. Wei, Succinic acid production from cellobiose by *Actinobacillus succinogenes*. Bioresour. Technol. 135 (2013) 469–474.

[74] M. Carvalho, M. Matos, C. Roca, M.A.M. Reis, Succinic acid production from glycerol by *Actinobacillus succinogenes* using dimethylsulfoxide as electron acceptor. New Biotechnol. 31 (2014) 133–139.

[75] W. Cao, Y. Wang, J. Luo, J. Yin, J. Xing, Y. Wan, Succinic acid biosynthesis from cane molasses under low pH by *Actinobacillus succinogenes* immobilized in luffa sponge matrices, Bioresour. Technol. 268 (2018) 45–51. https://doi.org/10.1016/j.biortech.2018.06.075.

[76] M. Carvalho, C. Roca, M.A.M. Reis, Improving succinic acid production by *Actinobacillus succinogenes* from raw industrial carob pods, Bioresour. Technol. 218 (2016) 491–497. http://dx.doi.org/10.1016/j.biortech.2016.01.140.

[77] K. Chen, M. Jiang, P. Wei, J. Yao, H. Wu, Succinic acid production from acid hydrolysate of corn fiber by *Actinobacillus succinogenes*, Appl. Biochem. Biotechnol. 160 (2010) 477–485. https://doi.org/10.1007/s12010-008-8367-0.

[78] K. Chen, H. Zhang, Y. Miao, M. Jiang, J. Chen, Succinic acid production from enzymatic hydrolysate of sake lees using *Actinobacillus succinogenes* 130Z, Enzyme Microb. Technol. 47 (2010) 236–240. https://doi.org/10.1016/j.enzmictec.2010.06.011.

[79] K. Chen, H. Zhang, Y. Miao, P. Wei, J. Chen, Simultaneous saccharification and fermentation of acid-pretreated rapeseed meal for succinic acid production using *Actinobacillus succinogenes*. Enz. Microb. Technol. 48 (2011) 339–344.

[80] I.B. Gunnarsson, D. Karakashev, I. Angelidaki, Succinic acid production by fermentation of Jerusalem artichoke tuber hydrolysate with *Actinobacillus succinogenes* 130Z, Ind. Crops Prod. 62 (2014) 125–129.

[81] Q. Li, M. Yang, D. Wang, W. Li, Y. Wu, Y. Zhang, J. Xing, Z. Su, Efficient conversion of crop stalk wastes into succinic acid production by *Actinobacillus succinogenes*. Bioresour. Technol. 101 (2010) 3292–3294.

[82] J. Li, X.Y.Y. Zheng, X.J.J. Fang, S.W.W. Liu, K.Q.Q. Chen, M. Jiang, P. Wei, P.K.K. Ouyang, A complete industrial system for economical succinic acid production by *Actinobacillus succinogenes*. Bioresour. Technol. 102 (2011) 6147–6152.

[83] M. Shamsuddin, I. Abdullah, R. Othaman, Celluloses filled ENR/PVC membranes for palm oil mill effluent (POME) treatment, AIP Conference Proceedings Vol. 1571, (2013) 753. https://doi.org/10.1063/1.4858745

[84] N. Shen, S. Liao, Q. Wang, Y. Qin, Q. Zhu, J. Zhu, Y. Li,R. Huang, Economical succinic acid production from sugarcane juice by *Actinobacillus succinogenes* supplemented with corn steep liquor and peanut meal as nitrogen sources, Sugar Tech. 6 (2016) 8. https://doi.org/10.1007/s12355-015-0401-2.

[85] C. Wan, Y. Li, A. Shahbazi, S. Xiu, Succinic acid production from cheese whey using *Actinobacillus succinogenes* 130 Z. Appl. Biochem. Biotechnol. 145 (2008) 111–119.

[86] E.R. Borges, J.N. Pereira Jr., Succinic acid production from sugarcane bagasse hemicellulose hydrolysate by *Actinobacillus succinogenes*. J. Ind. Microbiol. Biotechnol. 38 (2011) 1001–1011.

[87] J. Yu, Z. Li, Q. Ye, Y. Yang, S. Chen, Development of succinic acid production from corncob hydrolysate by Actinobacillus succinogenes, J. Ind. Microbiol. Biotechnol. 37 (2010) 1033–1040. https://doi.org/10.1007/s10295-010-0750-5.

[88] M.R. Kunduru, A. Pometto, Continuous ethanol production by Zymomonas mobilis and Saccharomyces cerevisiae in biofilm reactors, J. Ind. Microbiol. Biotechnol. 16 (1996) 249–256. https://doi.org/10.1007/BF01570029.

[89] C. van Heerden, W. Nicol, Continuous succinic acid fermentation by *Actinobacillus succinogenes*, Biochem. Eng. J. 73 (2013) 5–11. https://doi.org/10.1016/j.bej.2013.01.015.

[90] H. Flemming, J. Wingender, The biofilm matrix. Nat. Revs. Microbiol. 8 (2010) 623–633.

[91] K.C. Cheng, A. Demirci, J.M. Catchmark, Advances in biofilm reactors for production of value-added products. Appl. Microbiol. Biotechnol. 87 (2010) 445–456. https://doi.org/10.1007/s00253-010-2622-3.

[92] R. Gross, B. Hauer, K. Otto, A. Schmid, Microbial biofilms: new catalysts for maximizing productivity of long-term biotransformations, Biotechnol. Bioeng. 98 (2007) 1123–1134. https://doi.org/10.1002/bit.21547.

[93] N. Qureshi, B.A. Annous, T.C. Ezeji, P. Karcher, I.S. Maddox, (2005) Biofilm reactors for industrial bioconversion processes: employing potential of enhanced reaction rates. Microb. Cell Factories. 4 (2005) 24. https://doi.org/10.1186/1475-2859-4-24.

[94] H.G. Brink, W. Nicol, Succinic acid production by actinobacillus succinogenes in chemostat and biofilm cultures, Chem. Eng. Trans. 49 (2016) 613–618.

[95] J. Herselman, M.F.A. Bradfield, U. Vijayan, W. Nicol, The effect of carbon dioxide availability on succinic acid production with biofilms of *Actinobacillus succinogenes*, Biochem. Eng. J. 117 (2017) 218–225.

[96] Q. Yan, P. Zheng, S.T. Tao, J.J. Dong, Fermentation process for continuous production of succinic acid in a fibrous bed bioreactor. Biochem. Eng. J. 91 (2014) 92–98.

[97] M.F.A. Bradfield, W. Nicol, Continuous succinic acid production from xylose by *Actinobacillus succinogenes*, Bioproc. Biosyst. Eng. 39 (2016) 233–244. https://doi.org/10.1007/s00449-015-1507-3.

[98] M. II Kim, N.J. Kim, L. Shang, Y.K. Chang, S.Y. Lee, H.N. Chang, Continuous production of succinic acid using an external membrane cell recycle system, J. Microbiol. Biotechn. 19 (2009) 1369–1373. https://doi.org/10.4014/jmb.0903.03034.

[99] M.F.A. Bradfield, W. Nicol, The pentose phosphate pathway leads to enhanced succinic acid flux in biofilms of wild-type *Actinobacillus succinogenes*, Appl. Microbiol. Biotechnol. 100 (2016) 9641–9652. https://doi.org/10.1007/s00253-016-7763-7766.

[100] R.M. Donlan, Preventing biofilms of clinically relevant organisms using bacteriophage, Curr. Trends Microbiol. 17(2009) 66–72.

[101] M.E. Davey, G.A. O'Toole, Microbial biofilms: From ecology to molecular genetics. Microbiol. Mol. Biol. Rev. 64 (2000) 847–867.

[102] B. Vu, M. Chem, R.J. Crawford, E.P. Ivanova, Bacterial extracellular polysaccharides involved in biofilm formation. Molecules. 14 (2009) 2535–2554.

[103] J.W. Costerton, Introduction to biofilm, Int. J. Antimicrob. Agents. 11(1999) 217–239. https://doi.org/10.1016/s0924-8579(99)00018-7.

[104] H. Flemming, J. Wingender, U. Szewzyk, P. Steinberg, S.A. Rice, S. Kjelleberg, Biofilms: an emergent form of bacterial life. Nat. Rev. Microbiol. 14 (2016) 563–575. https://doi.org/10.1038/nrmicro.2016.94.

[105] M. Fletcher, Measurement of glucose utilization by *Pseudomollas fluorescells* that are free-living and that are attached to surfaces. Appl. Environ. Microbiol. 52 (1986) 672–676.

[106] H. Flemming, J. Wingender, The biofilm matrix, Nat. Rev. Microbiol. 8 (2010) 623–633. https://doi.org/10.1038/nrmicro2415.

[107] Z. Khatoon, C.D. McTiernan, E.J. Suuronen, T. Mah, E.I. Alarcon, Bacterial biofilm formation on implantable devices and approaches to its teatment and prevention, Heliyon. 4 (2018) e01067. https://doi.org/10.1016/j.heliyon.2018.e01067.

[108] T. Ebihara, P.L. Bishop, Effect of acetate on biofilms utilized in PAH bioremediation, Environ. Eng. Sci. 19 (2002) 305–319. https://doi.org/10.1089/10928750260418944.

[109] S.J. Edwards, B.V. Kjellerup, Applications of biofilms in bioremediation and biotransformation of persistent organic pollutants, pharmaceuticals/personal care products, and heavy metals, Appl. Microbiol. Biotechnol. 97 (2013) 9909–9921.

[110] K. Egli, F. Bosshard, C. Werlen, P. Lais, H. Siergrist, A.J.B. Zehnder, J.R. van der Meer, Microbial composition and structure of a rotating biological contactor biofilm treating ammonium-rich wastewater without organic carbon, Microb. Ecol. 45 (2003) 419–432. https:/doi.org/10.1007/00248-002-2037-5.

[111] T. Wik, Trickling filters and biofilm reactors modelling, Rev. Environ. Sci. Biotechnol. 2 (2003) 193–212.

[112] K.J. Martin, R. Nerenberg, The membrane biofilm reactor (MBfR) for water and wastewater treatment: principles, applications, and recent developments, Bioresour. Technol. 122 (2012) 83–94. https://doi.org/10.1016/j.biortech.2012.02.110.

[113] T. Vicsek, M. Cserzõ, V.K. Horvath, Self-affine growth of bacterial colonies, Physica Acta, 167 (2015) 315–321. https://doi.org/10.1016/0378-4371(90)90116-A.

[114] A.L.D. Moreau, G.S. Lorite, C.M. Rodrigues, A.A. de Souza, M.A. Cotta, Fractal analysis of *Xylella fastidiosa* biofilm formation, J. Appl. Phys. 106 (2009) 024702**.**

[115] H.J. Busscher, H.C. Van der Mei, How do bacteria know they are on a surface and regulate their response to an adhering state, PLoS Pathogens. 8 (2012) 1–3.

[116] J.B Kaplan, Biofilm dispersal, J. Dent. Res. 89 (2010) 205–218. https://doi.org/10.1177/002034509359403.

[117] M.C.M. van Loosdrecht, D. Gjatelma, A. Mulder, L. Tijhuis, J.J. Heijnen, Biofilm structures, Water Sci. Technol. 32 (1995) 35–43. https://doi.org/10.1111/j.1574-6941.1997.tb00434.x.

[118] B.S. Tseng, W. Zhang, J.J. Harrison, T.P Quach, J.L. Song, J. Penterman, P.K. Singh, D.L. Chopp, A.I. Packman, M.R. Parsek, The extracellular matrix protects *Pseudomonas*

aeruginosa biofilms by limiting the penetration of tobramycin, Environ. Microbiol. 15 (2013) 2865–2878.

[119] J.W.T. Wimpenny, R. Colasanti, A unifying hypothesis for the structure of microbial biofilms based on cellular automaton models, FEMS Microbiol. Ecol. 22 (2006) 1–16.

[120] J.A. Conchello, J.W. Lichtman, Optical sectioning microscopy. Nat. Methods 2 (2005) 920–931.

[121] D.M. Shotton, Confocal scanning optical microscopy and its applications for biological specimens. J. Cell. Sci. 94 (1989) 175–206.

[122] N. Cerca, F. Gomes, S. Pareira, P. Teixeira, R. Oliveira, Confocal laser scanning microscopy analysis of *S. epidermidis* biofilms exposed to farnesol, vancomycin and rifampicin, BMC Res. Notes 16 (2012) 244. https://doi.org/10.1186/1756-0500-5-244.

[123] J.W. Costerton, Z. Lewandowski, D.E. Caldwell, D.R. Korber, H.M. Lappin-Scott. Microbial biofilms. Ann. Rev. Microbiol. 47 (1995) 711–745. doi:10.1146/annurev.mi.49.100195.003431

[124] T.R. Neu, J.R. Lawrence, Innovative techniques, sensors, and approaches for imaging biofilms at different scales. Curr. Trends Microbiol. 23 (2015) 233–242.

[125] D.R. Korber, J.R. Lawrence, M. J. Hendry, D.E. Caldwell, Programs for determining statistically representative areas of microbial biofilms, Binary 4 (1992) 204–210.

[126] S.C. Mokwatlo, M.E. Nchabeleng, H.G. Brink, W. Nicol, Impact of metabolite accumulation on the structure, viability and development of succinic acid–producing biofilms of *Actinobacillus succinogenes*. Appl. Microbiol. Biotechnol. 103 (2019) 6205–6215. https://doi.org/10.1007/s00253-019-09888-8.

[127] S.C. Mokwatlo, W. Nicol, Structure and cell viability analysis of *Actinobacillus succinogenes biofilms* as biocatalysts for succinic acid production, Biochem. Eng. J. 128 (2017) 134–140. https://doi.org/10.1016/j.bej.2017.09.013.

[128] V.P. Venugopalan, M. Kuen, M. Hausner, D. Spring, P.A. Wilderer, S. Wuertz, Architecture of a nascent *Sphingomonas* sp. biofilm under varied hydrodynamic conditions. Appl. Environ. Biotechnol. 71 (2005) 2677–2686.

[129] C.A. Schneider, W.S. Rasband, K.W. Eliceiri, NIH Image to ImageJ: 25 years of image analysis, Nat. Methods 9 (2012) 671–675. https://doi.org/10.1038/nmeth.2089.

[130] A. Heydorn, A.T. Nielsen, M. Hentzer, M. Givskov, B.K. Ersbøll, S. Molin, Quantification of biofilm structures by the novel computer program COMSTAT, Microbiology 146 (2000) 2395–2407. https://doi.org/10.1099/00221287-146-10-2395.

[131] D. Hwang, Y.H. Lim, Resveratrol antibacterial activity against *Escherichia coli* is mediated by Z-ring formation inhibition via suppression of FtsZ expression, Sci. Rep. 5 (2015) 2–11. https://doi.org/10.1038/srep10029.

[132] T.H. Jones, K.M. Vail, L.M. McMullen, Filament formation by foodborne bacteria under sublethal stress, Int. J. Food Microbiol. 165 (2013) 97–110. https://doi.org/10.1016/j.ijfoodmicro.2013.05.001.

[133] M.A. Wortinger, E.M. Quadokus, Y.V. Brun, Morphological adaptation and inhibition of cell inhibition of cell division during stationary phase in *Caulobacter crescentus*. Mol. Microbiol. 29 (1998) 963–973.

[134] R. Janissen, D.M. Murillo, B. Niza, P.K. Sahoo, M.M. Nobrega, C.L. Cesar, M.L.A. Temperini, H.F. Carvalho, A.A. de Souza, M.A. Cotta, Spatiotemporal distribution of different extracellular polymeric substances and filamentation mediate *Xylella fastidiosa* adhesion and biofilm formation., Sci. Rep. 5 (2015) 9856. https://doi.org/10.1038/srep09856.

[135] M.C.M. van Loosdrecht, C. Picioreanu, J.J. Heijnen, A more unifying hypothesis for biofilm structures. FEMS Microbiol Ecol. 24 (1997) 181–183. https://doi.org/10.1111/j.1574-6941.1997.tb00434.x.

[136] C. Picioreanu, M.C.M. van Loosdrecht, J.J. Heijnen, Two-dimensional model of biofilm detachment caused by internal stress from liquid flow, Biotechnol. Bioeng. 72 (2000) 206–218. https://doi.org/10.1002/1097-0290(20000120)72:2<205::AID-BIT9>3.0.CO;2-L

[137] P. Stoodley, S. Yang, H. Lappin-Scott, Z. Lewandowski, Relationship between mass transfer coefficient and liquid flow velocity in heterogenous biofilms using microelectrodes and confocal microscopy, Biotechnol. Bioeng, 56 (1997) 681–688,

https://doi.org/10.1002/(SICI)1097-0290(19971220)56:6<681::AID-BIT11>3.0.CO;2-B.

[138] C. Pellicer-Nàcher, B.F. Smets, Structure, composition, and strength of nitrifying membrane-aerated biofilms. Water Res. 57 (2014) 151–161. https://doi.org/10.1016/j.watres.2014.03.026.

[139] D. Celmer, J.A. Oleszkiewicz, N. Cicek, Impact of shear force on the biofilm structure and performance of a membrane biofilm reactor for tertiary hydrogen-driven denitrification of municipal wastewater. Water Res. 42 (2008) 3057–3065, https://doi.org/10.1016/j.watres.2008.02.031.

[140] E. Paramonova, O.J. Kalmykowa, H.C. Van Der Mei, H.J. Busscher, P.K. Sharma, Impact of hydrodynamics on oral biofilm strength. J. Dent. Res. 10 (2009) 922–926. https://doi.org/10.1177/0022034509344569.

[141] Y. Shen, M. Wang, I.S. Chang, H.W. Ng, Effect of shear rate on the response of microbial fuel cell toxicity sensor to Cu(II). Bioresour. Technol. 136 (2013) 707–710. https://doi.org/10.1016/j.biortech.2013.02.069.

[142] S.C. Mokwatlo, H.G. Brink, W. Nicol, Effect of shear on morphology, viability and metabolic activity of succinic acid-producing *Actinobacillus succinogenes* biofilms. Bioproc. Biosyst. Eng. (2020). https://doi.org/10.1007/s00449-020-02322-8. [Epub ahead of print]

[143] D.R. Madhrani, Experimental investigation of the fluid velocity distribution in stirred tank reactors equipped with retreat blade impellers using laser doppler velocimetry. New Jersey Institute of Technology (2008). https://digitalcommons.njit.edu/cgi/viewcontent.cgi?article=1355&context=theses. (accessed 20 January 2020).

[144] S. Jachlewski, W.D. Jachlewski, U. Linne, C. Bräsen, J. Wingender, B. Siebers, Isolation of extracellular polymeric substances from biofilms of the thermoacidophilic archaeon *Sulfolobus acidocaldarius*. Front. Bioeng. Biotechnol. 3 (2005) 123. https://doi.org/10.3389/fbioe.2015.00123.

[145] M. Dubois, K.A. Gilles, J.K. Hamilton, P.A. Rebers, F. Smith, Colorimetric method for

determination of sugars and related substances. Anal Chem. 28 (1956) 350–356. https://doi.org/10.1021/ac60111a017.

[146] J.M. Walker, J.H. Waterborg, H.R. Matthews, The Lowry method for protein quantitation. In J.M. Walker (Ed.) The Protein Protocols Handbook. (2003). New York, Springer Science. https://doi.org/10.1385/0-89603-268-x:1.

[147] H. Wang, H. Cheng, F. Wang, D. Wei, X. Wang, An improved 3-(4,5-dimethylthiazol-2-yl)-2,5-diphenyl tetrazolium bromide (MTT) reduction assay for evaluating the viability of *Escherichia coli* cells. J. Microbiol. Methods. 82 (2010) 330–333. https://doi.org/10.1016/j.mimet .2010.06.014

[148] Y. Liu, J.H. Tay, The essential role of hydrodynamic shear force in the formation of biofilm and granular sludge. Water Res. 36 (2002) 1653–1665.

[149] Y.C. Choi, E. Morgenroth, Monitoring biofilm detachment under dynamic changes in shear stress using laser-based particle size analysis and mass fractionation. Water Sci. Technol. 47 (2003) 69–76.

[150] I.P. Molobela, F.M. Ilunga , Impact of bacterial biofilms: The importance of quantitative biofilm studies. Ann. Microbiol. 62 (2012) 461–467. https://doi.org/10.1007/s13213-011-0344-0.

[151] P.S. Qi, W. Bin Wang, Z. Qi, Effect of shear stress on biofilm morphological characteristics and the secretion of extracellular polymeric substances. Proceedings, 2nd Int. Conf. Bioinforma. Biomed. Eng. (2008) 3438–3441. https://doi.org/10.1109/ICBBE.2008.363.

[152] J. Yang, S. Cheng, C. Li, Y. Sun, H. Huang, Shear stress affects biofilm structure and consequently current generation of bioanode in microbial electrochemical systems (MESS). Front. Microbiol. 10 (2019) 398. https://doi.org/10.3389/fmicb.2019.00398.

[153] A.D. Jones, C.R. Buie, Continuous shear stress alters metabolism, mass transport, and growth in electroactive biofilms independent of surface substrate transport. Sci. Rep. 9 (2019) 2602. https://doi.org/10.1038/s41598-019-39267-2.

[154] M. Trulear, W.G. Characklis, Dynamics of biofilm processes. J. Water Pollut. Control

Fed. 16 (1982) 1207–1217. https://doi.org/10.2307/25041684.

[155] Y. Liu, J.H. Taylor, Metabolic response of biofilm to shear stress in fixed film culture. J. Appl. Microbiol. 90 (2001) 337–342. https://doi.org/10.1046/j.1365-2672.2001.01244.x.

[156] P.S. Stewart, Diffusion in biofilms, J. Bacteriol. 185 (2003) 1485–1491. https://doi.org/10.1128/JB.185.5.1485-1491.2003.

[157] M.C.M. van Loosdrecht, J. Lyklema, W. Norde, A.J.B. Zehnder, Bacterial adhesion: A physicochemical approach, Microb. Ecol. 17 (1989) 1–15. https://doi.org/10.1007/BF02025589.

[158] R. Patel, Biofilms and antimicrobial resistance, Clin. Orthop. Relat. Res. 43 (2005) 41–47. https://doi.org/10.1097/01.blo.0000175714.68624.74.

[159] P.S. Stewart, A review of experimental measurements of effective diffusive permeabilities and effective diffusion coefficients in biofilms, Biotechnol. Bioeng. 59 (1998) 261–272. https://doi.org/10.1002/(SICI)1097-0290(19980805)59:3<261::AID-BIT1>3.0.CO;2-9.

[160] G.E. Briggs, J.B.S. Haldane, A note on the kinetics of enzyme action, Biochem. J. 19 (1925) 338–339. https://doi.org/10.1042/bj0190338.

[161] J.J.J.H. Nielsen, J. Villadsen, G. Lidén, J.J.J.H. Nielsen, J. Villadsen, G. Lidén, J. Villadsen, G. Lidén, Bioreaction Engineering Principles, 3rd ed. Springer, New York, 2011. https://doi.org/10.1007/978-1-4419-9688-6.

[162] R.K. Hinson, W.M. Kocher, Model for effective diffusivities in aerobic biofilms, J. Environ. Eng. 122 (1996) 1023–1030. https://doi.org/10.1061/(ASCE)0733-9372(1996)122:11(103).

[163] E.W. Thiele, Relation between catalytic activity and size of particle, Ind. Eng. Chem. 31 (1939) 916–920. https://doi.org/10.1021/ie50355a027.

[164] H.S. Fogler, Elements of Chemical Reaction Engineering, 4th edition. London, Pearson, 2006.

[165] H.G. Brink, W. Nicol, Succinic acid production by *Actinobacillus succinogenes* in chemostat and biofilm cultures, Chem. Eng. Trans. 49 (2016) 613–618. https://doi.org/10.3303/CET1649103.

[166] T.H. Chilton, A.P. Colburn, Mass transfer (absorption) coefficients: Prediction from data on heat transfer and fluid friction, Ind. Eng. Chem. 26 (1934) 1183–1187. https://doi.org/10.1021/ie50299a012.

[167] I. Bechthold, K. Bretz, S. Kabasci, R. Kopitzky, A. Springer, Succinic acid: A new platform chemical for biobased polymers from renewable resources, Chem. Eng. Technol. 31 (2008) 647–654. https://doi.org/10.1002/ceat.200800063.

APPENDIX

A. DISCRETISATION OF THE PSEUDO-STEADY-STATE REACTOR MODEL

Under pseudo-steady-state conditions, there is no mass accumulation within the biofilm layer, and therefore the rate of reaction equals the rate of diffusion at any point in the biofilm. Equation A-1 gives the general mass balance used to solve for the concentration profiles.

$$D_{e_j} \frac{d^2 C_j}{dz^2} = r_j' C_X \tag{A-1}$$

The second-order differential equations in the pseudo-steady-state model were discretised using a central finite difference method. As an example, the discretisation of the SA mass balance leads to

$$z_0 = 0, \dots, z_i = i\Delta z, \dots, z_n = L = n\Delta z$$

$$\frac{d^2 C_{SA}}{dz^2} \approx \frac{C_{SA_{i+1}} - 2C_{SA_i} + C_{SA_{i-1}}}{\Delta z^2} \tag{A-2}$$

By applying these transformations to Equation A-1 for i = 1 to i = n −1, we get the discretised system presented in Equations A-3 and A-4:

$$De_{SA} \frac{C_{SA_{i+1}} - 2C_{SA_i} + C_{SA_{i-1}}}{\Delta z^2} = \left(\phi 0.82 \left(1 - e^{-6e^{-0.54 C_{SA}i}}\right) + \frac{k C_{SA_i}}{K_P + C_{SA_i} + \frac{C_{SA_i}^2}{K_I}} \right) C_X \tag{A-3}$$

$$C_{SA_{i+1}} = 2C_{SA_i} - C_{SA_{i-1}} + \left(\phi 0.82 \left(1 - e^{-6e^{-0.54 C_{SA}i}}\right) + \frac{k C_{SA_i}}{K_P + C_{SA_i} + \frac{C_{SA_i}^2}{K_I}} \right) C_X \frac{\Delta z^2}{De_{SA}} \tag{A-4}$$

with the following boundary conditions:

$$\begin{cases} C_{SA_n} = C_{SA_{aq}} & succinic\ acid\ concentration\ in\ the\ bulk\ conditions \\ C_{SA_1} = C_{SA_0} & so\ that\ the\ flux\ at\ the\ solid - biofilm\ interface\ is\ zero \end{cases}$$

A second-order Newton-Raphson method is consequently employed to solve the n −1 system of equations with n −1 unknown variables.

B. DISCRETISATION OF THE BATCH REACTOR MODEL

The batch system consists of the bulk liquid phase and the biofilm phase. In the liquid phase suspended cells grow and convert the substrate to products, and there is diffusion of metabolic products and the substrate out of and into the biofilm phase, respectively. Equations A-5 and A-6 give a generic mass balance in the liquid phase.

$$\frac{dC_{jaq}}{dt} = r_j' C_{X,aq} + J_j \tag{A-5}$$

where the mass flux Jj, is given by Equation A-6 which can

$$J_j = D_{e-j} A_p \frac{dC_j}{dz}|_{z=L} \tag{A-6}$$

In the biofilm phase, the general mass balance is as presented in Equation A-7.

$$\frac{dC_j}{dt}|_z = -D_{e-j} \frac{d^2 C_j}{dz^2} + r_j' C_{XB} \tag{A-7}$$

First-order and second-order differential equations were discretised using the central difference method in order to solve the batch system of equations numerically with an iterative process that uses a finite difference method. Time and the biofilm thickness domains were first discretised as follows:

$$z_0 = 0, \ldots, z_i = i\Delta z, \ldots, z_n = L = n\Delta z$$

$$t_0 = 0, \ldots, t_m = m\Delta t, \ldots, t_p = T = p\Delta t$$

Using SA as an example, Equation (A-7) for the general mass balance in the biofilm layer is discretised as follows:

$$\frac{C_{SA_i}^{m+1} - C_{SA_i}^{m}}{\Delta t} = -De_{SA} \frac{C_{SA_{i+1}}^{m} - 2C_{SA_i}^{m} + C_{SA_{i-1}}^{m}}{\Delta z^2} + \left(\phi\mu + \frac{kC_{SA_i}^{m}}{K_P + C_{SA_i}^{m} + \frac{\left(C_{SA_i}^{m}\right)^2}{K_I}} \right) C_{XB} \tag{A-8}$$

By rearranging Equation A-8, we end up with a discretised Equation A-9 which solves for the mass balance in the biofilm phase of the system.

$$C_{SA_i}^{m+1} = C_{SA_i}^{m} + \left(C_{SA_{i+1}}^{m} - 2C_{SA_i}^{m} + C_{SA_{i-1}}^{m}\right)\left(\frac{-De_{SA}\Delta t}{\Delta z^2}\right) + \left(\phi\mu + \frac{kC_{SA_i}^{m}}{K_P + C_{SA_i}^{m} + \frac{\left(C_{SA_i}^{m}\right)^2}{K_I}}\right)\Delta t C_{XB} \quad \text{(A-9)}$$

Equations A-5 and A-6 are then combined and discretised as follows to give the general mass balance for the bulk liquid phase

$$\frac{C_{SA,aq}^{m+1} - C_{SA,aq}^{m}}{\Delta t} = \left(\phi\mu + \frac{kC_{SA,aq}^{m}}{K_P + C_{SA,aq}^{m} + \frac{\left(C_{SA,aq}^{m}\right)^2}{K_I}}\right)C_{X,aq} + D_{e_{SA}}A_p\left(\frac{C_{SA_n} - C_{SA_{n-1}}}{\Delta z}\right) \quad \text{(A-10)}$$

Finally, the general mass balance in the bulk liquid phase becomes

$$C_{SA,aq}^{m+1} = C_{SA,aq}^{m} + \left(\phi\mu + \frac{kC_{SA,aq}^{m}}{K_P + C_{SA,aq}^{m} + \frac{\left(C_{SA,aq}^{m}\right)^2}{K_I}}\right)\Delta t C_{X,aq} + D_{e_{SA}}A_p\Delta t\left(\frac{C_{SA_n} - C_{SA_{n-1}}}{\Delta z}\right) \quad \text{(A-11)}$$

C. THEORETICALLY GENERATED DATA

Table A-1: Realistic pseudo-steady state data generated for a hypothetical *A. succinogenes* biofilm.

$C_{SA,aq}$ ($g.L^{-1}$)	$C_{Glc,aq}$ ($g.L^{-1}$)	C_{XB} ($g.L^{-1}$)	L^* (μm)	ε_{cells}	ε_{EPS}
10	86.6	57.6	834	0.5	0.3
25	68.2	57.6	790	0.5	0.3
45	47.0	57.6	740	0.5	0.3
10	86.6	34.2	730	0.3	0.5
25	68.2	34.2	695	0.3	0.5
25	68.2	57.6	200	0.5	0.3
25	68.2	57.6	400	0.5	0.3
25	68.2	57.6	600	0.5	0.3
25	68.2	57.6	790	0.5	0.3
25	68.2	57.6	790	0.5	0.3
45	47.0	57.6	200	0.5	0.3
45	47.0	57.6	400	0.5	0.3
45	47.0	57.6	600	0.5	0.3
25	68.2	10.9	500	0.1	0.7
25	68.2	22.6	500	0.2	0.6
25	68.2	34.2	500	0.3	0.5
25	68.2	45.9	500	0.4	0.4
25	68.2	57.6	500	0.5	0.3
45	47.0	10.9	500	0.1	0.7
45	47.0	22.6	500	0.2	0.6
45	47.0	34.2	500	0.3	0.5
45	47.0	45.9	500	0.4	0.4
45	47.0	57.6	500	0.5	0.3
25	68.2	61.5	500	0.53	0.267
25	68.2	61.5	500	0.57	0.283

25	68.2	61.5	500	0.6	0.3
25	68.2	61.5	500	0.63	0.317
25	68.2	61.5	500	0.65	0.325
25	68.2	22.6	500	0.2	0.6
25	68.2	22.6	500	0.213	0.6375
25	68.2	22.6	495	0.225	0.675
25	68.2	22.6	352	0.238	0.7125
25	68.2	22.6	250	0.244	0.73125
25	68.2	8.5	500	0.08	0.72
25	68.2	8.5	500	0.085	0.765
25	68.2	8.5	500	0.09	0.81
25	68.2	8.5	500	0.095	0.855